Seafloor Anchoring for Platforms in the Messina Strait

by

Antonioluca Manno

B.S. Environmental Engineering
La Sapienza Università di Roma, 2007

SUBMITTED TO THE DEPARTMENT OF CIVIL AND ENVIRONMENTAL ENGINEERING IN PARTIAL FULFILLMENT OF THE REQUIREMENTS FOR THE DEGREE OF

MASTER OF ENGINEERING IN CIVIL AND ENVIRONMENTAL ENGINEERING

AT THE

MASSACHUSETTS INSTITUTE OF TECHNOLOGY

JUNE 2010

Signature of Author: _____

Department of Civil and Environmental Engineering
May 7th, 2010

Certified by: _____

Herbert H. Einstein
Professor of Civil and Environmental Engineering
Thesis Supervisor

Accepted by: _____

Daniele Veneziano
Professor of Civil and Environmental Engineering
Chairman, Departmental Committee for Graduate Students

Seafloor Anchoring for Platforms in the Messina Strait

by

Antonioluca Manno

Submitted to the Department of Civil and Environmental Engineering
on May 7th, 2010 in Partial Fulfillment of the
Requirements for the Degree of Master of Engineering in
Civil and Environmental Engineering

ABSTRACT

The importance of properly designing and selecting an anchor is key to reliable techniques for floating offshore platforms including power generation from marine currents. Numerous studies have demonstrated how the uplift capacity of embedment anchors is highly dependent on the soil properties and the anchor geometry. This work focuses in detail on the behavior of vertically loaded circular anchors to keep a floating structure stationary in the offshore environment. The main goal of this research was to find and evaluate an alternative to the foundations employed in the M. Eng. 2009/10 offshore project. The initial option consisted of drag embedment anchors and suction anchors as the foundations for the floating structure located in the Messina Strait that carries a horizontal-axis marine current turbine. Examining past theories and tests, and using dimensional analysis, we determined that circular plate anchors of 4.22 m and 2.72 m in diameter represent a good alternative design for the foundations of the front and back floating platforms. These anchors have an embedment depth-to-diameter ratio of 3 and a plate thickness-to-diameter ratio of 3%. Therefore, in comparison to the initial foundation options developed in the M. Eng. project, the solution with circular anchors has the advantage to reduce the overall dimensions of the anchors, reduce the material necessary for their manufacture, minimize the duration and cost of installation, and provide an efficient anchoring system independent of the local current direction.

Thesis Supervisor: Herbert H. Einstein

Title: Professor of Civil and Environmental Engineering

Acknowledgments

I am glad to express my gratitude to my advisor and thesis supervisor Professor Herbert H. Einstein whose expertise and understanding added considerably to my graduate experience. I would like to thank him for his patience, enthusiasm, and dedication demonstrated for my thesis.

Furthermore, many thanks to my friends, colleagues, and team companions Fernando, Geoffroy, and Mohamed who worked hard with me to make our HPS Master of Engineering project successful and of inspiration for this thesis.

I am significantly grateful to my girlfriend and life partner Federica who has supported me throughout this academic year. She incited me, she cheered me up in though times, and she demonstrated her strong feelings more and more over time helping me find the strength and the way of success.

I am pleased and delighted to acknowledge my sister and all my family relatives, who always encouraged me, but special thanks to my lovely parents who supported me with their efforts and joyful spirit toward and along this wonderful and unique experience at MIT.

Finally, I am happy to thank the Honors Center of Italian Universities (H2CU) to make great part of this dream possible.

Table of Contents

List of Figures

List of Tables

1 Introduction

This thesis draws its motivation from a team project that focused on the design of a marine current turbine farm to generate enough renewable energy to supply a medium sized city. The project involved four students from the 2010 CEE Master of Engineering Program at MIT who have worked on the major aspects of the design throughout the academic year. After an initial investigation into the available technologies for marine current power generation, Fernando Pereira-Mosqueira, Mohamed Abdellaoui Maane, and Geoffroi Larrecq developed the structural design, while the author has been in charge of the foundation analyses. The team selected the Messina Strait as the site for the project because of the steady current velocity and, given the bathymetry profile under consideration, proposed and analyzed the following design options.

Option 1. The reference depth is 30 m under mean sea level (m.s.l.), so the design comprises a jacket structure (tripod) resting on driven steel pipe piles with a vertical-axis turbine connected on its top (see Fig. 1.1).

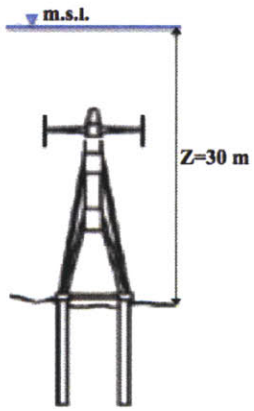

Figure 1.1: Tripod structure bearing a vertical-axis turbine and resting on driven piles (lateral view).

Option 2. The reference depth is 80 m under m.s.l.; the design consists of a three-platform floating structure bearing a horizontal-axis turbine by use of a tripod structure attached to its bottom. Additionally, in order to keep it in place, two mooring anchors are connected to the front floating platforms by a catenary system and one suction caisson is connected at the back platform in a tension-leg fashion (see Fig. 1.2).

Figure 1.2: Three-platform floating structure bearing a horizontal-axis turbine.

Since the present research focuses on the anchor design, the second of the aforementioned options will be studied.

Floating platforms are leading the search for oil and gas, and the attempt to harness alternative energy sources offshore. Indeed, an offshore platform is used mainly for drilling and installation of mechanical systems for renewable energy. As technical solutions drive the offshore industry into deeper waters, the use of floating production units (FPUs), mobile drilling rigs (MODUs) or Single Buoy Moorings (SBMs) has increased significantly (see Fig. 1.3).

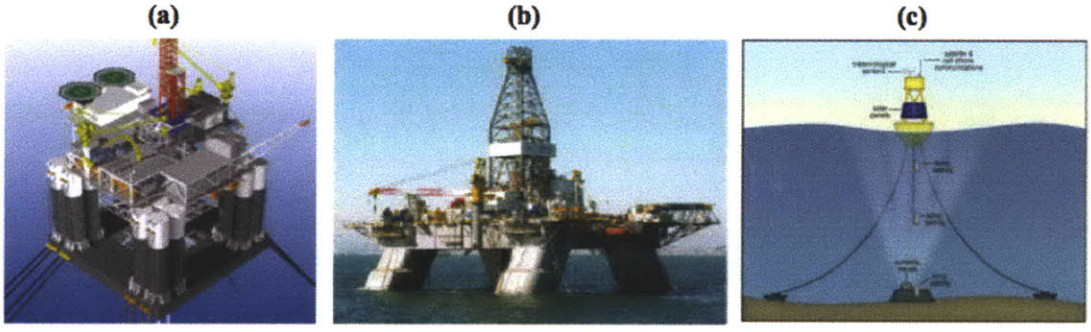

Figure 1.3: a) Floating Production Unit (FPU), (Navarre, 2008),
b) Mobile Drilling Rig Unit (MODU) (Moore, 2000),
c) Single Buoy Mooring (SBM) (Marine Sciences at UNC Chapel Hill).

These units need to be held in position using proper anchoring systems. So far, moorings anchored to the seabed (see Fig. 1.5) or dynamic positioning (see Fig. 1.4) have been deployed, with the former more frequently used. (Riemers and Kirstein, 1999; Riemers, 2004).

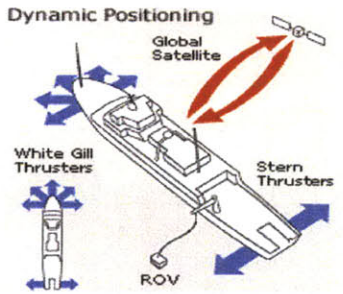

Figure 1.4: Dynamic positioning system applied to a ship: it consists of a computer- and satellite-based system that helps the vessel maintain its position by use of its thrusters (Hunt for the Hood).

The foundations of offshore floating structures are expected to receive forces coming from the superimposed fluctuating platform/vessel and primarily due to the motion caused by wind and waves. To meet the stability requirements during even the harshest circumstances, several anchoring systems have been developed, and those available on the market mainly differ in terms of load capacity, size, installation procedure, reliability, and cost. Most systems generally have a good vertical load capacity, but this characteristic may be associated with inherent weaknesses, for instance, difficult installation and soil condition limitations. Moreover, moving into deeper waters, the load transferred to the anchors tends to shift from a pure horizontal load, typical with catenary mooring, towards a combined horizontal and vertical load (taut moorings) to a completely vertical load (as for Tension Leg Platforms – TLPs), as shown in Fig. 1.5. (Riemers and Kirstein, 1999; Riemers, 2004).

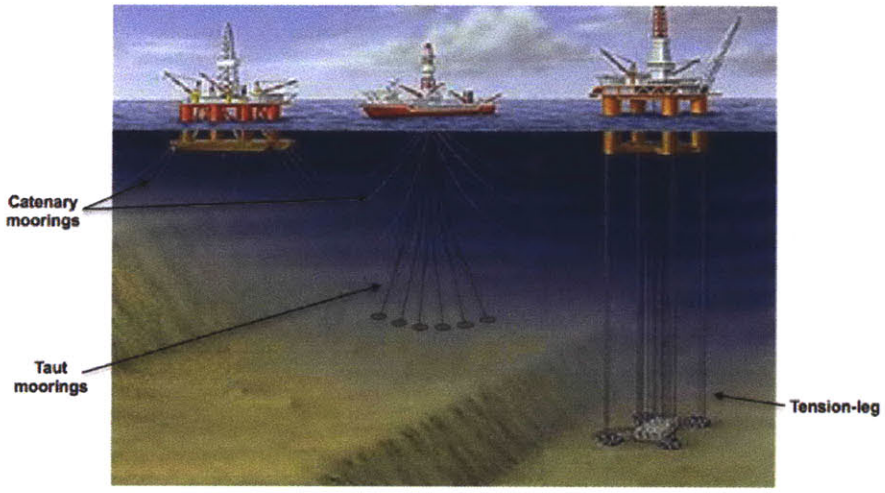

Figure 1.5: Mooring anchor systems: the first system on the left allows anchoring a floating platform using only catenary moorings, the intermediate system combines both catenary moorings and taut mooring anchors to keep the vessel in station in a deeper seabed, and the last system on the right anchors the floating platform by using only tension-legs in the deepest possible seabed, (C&C Technologies Survey Services).

Multiple factors influence anchor selection, and the leading ones are the type and magnitude of loading, soil and site conditions, and the type of floating structure. Thus, if the site belongs to a seismic area, the loading generated by earthquakes should be added to the cyclic loading caused by wind and waves acting on the floater. In fact, the behavior of anchors under repetitive loads involves the soil, water, anchor, and loading pattern in complex relations, (Hermann, 1981). For these reasons, an efficient design requires the anchors to provide a sufficient holding capacity either under static or cyclic loading, or a combination of the two.

Given multiple aspects of the problem, this work addresses the behavior of embedment anchors subjected to static and dynamic loadings in granular soil. Such behavior is important since anchors might be employed in a temporary or permanent fashion either onshore or offshore. This thesis presents an overview of possible anchor alternatives, investigates the mechanisms that control the anchor capacity, and deals with all factors that influence the anchor pullout capacity. The following background chapter focuses on how the static and dynamic pullout resistance of anchors is affected by some soil properties and by geometric properties of the anchor. Overall, analyzing the phenomena should give a better understanding of the mechanisms that are involved in an anchor system.

The final objective of this analysis was to predict the vertical uplift capacity of circular anchors for the specific application of the aforementioned **Option 2**. We started with important results on model tests conducted either in a conventional way (Clemence and Veesaert, 1977) or by means of a centrifuge (Ovesen, 1981). Then, we analyzed the phenomenon through dimensional analysis as suggested by Langhaar (1951) and Ovesen (1981). Finally, we extrapolated important results to the prototype scale, so we assessed the design and uplift capacity of those circular anchors that ought to keep the three-platforms floating structure stationary in the harsh conditions of the Messina Strait.

The rest of this thesis is organized as follows:

Chapter 2: Background regarding the anchor behavior ranging from soil-anchor interaction to loading dependence;

Chapter 3: Analyses and discussion about the theory for pullout capacity of circular anchors subjected to static and cyclic loading during conventional model tests proposed by Clemence S. P., Veesaert C. J, (1977);

Chapter 4: Dimensional analysis for the static uplift resistance of circular anchors suggested by Ovesen (1981): application to the prototype case study. Design of the anchors for the floating structure under consideration using both C&V's (1977) and Ovesen's (1981) theories for static and total dynamic loading;

Chapter 5: Discussion about the discrepancies between theory and reality for the installation of the designed anchors in the Messina Strait. Revision of the anchor designs;

Chapter 6: Summary and final conclusions.

2 Background

This chapter provides an overview of the main notions that characterize the project in discussion. Firstly, we present a geological and geotechnical report of the Messina Strait. The geomorphology and hydraulics of this site have determined the design of the overall project and the alternative anchor design that we propose is intimately related to the local ground conditions. Secondly, few of the most common type of offshore anchors are illustrated and described. The description intends to portray the advantages and disadvantages that characterize each anchor type. Finally, we provide an extensive section about the anchor's behavior during static and dynamic loading conditions. The soil-anchor interaction is the main objective and it will be covered through the investigation of past theories.

2.1 Geological and Geotechnical Site Characterization

The Messina Strait consists of several geological strata close to the surface, as illustrated in Fig. 2.1 and Fig. 2.2;

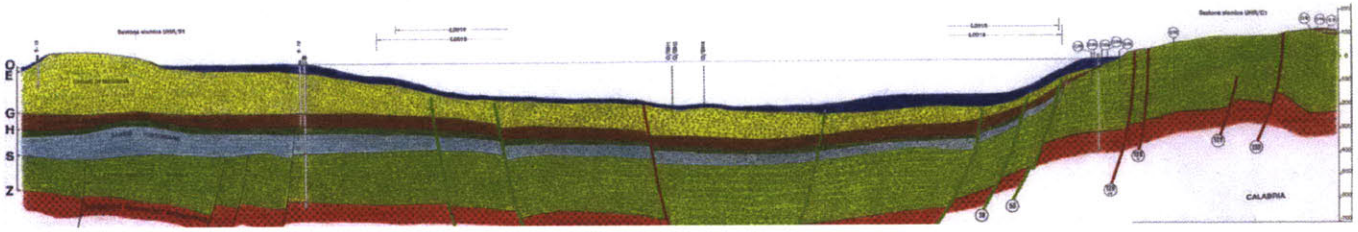

Figure 2.1: Geological cross section (for a larger view see Appendix 8.1).

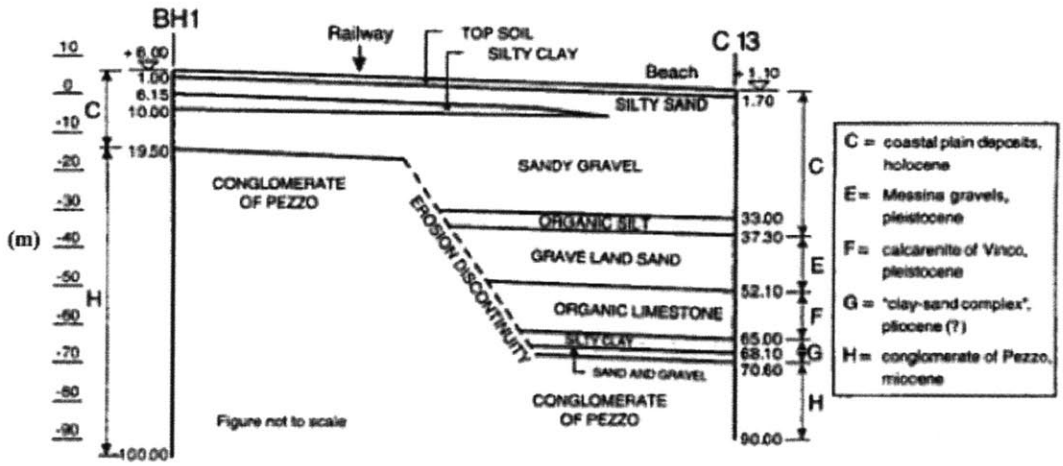

Figure 2.2: Soil profile of the Calabrian shore, (Jamiolkowski and Lo Presti, 2003).

As Jamiolkowski and Lo Presti (2003) describe, two formations characterize the site in the first 100 m. They are from top to bottom: the Coastal Plain Deposit (CPD) and the Messina Gravels (MG).

The CPD features sandy-gravelly layers rarely alternating with lenses and layers with abundant organic material. The formation thickness varies from 10 m to 70 m along the Strait. CPD samples retrieved from boreholes were classified as "rounded gravels, often well graded, with sand or subangular medium to coarse sand with gravel", (Jamiolkowski and Lo Presti, 2003). On the Sicilian shore the total unit weight has been estimated as ranging from 18.6 kN/m^3 to 19.6 kN/m^3. The relative density (D_R) tends to decrease with depth ranging from 40% to 60%. The earth pressure coefficient at rest (K_0) has been estimated in the range of 0.4 to 0.65 moving from the Calabrian to the Sicilian shore.

Pumping tests were performed on both the Calabrian and Sicilian shore to assess the hydraulic conductivity of the formation. The aquifer was qualified as unconfined, and tests yielded a range of permeability for horizontal flow from 5×10^{-3} m/s to 2.6×10^{-3} m/s with an anisotropy coefficient (k_h/k_v) at least equal to 5.

As for the stiffness, relating the shear strain (γ), the effective consolidation stress (σ'_c), and the shear modulus (G) to the small strain shear modulus (G_0), it becomes apparent that the consolidation pressure and the grain size distribution influence the shear modulus and the damping ratio. In particular, as Fig. 2.3 and Fig. 2.4 show, when the consolidation

stress and the shear strain go up the shear modulus slightly decreases, while the damping ratio also assumes lower values with increase in consolidation pressure, but higher values with increase in shear strain.

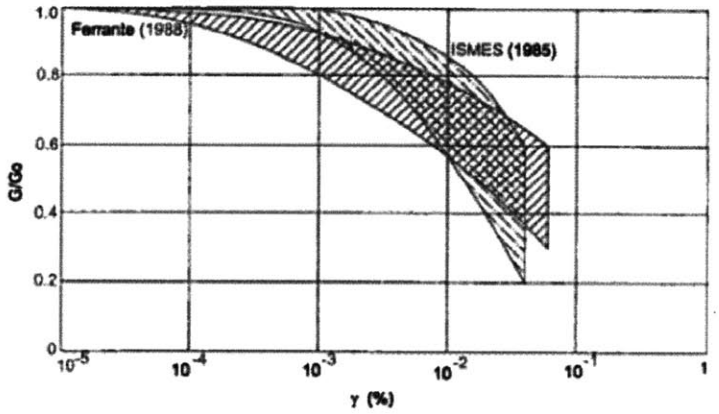

Figure 2.3: Shear modulus decay vs. shear strain of CPD from laboratory tests, (Jamiolkowski and Lo Presti, 2003).

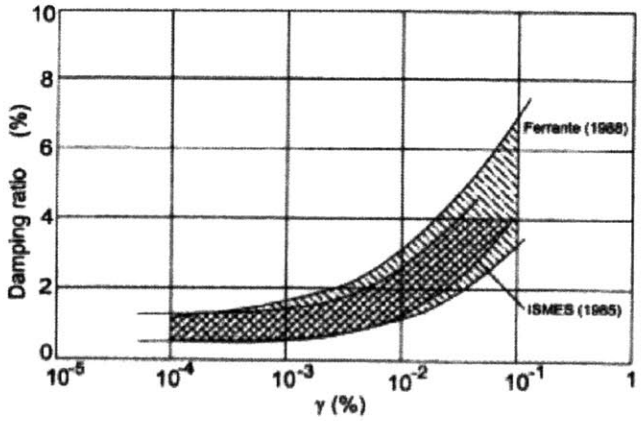

Figure 2.4: Damping ratio vs. shear strain of CPD from laboratory tests, (Jamiolkowski and Lo Presti, 2003).

In addition, the following empirical correlation has been used to estimate the peak friction angle of the deposit.

$$\phi'_p = \sqrt{20 \cdot (N_1)_{SPT}} + 20 \pm 3 \qquad (2.1)$$

where $(N_1)_{SPT}$ is the blow count for the SPT test corrected to account for the overburden pressure. Therefore, data gathered from the dynamic penetration tests and Eq. (2.1) yielded a friction angle (ϕ'_p) ranging from 36° to 47°.

The MG features gravel and pebbles with an average grain size of 10 mm and a maximum grain size of about 100 mm. Strata of sand with a thickness of 0.5 m to 1.0 m, and with an inclination of 35° to 45° toward the Strait axis, form the global matrix in which pebbles are randomly located. The overall formation is part of the medium Pleistocene and it has a thickness varying from few meters to 400 m at most. On the Sicilian shore the total unit weight has been estimated as ranging from 18.6 kN/m^3 to 20.5 kN/m^3. The relative density (D_R) does not show remarkable variations with depth, yet it maintains similar values within the range 40% to 60%. The effect of aging and mechanical overconsolidation has been considered suggesting an earth pressure coefficient at rest in the range 0.15 to 0.3. With the same procedure indicated for CPD using Eq. (2.1), the peak friction angle (ϕ'_p) for MG has been evaluated as between 37° to 45°.

For either formations, the suggested constant volume friction angle (ϕ'_{cv}) ranges between 35° to 37° degrees, and the stress dependence of the friction angle is supposed to be properly evaluated using the Bolton (1986) approach. It consists of determining the peak friction angle of soil by adding to ϕ'_{cv} an increment $\Delta\phi'$ that depends on the relative density of the deposit and on the magnitude of stresses.

Geophysical tests, based on shear wave velocity measurements from cross-hole tests, allowed one to define the small strain shear modulus G_0 for both formations. In particular, as shown by Fig. 2.5 and Eq. 2.2, a relation has been established between G_0 and the dimensionless constant K_2 (as defined by Seed et al., 1985) along with the mean effective stress σ'_m and the atmospheric pressure p_a:

$$G_0 = K_2 \cdot p_a^{1-n} \cdot (\sigma'_m)^n \qquad (2.2)$$

where n=modulus exponent, which depends on the coefficient of uniformity, and in this case n was assumed equal to 0.5. K_2 was determined both through geophysical measurements of the shear wave velocity and by means of the following empirical expression (Ismes, 1985; Ferrante, 1988):

$$G_0 = 1710 \cdot (\sigma'_c)^{0.54} \cdot p_a^{0.46} \cdot \frac{(1.32 - e)^2}{(1 + e)} \tag{2.3}$$

The two deposits show significant differences in their shear moduli; this may be due to the difference in age between them since they essentially have a similar composition. In fact, the MG belonging to the Pleistocene Era features bonding due to cementation, whereas the CPD of the Holocene Era does not show any trait of aging or cementation.

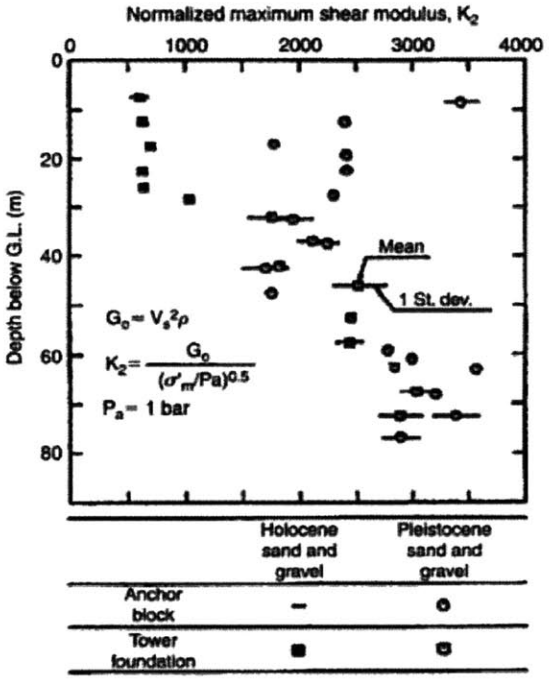

Figure 2.5: Shear modulus of sand and gravel from geophysical tests normalized with respect to σ'_m/p_a, (Jamiolkowski and Lo Presti, 2003).

Below the MG, the following geological strata have been identified with increasing depth:

- Vito Superiore Clays, which dates back to lower Pliocene. This formation features alternating layers of clays, marly clays and sandy clays, and reaches a maximum thickness of 50 m.
- Calcarenite of Vinco, whose age is also Pliocene. It consists of sands and calcarenite in sequence, and it ranges in thickness from 20 m to 100 m.
- Trubi formation, which consists of marls formed during the Pliocene and reaches its maximum thickness of 5 m to 20 m on the Calabrian shore.

- Conglomerate of Pezzo, whose origins belong the Miocene. It features a sandy-silty matrix with pebbles of metamorphic nature, and it varies in thickness reaching hundreds of meters.
- Metamorphic rock, which dates back to the Triassic Period and mainly consists of gneiss.

The area of interest is located in one of the regions with the highest seismicity within the European continent. The site comprises active faults and it is where on December 28th, 1908 the strongest earthquake ever recorded in southern Italy occurred with a Richter magnitude of 7.5 (see Fig. 2.6 and Fig. 2.7).

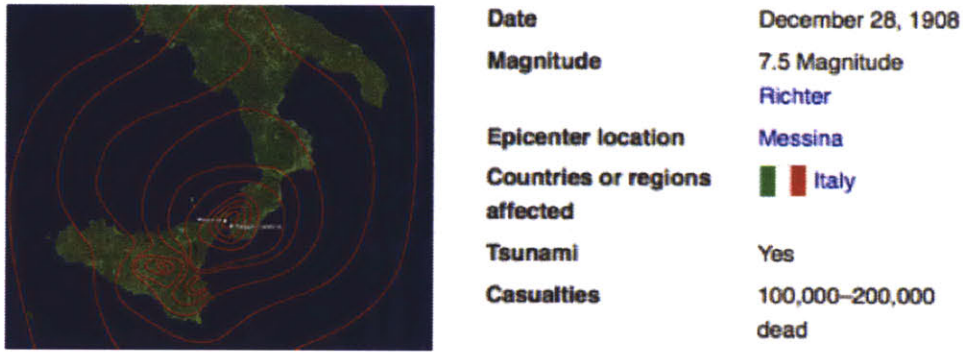

Figure 2.6: Messina 1908 quake, (Wikipedia, 1908 Messina Earthquake).

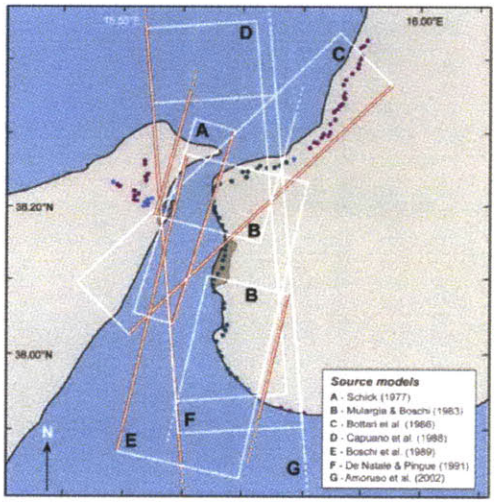

Figure 2.7: Surface projection of the published fault planes for the 1908 earthquake, (Pino et al., 2009).

According of the seismogenetic zonation (see Fig. 2.8) elaborated by the National Research Council (CNR) and the major Italian geophysical observatories, the Messina

area belongs to the most hazardous zones in the Italian territory with a peak ground acceleration (PGA) greater than 0.36g.

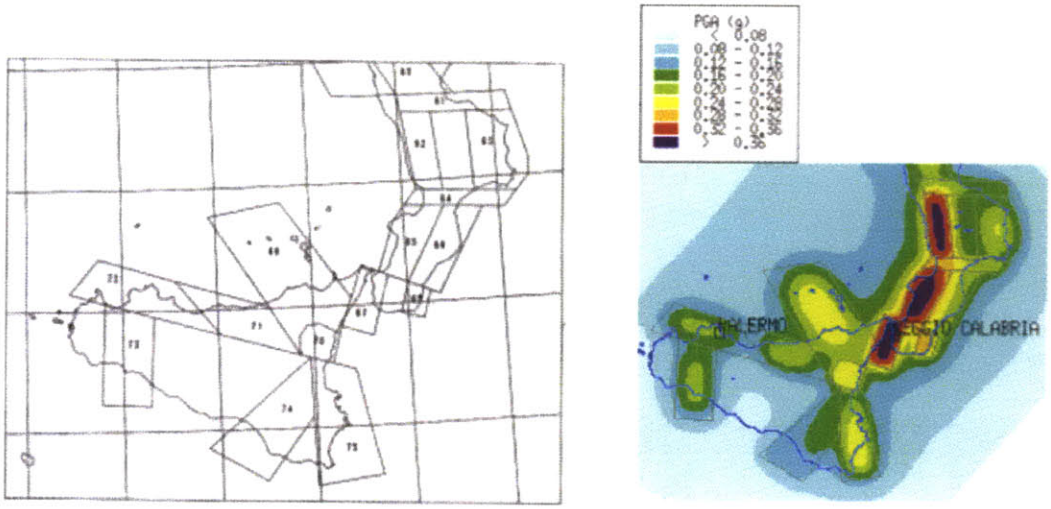

Figure 2.8: Left – Seismogenic zonation (CNR, Italy),
Right – Horizontal peak ground acceleration map, (Slejko et al., 1996).

Therefore, numerous geophysical investigations have been performed to locate the main faults and define a seismotectonic model. Surveys took place both on land and offshore, and they utilized multiple advanced techniques such as:

- mono- or multi-channel analogue and digital sparker for detailing the bathymetry and superficial seismography;
- hydropulse;
- seismic reflection and refraction; and,
- electric seismic.

The obtained seismic-stratigraphic cross section presents diverse seismic reflective horizons. They have been identified and mapped as follows (see Fig. 1 in Appendix 8.1):

- Horizon E: top of "Messina Gravels";
- Horizon G: bottom of "Messina Gravels";
- Horizon H: top of "Trubi Formation";
- Horizon S: top of "Pezzo Conglomerate"; and,
- Horizon Z: top of "Metamorphic rock".

Numerous faults were detected: 82 were counted on the Calabrian side, 80 on the Sicilian side, and 128 offshore. Some of them are inactive, while others are too shallow to be considered dangerous. Those that are active have inclinations averaging between 60 and 80 degrees. Four different systems of faults can be distinguished in terms of orientation, but the most critical one has a strike (NE-SW).

For this reason, some samples of the superficial deposit were reconstituted to run proper tests for determining the liquefaction susceptibility. It turned out that the CPD is at risk, as shown by historical episodes, and its cyclic resistance ratio mainly depends on the density and gradation of soil, which slightly vary within the area; in particular, the volumetric strains at liquefaction (when the normalized excess pore pressure $R_u=\Delta u/\sigma'_c \approx 100\%$) is about 2%, (Jamiolkowski and Lo Presti, 2003). However, as observed by Faccioli (1994) and, then, proven through in-situ seismic analysis, the CPD deposit does not reach liquefaction in the first 30 m within the volume of influence of overloaded foundations if it is previously jet-grouted, (Jamiolkowski and Lo Presti, 2003; Faccioli, 1994).

2.2 Site Investigation Recommendations

Marine anchors need to satisfy more demanding design requisites than those used on land. Indeed, they are continuously subjected to dynamic loads, they are expected to operate for a very long time in a harsh environment, and their repair and maintenance is far more difficult, (Ponniah and Finlay, 1988).

In contrast to the onshore anchors, the soil characterization for offshore design is more uncertain. Therefore, a thorough geotechnical investigation should be run in the specific area of interest of all anchors. It should involve the soil at least as deep as the anchor will penetrate and as close as possible to the installation point. The soil investigation can consist of boreholes, vibrocores, penetration tests, or a combination of these.

For cohesive soils, a combination of cone penetration tests, with measurement of the skin friction, and few samples per site are necessary to evaluate the soil composition and run lab tests to assess the strength properties.

On the other hand, in case of granular soil particular focus should be on performing dynamic penetration tests. A good estimate of the drained friction angle can be obtained from the blow counts of the tests (N_{SPT}) accounting for the proper corrections for submergence, overburden pressure, and test methods ($N_{1\text{-}60}$). The samples retrieved with the split spoon can be sufficient in evaluating the soil composition and classifying it, yet meaningful lab tests can be run only on high quality undisturbed samples retrieved by using proper techniques to conserve the state of stress (for instance, by freezing the soil).

As Fig. 2.9 shows, depending on the soil conditions different tests either in situ or in the lab may be carried out, and their results must be carefully presented in the survey report.

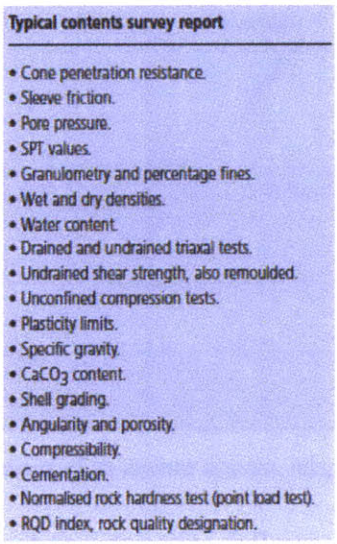

Figure 2.9: Typical data from different possible tests presented in a survey report, (Vryhof Anchors).

Still, most of the time the geotechnical foundation design is constrained by a limited exploration conducted on a much larger scale than the anchor zone of influence. This will result not only in initial savings from the partial investigation, but also in a more expensive standardized and conservative foundation design: for example, the lack of soil data can be compensated by choosing a larger anchor size, (Vryhof Anchors).

Conversely, investing more money in a precise geotechnical exploration is more likely to be reflected in a site-specific design with more reliable results and more savings both for the foundation size and their installation. Therefore, besides punctual investigation techniques, geophysical methods and the study of the site geology are useful to get an overview of the range of soil properties that can be encountered.

2.3 Anchor Options

A mooring system is an ensemble of different components such as: a floating vessel/platform, a mooring line, one or multiple fairleads, and the anchor itself (see Fig. 2.10 adapted from Vryhof Anchors).

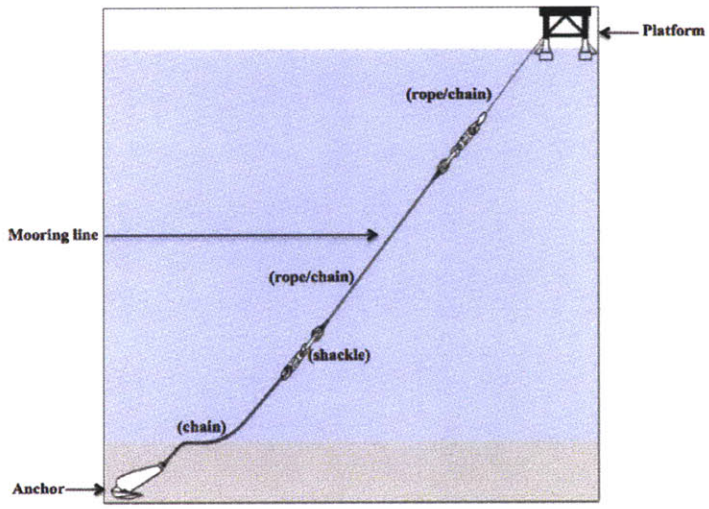

Figure 2.10: Typical components of an anchor system, adapted from (Vryhof Anchors).

A brief overview of different anchor categories follows, and it points out some of their specifics along with advantages and disadvantages:

2.3.1 Driven Piles

According to API standard RP2A, pile design is strongly affected by the lateral resistance of soil, installation techniques, and scour during operation. Driven piles are an

appropriate type of foundation in a wide range of ground conditions. They are the fastest deep foundation to install and are suitable for marine-based structures, especially offshore structures. They are well suited because they are almost insensitive to scour and to damage. In fact, given the intense and steady current in the Messina Strait, drilled-shafts could be much more affected by scour than driven piles, and partial damage of concrete might occur with subsequent direct exposure of the steel bars to the salt water.

Driven piles can be high performance foundations with high maximum design loads, yet the main problem when it comes to driving a pile is the grain size of the soil to penetrate. Indeed, driven piles are not suited for geotechnical conditions with clusters of boulders. It could be an issue to drive a large diameter pile in granular soil, but it depends on the pile diameter to grain size ratio; it might be impossible or it might require a technical support that is too costly. In fact, driving a pile requires proper equipment such as a hammer and a cushion to push the pile into the ground, as well as a crane and a jack-up platform/barge (see Fig. 2.11).

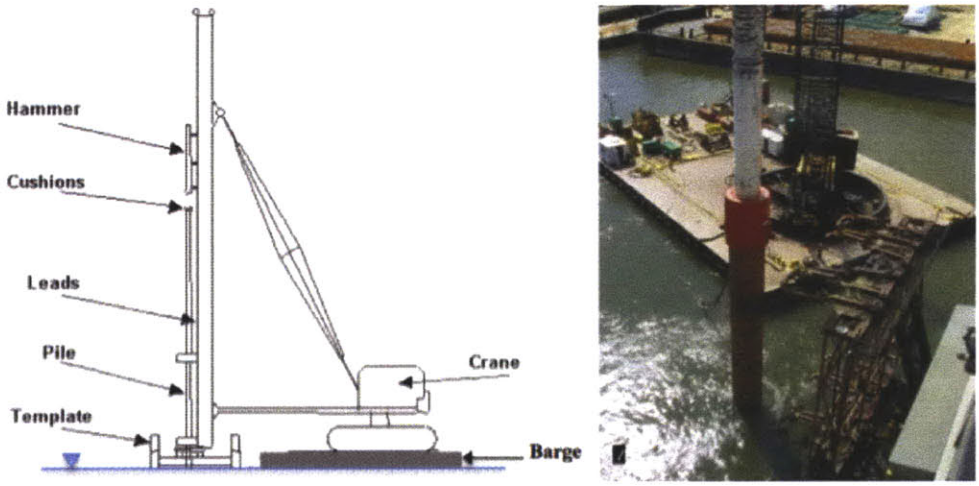

Figure 2.11: Left – Sketch of pile driving and necessary components, adapted from (Lee, 2009); Right – Pile being driven offshore by use of a template and pile extension, (Roadtraffic-technology.com).

Moreover, in deep water the hydraulic piling hammer might involve longer hoses and larger hose reels on the deck of the installation vessel, so it might affect the practicality of the work. However, boulders and cobbles are no longer an obstacle as initially feared, because evidence demonstrates how they are displaced through the granular soil matrix during the pile installation. In addition, it may be decided to aid the pile penetration by

inducing soil liquefaction with a free jet ahead or just behind the pile tip (see Fig. 2.12), but with possible repercussions on the mobilized soil resistance; thus, piling should be driven for a certain number of blows after the jetting in order to insure reconsolidation. In conclusion, driven piles can be a very costly type of foundation.

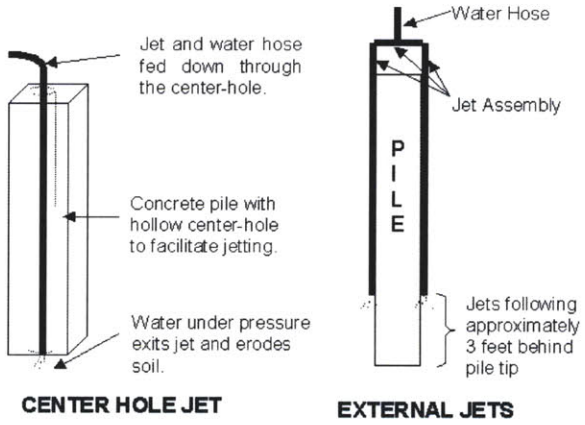

Figure 2.12: Jetting ahead or just behind the pile tip, (U.S. Department of Transportation).

Driving a pile below water requires at least the use of a template. It is a guiding frame that can be laid on the seafloor or cantilevered out from an offshore barge. Due to the sea motion, the lack of fixed points, and the length of piles, the template allows the pile to be driven in the proper direction (see Fig. 2.11), (Gerwick, 1999).

As Fig. 2.13 illustrates, new technological solutions such as seabed power packs (or submergible hammers) are being developed to drive single piles very deep, but they still are more complicated and expensive to operate than other options.

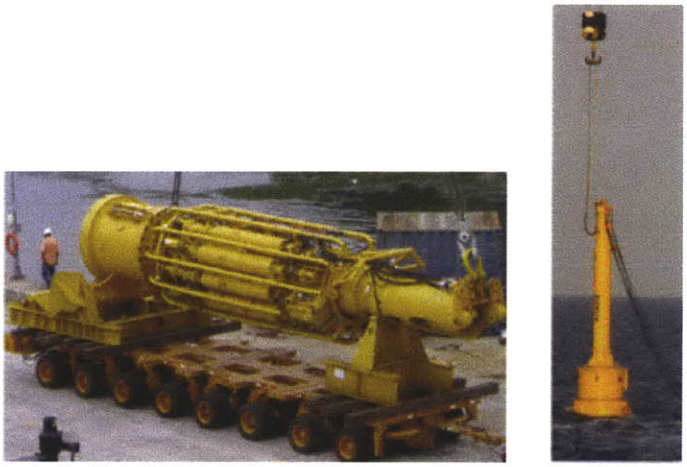

Figure 2.13: Submergible hammer for new offshore practice and deep installations, (Menck).

2.3.2 Gravity Anchors

The proposed structures are either of concrete design consisting of cellular concrete construction with a large concrete-mat foundation, or a gravity block combining concrete and rock aggregates, or, rarely, a hybrid design that features a typical steel-template structure supported by a concrete mat, (Gerwick, 1999); an example of gravity anchor is provided in Fig. 2.14.

The advantages of this option are the following:

- it is easy to design, construct, and put in place;
- it can be easily recovered or moved to another position; and,
- it is cheap because of the material used for its manufacture.

However, this type of anchor also has significant and limiting disadvantages, such as:

- it is sensitive to scour, which affects its stability;
- it requires a thorough seabed preparation; and,
- it may be uneconomical for very deep water as the required size and mass can be very large.

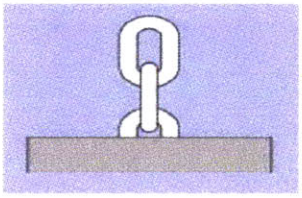

Figure 2.14: Gravity anchor example, (Vryhof Anchors).

2.3.3 Suction Piles

A typical suction anchor comprises a large diameter open-ended steel pipe pile with a sealed top cap (see Fig. 2.15). As Fig. 2.16 illustrates, the pile is lowered to the seabed and, then, it initially penetrates the sediment under its own buoyant self-weight (step 1). Thereafter, (step 2) water is pumped from inside the top chamber to produce a differential

pressure that enables further penetration, $\Delta p = (p_w - p_i)$, where p_w is the pressure in the surrounding seawater (γ_w = 10.1 kN/m^3) and p_i is the pressure inside the chamber: this stage must be accurately controlled to avoid the soil to fail for basal heave. The inverse process, applying a positive pressure inside the pile, is used to eventually recover the pile, (Gerwick, 1999). Finally, (step 3) the suction pump is recovered and the anchor chain/cable is tensioned from surface.

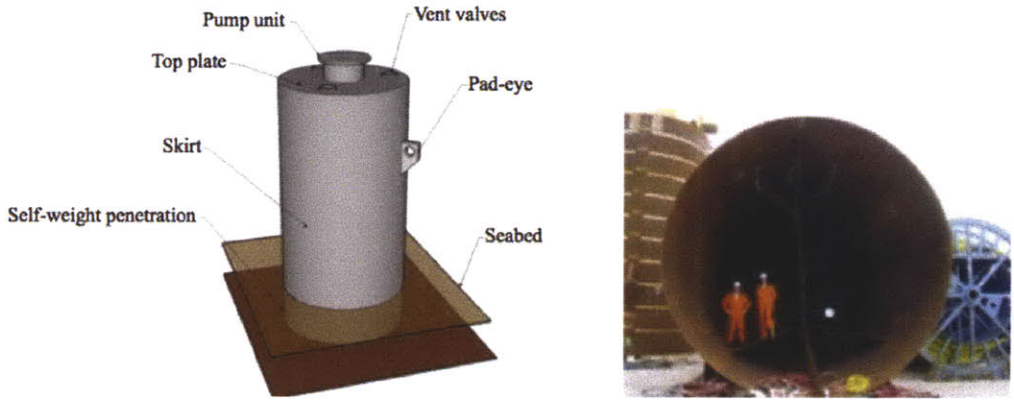

Figure 2.15: Left – Model of a suction pile, (Bakker et al., 2006);
Right – Large diameter suction pile, (SPT Offshore).

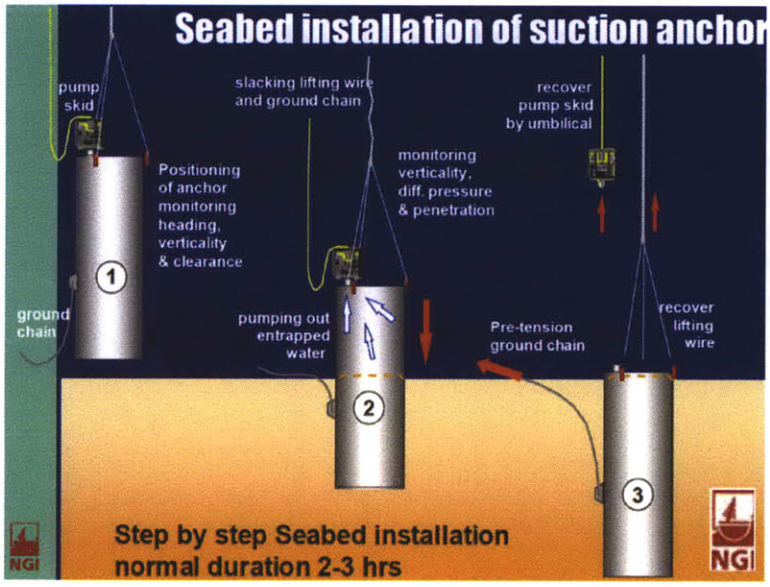

Figure 2.16: Installation sequence of suction anchor, (NGI).

Suction anchors are excellent for holding vertical loads and provide better lateral resistance than driven piles. Their design is more reliable than that for conventional piles, and, therefore, no additional load testing is required. Another advantage is the ease and

control of installation with the drawback that their big mass and large size can increase the installation cost.

As proven by past experience and shown in Fig. 2.17, when designed for cohesive soils suction anchors typically have a large length-to-diameter ratio, whereas when designed for granular soil they are shorter with a lower length-to-diameter ratio. This difference is dictated by the second step of installation that is the suction-assisted penetration. In fact, to push the pile into the seabed and achieve the full-length penetration, a suction pump is used to create a pressure gradient between the outside and the inside of the pile. However, the gradient can not overcome a certain value otherwise piping can occur at the tip causing the vertical effective stresses to fall to zero with subsequent water inflow into the pile without further penetration of it. Moreover, as the pile penetrates a skin friction develops along the penetrated skirt and it counteracts the pile penetration requiring to increase the suction. Therefore, the right compromise must be found between the imposed suction and the pile dimension. In contrast to cohesive soils, in granular soils this compromise leads the design toward a suction anchor with diameters that are larger than the length.

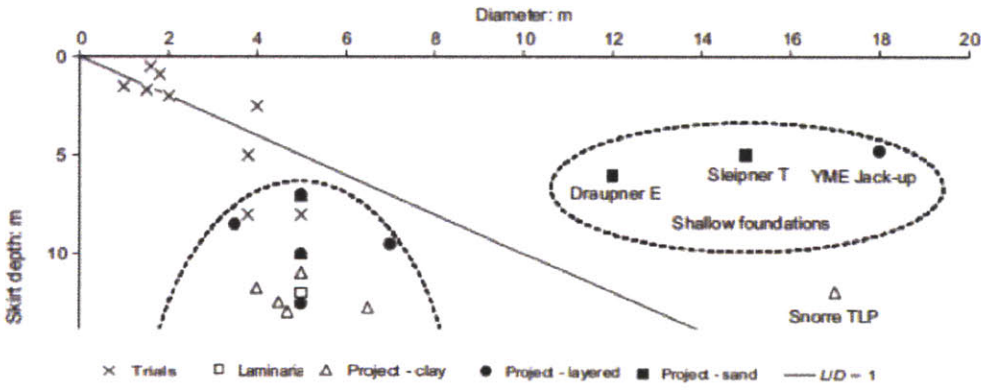

Figure 2.17: Summary of uses of caisson foundations, (Houlsby and Byrne, 2005).

2.3.4 Drag Embedment Anchors

Different types of drag anchors are available. Most of them work in a catenary or taut leg-mooring configuration (see Fig. 2.18) because the depth of installation not only

affects their size, but it also affects the loading distribution as already described in Fig. 1.5, (Vryhof Anchors).

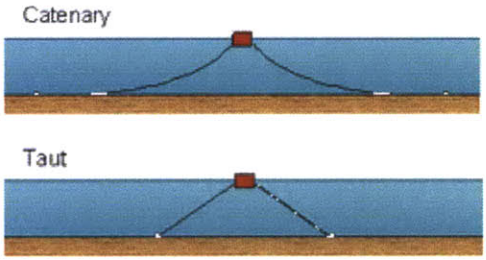

Figure 2.18: Catenary and taut-leg mooring configurations, (TTI, 2003).

The type of anchor, its configuration, and resistance are dictated by the type of soil present at the site, then the maximum calculated load leads the anchor design. Some anchors are especially designed for clay, while others for granular soil. In sands and hard clays they provide a higher holding capacity than in soft clays. On average, the larger the surface area of the anchor, the greater its holding capacity because both the anchor and the mobilized soil volume within the failure surface are bigger and heavier. They can generate a holding capacity of 100 to 150 times the anchor weight. The required holding capacity has to be 1.5 - 2 times the maximum load, and the installation load generally equals 80% to 100% of the maximum load, (Vryhof Anchors).

Drag embedment anchors can resist only if pulled horizontally. This means that, even when employed in taut-leg mooring configurations, they require the portion of the mooring line immediately ahead of them to be heavy enough to be seated on the seabed still when the line is under full tension (see Fig 2.19 and Fig. 2.10). This results in a lower FS for the anchor with respect to the mooring line because the anchor needs to drag before the line breaks, (Vryhof Anchors).

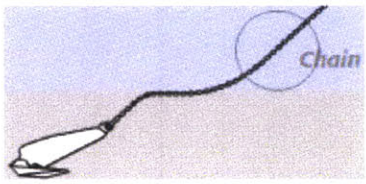

Figure 2.19: Particular of the anchor system in operation – the heavy chain sits on the seabed and pulls the anchor horizontally, (Vryhof Anchors).

Their final embedment can be predicted, but they need to be tested to verify their holding capacity. (Vryhof Anchors). Fig. 2.20 illustrates both a sketch and a real drag embedment anchor.

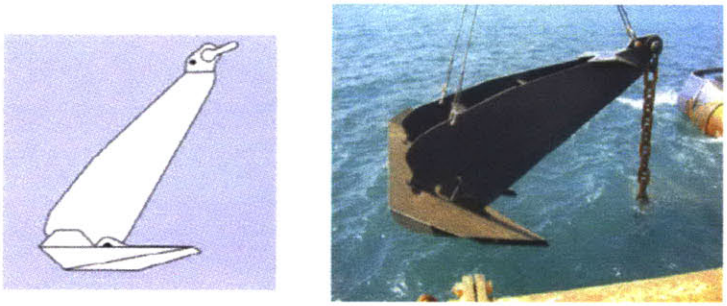

Figure 2.20: Drag Embedment Anchor – Stevpris, (Vryhof Anchors).

A particular category of drag anchors are ***Drag-in Plate Anchors***:

They can resist both vertical and horizontal loads and have a ratio of ultimate capacity to working load of 2.5 to 3.5. This anchor can penetrate deep in soft clay, and more superficially in granular soils. It is installed as a conventional fluke: by self-embedding in the seafloor and pulled horizontally, the holding force comes from the mobilized shear strength of the soil, (Vryhof Anchors).

They have some advantages like: efficient design, easy installation, low fabrication and transportation costs due to their small size. Unfortunately, their performance mostly depends on their penetration into the seabed, and consequently on the actual soil conditions. Although their final embedment depth can be predicted, they need to be proof-loaded to verify their holding capacity (Vryhof Anchors). Fig. 2.21 shows both a sketch and a real drag-in-plate anchor.

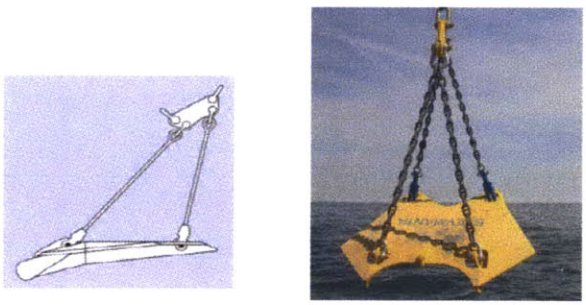

Figure 2.21: Drag-in-plate Anchor – Stevmanta, (Vryhof Anchors).

2.3.5 Suction Embedded Anchors (SEA)

The SEA consists of two half shells and, as displayed in Fig. 2.22, a SEA is installed using a suction pile follower, which pushes the anchor to the prescribed depth. The SEA is initially placed at the bottom of the suction pile with the two half shells closed that act as the extension of the pile tip. The pile begins penetrating into the seabed and, once it reaches the desired anchor depth, the suction pile is retrieved to the surface and the SEA anchor is left in place. As the suction pile is recovered, tension is applied to the SEA anchor in order to open its shells and let them form a strong anchor point for any kind of mooring from full catenary (horizontal) to tension leg (vertical). The capacity of the SEA anchor comes from the weight and shearing strength of the mobilized soil.

They combine several advantages such as: efficient design, easy and reliable installation, low fabrication and transportation costs due to their small size, high holding capacity that does not depend on the load inclination, and, moreover, they have a high holding capacity to weight ratio (from 50 to 100), (Riemers and Kirstein, 1999; Riemers, 1982).

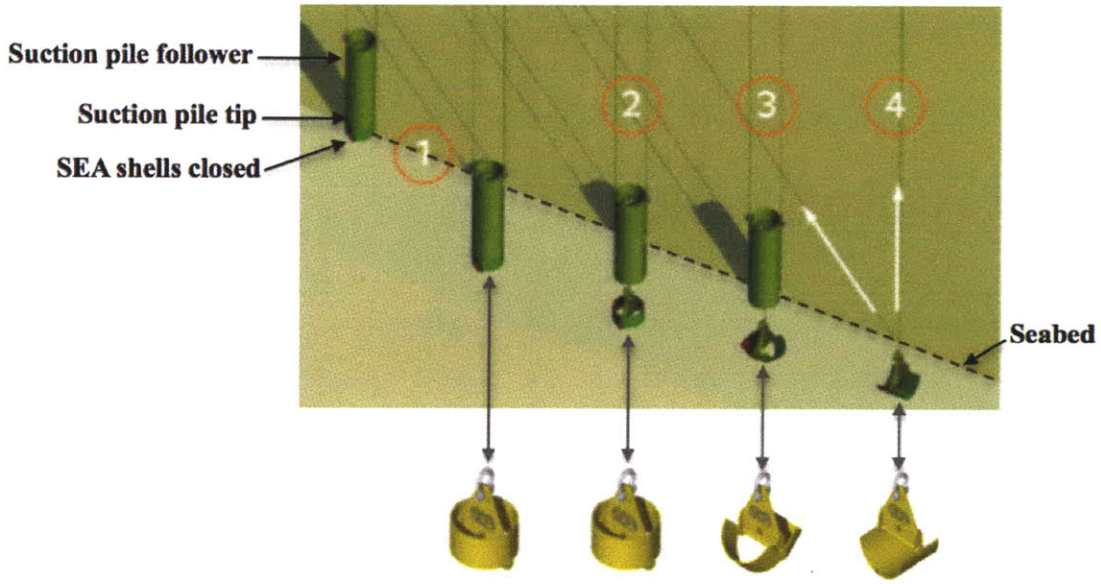

Figure 2.22: SEA opening sequence during installation: (1) the suction pile follower penetrates into the seabed with the SEA anchor placed at its tip with the two half shells closed; (2) the pile follower has reached the prescribed depth and has left the SEA anchor in place with its two half shells still closed; (3) retrieving the pile follower and applying tension, the SEA shells starts opening; (4) the SEA shells are completely open and the tension load can now eventually be applied in a direction other than vertical. Adapted from (SPT Offshore).

2.3.6 Jetting-in Driven Plate Anchors

The anchor consists of a steel plate welded to a steel beam section where the padeye for connection is located on top (see Fig. 2.23).

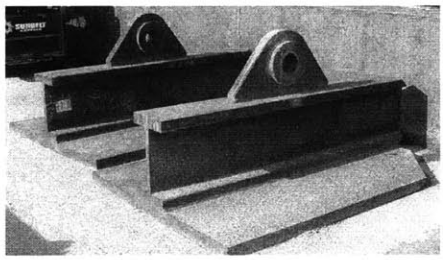

Figure 2.23: Jetting-in driven plate anchors, (Safaqah and Gerin, 2004).

The anchor is installed by driving it into the seafloor using a follower (usually a H-pile) until the maximum embedment depth is reached. Then, the follower is retrieved and the cable is tensioned in order to make rotate the anchor and find the configuration of highest pullout resistance (keyed depth); this sequence is illustrated in the following Fig. 2.24.

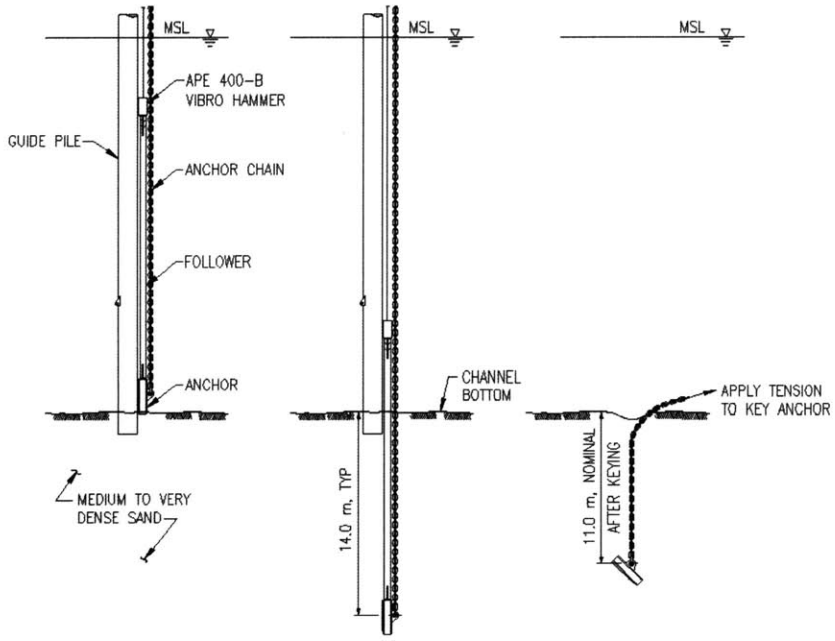

Figure 2.24: Jetting-in driven plate anchors: left – a pile follower is driven with the anchor connected sideways to it; middle – the pile follower reaches the desired depth, the anchor is released, and the pile is retrieved; right – the anchor is keyed by chain/cable tensioning to adjust it to the correct position, (Safaqah and Gerin, 2004).

The installation in dense soils may be facilitated by jetting water at the tip of the pile follower so forcing the soil to liquefy and impose less resistance to penetration. To

recover part of the soil strength lost during jetting, the retrieval of the follower occurs by vibrating it in order to densify back the surrounding material.

The anchor resists by mobilizing the shear strength of the soil, and its holding capacity depends on the failure mode; deeply embedded anchors have higher capacity than shallow anchors because the rupture surface either involves a greater soil volume or it develops after larger displacements of the anchor. The final capacity depends also on the anchor orientation, so it has to be tested, but, however, jetting-in driven anchors are an effective alternative whose main advantages are low cost, easy installation, and small size, (Safaqah and Gerin, 2004).

2.4 Anchor Behavior

Offshore anchors can be subjected to different kind of loadings. The design holding capacity at any water depth has to account for the static loads as well as the cyclic loads resulting from earthquakes, wind, waves, cable strumming, and loads coming from dynamic impacts during the installation process or operational life. Under these conditions it is important to predict and, then, try to measure the keyed anchor depth (see Fig. 2.25), a fundamental input parameter for the anchor holding capacity.

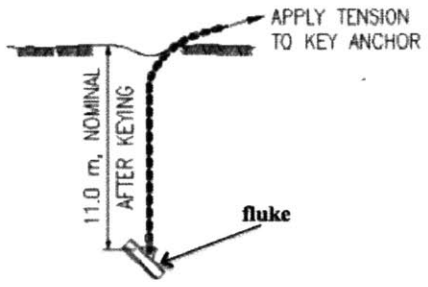

Figure 2.25: Anchor keying after penetration, (Safaqah and Gerin, 2004).

As Hermann (1981) describes, the basic loading condition is the so-called "short-term quasi-static" and other loading pattern computations usually refer to this. It is named "quasi-static" because it can be either a static load or load whose magnitude varies over

time within a minimum extent. In this context a valuable parameter is t_{CD} defined as the minimum amount of time the soil needs in order to dissipate the induced excess pore pressure; It is, essentially, a function of the soil permeability.

Consequently, if the load is applied at a rate slower than the pore pressure dissipation the soil will respond as drained, yet when the load is applied faster the pore pressure has not enough time to dissipate, but rather it builds up leading to an undrained response. In general, the short-term quasi-static loading condition corresponds to the drained condition for granular soils because the deposit permeability is sufficiently high to allow for a fully developed steady-state seepage pattern, whereas for cohesive low-permeable soils it corresponds to an undrained response.

On the other hand, a "long-term static-loading" implies that the consolidation is over, and the soil has reached the drained equilibrium.

Hence, for granular soils both conditions are equivalent because of the short time required for drainage, but the response of cohesive soils depends on how the loading time relates to t_{CD}.

2.4.1 Static Loading Conditions

The quasi-static holding capacity is defined as the load that causes the anchor to fail when such load is applied with a steady increase in magnitude within a certain time interval (usually shorter then 15 minutes). The actual working load is then computed considering a proper factor of safety, FS, (Hermann, 1981).

This holding capacity is representative for the vertical direction, but, in case the load acts at an angle to the vertical different than zero, an increase in FS is recommended. In a single-point mooring system (see Fig. 2.26) the loading direction may vary more than 90 degrees in azimuth, therefore one is expected to increase the FS by 100% to 250%, (Hermann, 1981).

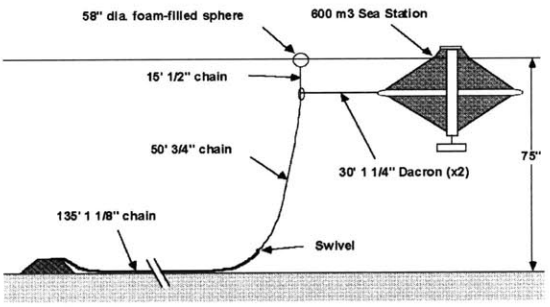

Figure 2.26: Single-point mooring system, (OAC, 2002).

As Balla (1961) and Baker and Konder (1965) observed, the embedment depth of the anchor influences its holding capacity. The first reason relates to the soil strength, which generally increases with depth leading to a larger capacity. Second, the deeper the anchor the larger is the shearing zone around it; hence, the holding capacity is proportional to the weight of the soil wedge above the anchor with slight differences in the failure wedge depending on whether it is an homogeneous or a layered soil as shown in Fig. 2.27 (Bouazza and Finlay, 1991).

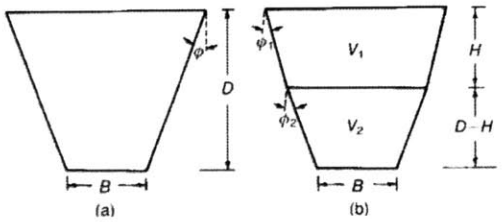

Figure 2.27: Failure wedges for (a) homogeneous soil and (b) two-layered system, (Bouazza and Finlay, 1991).

Moreover, the embedment depth may influence the anchor failure mechanism, which progresses toward the surface in case of shallow anchors or develops locally around it in case of high embedment (see Fig. 2.28).

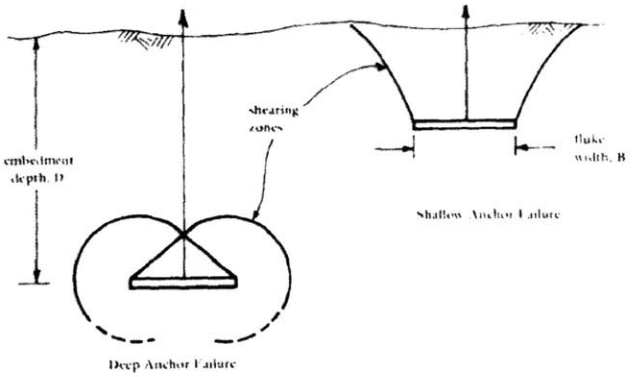

Figure 2.28: Behavior mechanisms for deep and shallow anchors, after (Beard, 1980) in (Hermann, 1981).

During the anchor penetration the fluke, or the pile skirt, penetrates into the soil down to the deepest point and, then, when tension is applied the soil experiences disturbance that may lead to a reduction of the system capacity; therefore, once installed, all anchors have to be tested. To prove its holding capacity, the anchor is loaded up to its working load either vertically or in the foreseen loading direction: a complete proof-load test requires tracking the anchor displacements under loading and to monitor also the anchor depth versus time (see Fig. 2.29).

Additionally, the keyed embedment depth can be measured in two different ways (Hermann, 1981):

- in shallow water, divers can read the penetration depth on a marked-cable extending out of the seafloor and connected to the anchor fluke;
- in deep water, a full-instrumented acoustic procedure has to be set up.

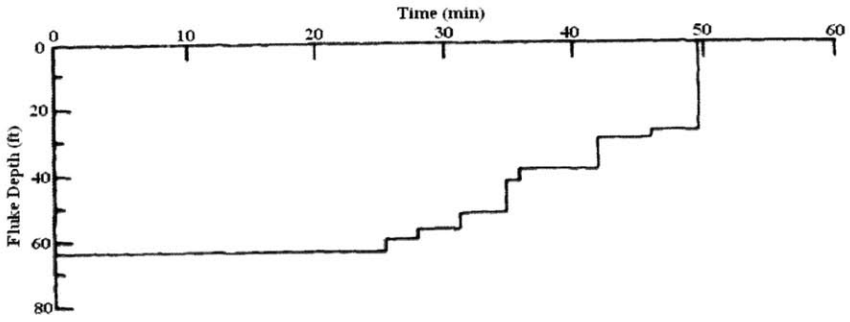

Figure 2.29: Data showing anchor keying with depth vs time during a slow load test up to failure, (Hermann, 1981).

Nowadays, the enormous advances in technology provide the possibility to monitor the mooring system in real time from installation to operation through wireless data transmission using sensors generally installed in the fluke of the anchor. Mooring location and field layout are only two of all parameters that can be tracked. Fig. 2.30 shows how this innovative technique allows one to record load and position during penetration till final embedment depth, and it gives justification of the design and proof loads, (Vryhof Anchors).

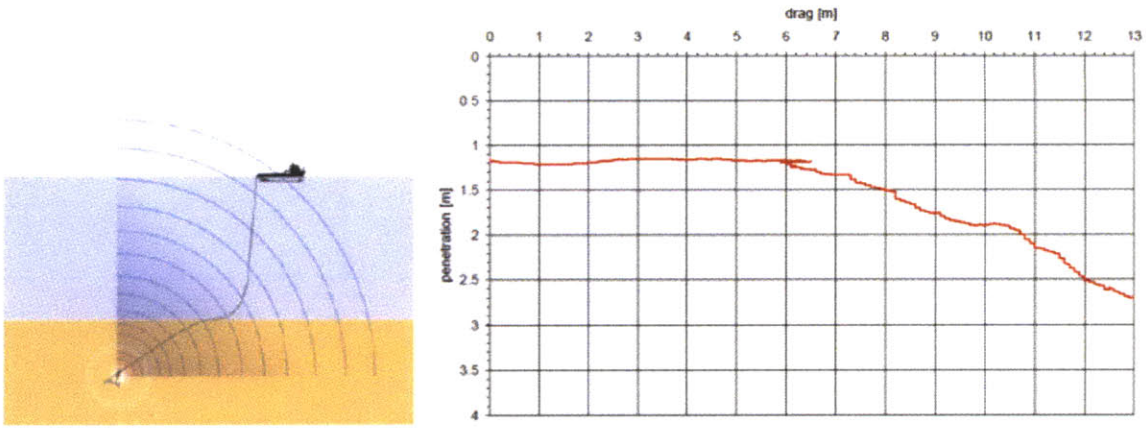

Figure 2.30: Wireless data transmission system during proof-load test plotting drag vs penetration, (Vryhof Anchors).

As with piles, if several identical anchors are to be installed in an area of uniform soil properties, only few (about 2% of all needed) should be tested and loaded up to failure for having evidence of their ultimate holding capacity. During the actual installation, each anchor will be proof-tested up to the working load in order to let it reach the keyed depth and provide it with the requested tension.

However, for a preliminary design, the anchor fluke penetration and its ultimate holding capacity can be empirically predicted using proper expressions: for instance, True (1975) developed an analytical model to calculate the keyed depth of NCEL propellant-embedded anchors, but his procedure can be applied to other anchors whose installation follow the same physical principles. Likewise, as discussed later in the thesis, Clemence and Veesaert (1977) and Ovesen (1981) proposed other expressions to compute the uplift capacity of plate circular anchors in granular soil basing their results on conventional or centrifugal model tests.

Rowe and Davis (1982) observed that plate anchors undergoing static loading have the failure load primarily influenced by the anchor orientation, embedment depth, surface roughness, and some fundamental soil strength parameters such as: friction angle (ϕ), angle of dilatancy (ψ), and state of stress (K_0). Fig. 2.31 shows how for a homogenous sand with $\phi=30°$ and $\psi=0°$ the failure zone depends not only on the embedment depth but also on the anchor orientation. In particular, loading an anchor results in elastic (white area) and plastic (dashed area) deformations of the soil. As illustrated in Fig. 2.31a, for

shallow anchors with vertical axis the soil in close contact with the anchor experiences elastic deformations, but plastic deformations also develop in a limited area toward the surface. In contrast, a horizontal axis anchor loaded to the same load P not only has a larger area of influence, but also induces simply plastic deformations in it. In addition, Fig. 2.31b is evidence for a large volume of soil that deep anchors mobilize. The vertical axis anchor always causes elastic and plastic deformations in the surrounding soil with the former contained within a certain distance from it, whereas the horizontal axis anchor produces a larger region of plastic deformation and two isolated regions of plastic deformations.

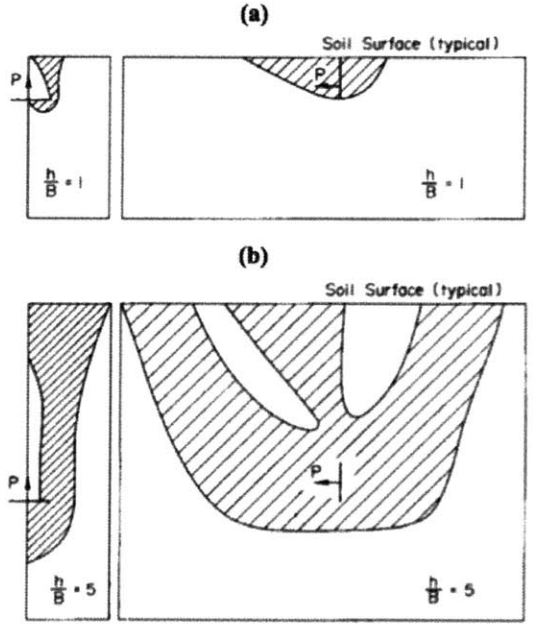

Figure 2.31: Plastic and elastic regions for horizontal axis and vertical axis plate smooth anchors in homogeneous soil with ϕ=30° and ψ=0°: a) shallow anchors, b) deep anchors, (Rowe and Davis, 1982).

The average ultimate resistance per unit length of a plate anchor with vertical axis can be expressed as:

$$p_u = \gamma_b D N_q \tag{2.4}$$

where γ_b=buoyant unit weight of soil, D=h=maximum embedment depth of the anchor, B=width of the anchor, N_q=bearing capacity factor.

N_q increases with the relative embedment depth λ=D/B (Balla, 1961) reaching a constant value at a certain depth (characteristic relative depth = $f(\phi)$ – see Fig. 2.32) where the failure mechanism changes from shallow to deep (McDonald's, 1963; Baker and Konder, 1965). Clemence and Veesaert (1977) noticed that "the movement occurred within a vertical column with no well defined failure surface".

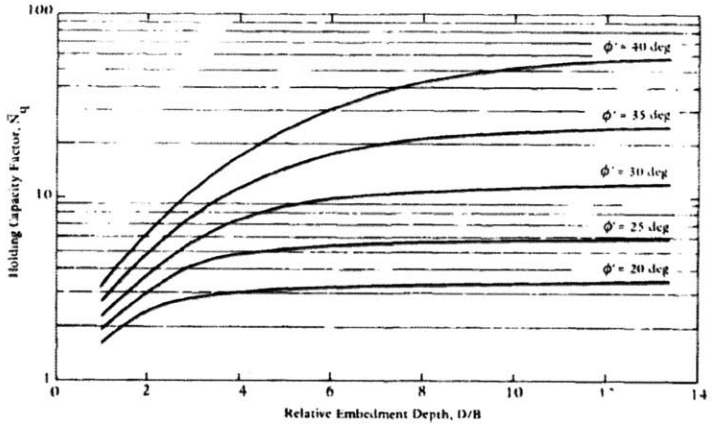

Figure 2.32: Holding capacity factor for cohesionless soil, from (Beard, 1980) in (Hermann, 1981).

In particular, Andreadis, Harvey, and Eldon (1981) performed static load tests in granular soil with anchors of different shapes, such as: cylindrical, circular, and conical anchors (see Fig. 2.33). They observed that for shallow depths (generally $\lambda \leq$5-6) the anchor uplift capacity increases more than proportionally with D^2, whereas for deep embedment ($\lambda \geq 6$) the relation tends to become linear, as shown in semi-logarithmic scale in Fig. 2.34. They also highlighted that this relationship is influenced by the soil relative density and the anchor installation method.

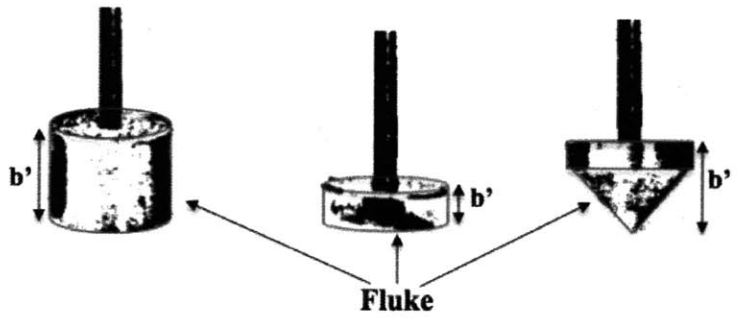

Figure 2.33: From left to right: cylindrical, circular, and conical anchor; b' is the fluke thickness. Adapted from (Andreadis et al., 1981).

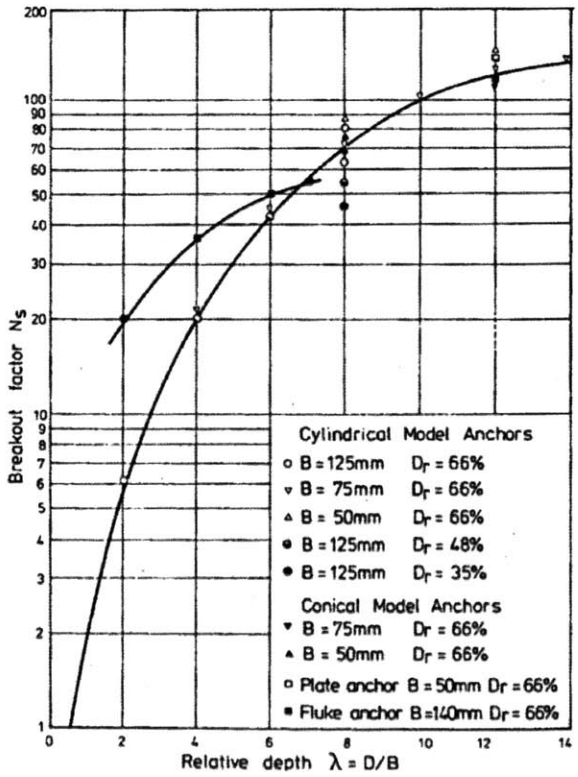

Figure 2.34: Bearing capacity factor-relative depth relationship, (Andreadis et al., 1981).

True (1975) stated that knowing the dimensions of a rectangular-shaped anchor, its quasi-static ultimate loading capacity can be estimated as follows (from True (1975) in Hermann (1981)):

$$F_T = N_q A \gamma_b D \left(0.84 + 0.16 \frac{B}{L}\right) \tag{2.5}$$

where A=bearing area of the fluke, B=width of the fluke, L=length of the fluke, as illustrated in Fig. 2.35. This expression is still valid for all other types of anchor that are provided with a fluke, whereas the capacity of driven piles and suction anchors is essentially determined through one of the methods used for deep foundation in computing the shaft capacity.

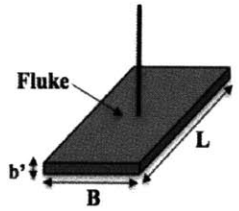

Figure 2.35: Rectangular-shaped plate anchor where b' is the fluke thickness.

As roughly reported above, the quasi-static working load of an anchor can be calculated dividing its ultimate holding capacity by a proper FS.

$$F_{all} = F_T / FS \tag{2.6}$$

The value of FS varies with the confidence in the loading conditions and soil properties, as well as the perceived seriousness of the possible anchor failure scenarios. Consequently, less confidence and more severe consequences result in a higher FS, vice versa high confidence implies a lower FS, (Hermann, 1981).

API standard API-RP2SK suggests the value of FS to use for permanent and temporary moorings both for intact and damaged conditions (see Tables 2.1 and 2.2).

Table 2.1: FS for permanent mooring (Vryhof Anchors).

Permanent mooring	Quasi-static load	Total dynamic load
Intact load condition	1.8	1.5
Damaged condition	1.2	1.0

Table 2.2: FS for temporary mooring (Vryhof Anchors).

Temporary mooring	Quasi-static load	Total dynamic load
Intact load condition	1.0	0.8
Damaged condition	Not required	Not required

The main task in evaluating the anchor capacity is the proper selection of N_q. It is a function of the soil strength parameters and the anchor roughness; therefore it can be approximated as (Rowe and Davis, 1982):

$$N_q = N'_q \cdot R_\psi \cdot R_R \cdot R_K \tag{2.7}$$

Where N'_q is the bearing capacity factor for the basic configuration of a smooth anchor in a soil with no dilatancy ($\psi=0°$) and state of stress represented by $K_0=1$, and R_ψ, R_R, R_K are useful factors to account for the influence of the aforementioned parameters: angle of dilatancy (ψ), roughness, and state of stress (K_0) respectively.

In the basic case of smooth anchors, Meyerhof & Adams (1968) and Vesic (1971) predicted that the capacity of vertical axis anchors increases linearly with the relative depth (see Fig 2.36a). However, Rowe and Davis, (1982) demonstrated that this trend is

no longer satisfied for $\lambda>8$ because deformations at failure appear to be too large to be correctly captured by an elastic analysis. Horizontal axis anchors do not abide by the same linear relationship; in fact, their holding capacity has a much higher increase with the friction angle especially when the embedment ratio λ is greater than 8 (see Fig 2.36b).

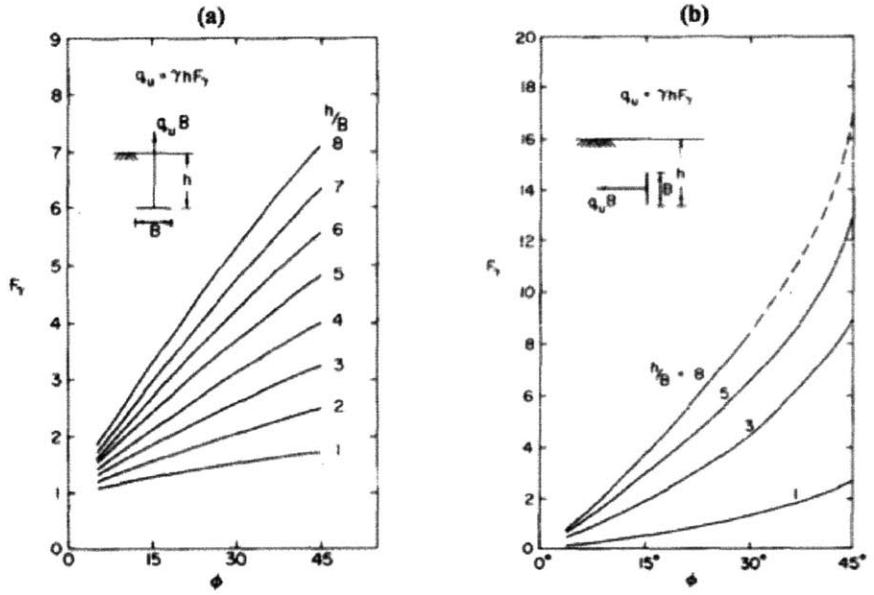

Figure 2.36: Variation of the basic bearing capacity factor F_γ for vertical-axis anchor (a), for horizontal-axis anchor (b), (Rowe and Davis, 1982).

Except for loose material, granular soils tend to dilate during plastic deformations leading to an extensive plastic region before failure occurs. The eventual rise of capacity due to dilatancy can be accounted for by introducing the correction factor R_ψ, which is related almost linearly with ψ for a given friction angle. For both vertical and horizontal axis anchors, when the angle of dilatancy equals the friction angle ($\psi=\phi$) the failure load is independent of the loading path and stress state, whereas for a material with ϕ and ψ not associated ($\psi\neq\phi$) the collapse load varies with K_0 : for $K_0>1$, p_u is higher than the basic case because the horizontal stresses that govern the shearing resistance along a vertical sliding surface are higher than they are for $K_0=1$, whereas for $K_0<1$ the horizontal stresses are lower leading to p_u lower than the basic case.

In regard to the initial stress ratio K_0, it barely influences the ultimate load of a plate anchor with any orientation. Therefore, the effect of the initial K_0 can be neglected to an accuracy of better than 10%; in particular, its effect gets more and more negligible when

ψ increases and dictates the anchor response. Hence, the introduced correction factor RK is essentially assumed to be unity.

As a consequence, Fig. 2.37 shows that high relative density causes the failure mode to be in local shear (higher N_q) governed by the friction angle, whereas with low relative density the rapture surface cannot propagate throughout zone of influence resulting in punching shear mode (lower N_q), (Bemben and Kupferman, 1975).

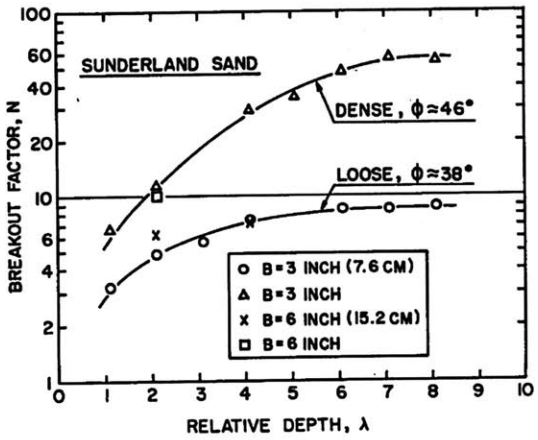

Figure 2.37: Bearing capacity factor-relative depth relationship, (Bemben and Kupferman, 1975).

Finally, R_R accounts for the surface roughness of the anchor, which does not have any influence on the collapse load of vertical axis anchor, but, as Fig. 2.38 illustrates, it has a significant effect for very shallow anchors with horizontal axis.

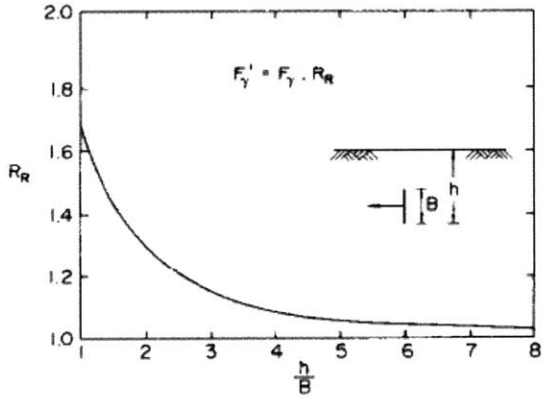

Figure 2.38: Correction factor for effect of roughness on horizontal axis plate anchor, (Rowe and Davis, 1982).

The last factor that affects the static capacity of a vertical axis anchor is the thickness (b') of its resistant element at the base, the fluke (see Fig. 2.33 and 2.35). When the anchor is

being pulled upward, part of the soil standing above the fluke tends to displace out and fill partially the created void beneath the anchor. As Fig. 2.39 illustrates, with a thicker fluke a lower amount of soil around its edges would move, so the anchor uplift resistance increases.

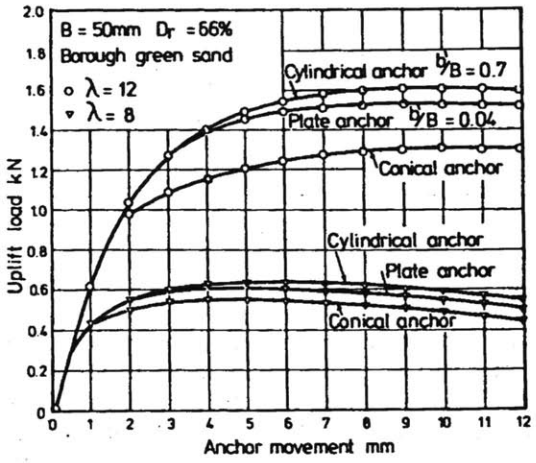

Figure 2.39: Static load test – Uplift load-anchor movement relationship for different anchor size and relative depth, (Andreadis et al., 1981).

In conclusion, there is evidence that the magnitude of stresses around the anchor is affected by both anchor size and relative depth. The value of the horizontal stress rises getting closer to the anchor where the horizontal stress reaches its peak value; particularly, for a deep anchor in sand, the magnitude of the horizontal stress maintains a significant value within an area of more than 10 diameters around the anchor (see Fig. 2.40).

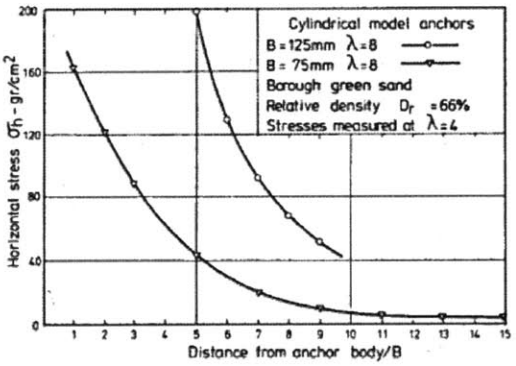

Figure 2.40: Static load test – horizontal stress vs relative distance from anchor body, (Andreadis et al., 1981).

2.4.2 Dynamic Loading Conditions

Dynamic loads differ from static loads because they are applied quickly (t<1min), and often in a cyclic pattern. The foundation response to dynamic loading is controlled by the soil shear modulus (G) and damping (D); the shear modulus is non-linear, and it decreases with the soil strain level.

The resulting conditions are the most crucial for embedded anchors because they cause the fluke or the pile skirt to be pulled out with direct decrease of embedment depth and capacity. Dynamic loads are essentially of two types: impact loads (single events), and cyclic loads, which encompass earthquake-loading conditions as a special case, (Hermann, 1981).

The following Fig. 2.39 illustrates impact and cyclic dynamic loads with respect to the ultimate static load (F_T) and static working load (F_{all}). The latter is simply defined by Eq. (2.6) where FS=2.5 for the illustrated example. Definition of each type of load is given in the following paragraphs.

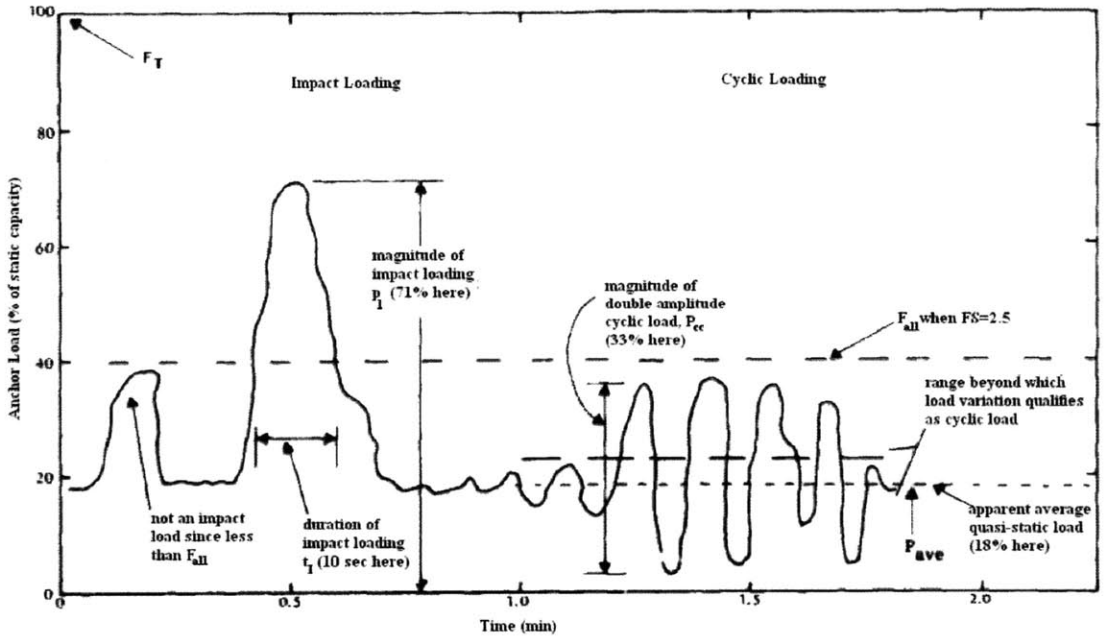

Figure 2.41: Example of dynamic time-load history, illustrating definitions and parameters, (Hermann, 1981).

2.4.2.1 *Impact Loads*

Impact loads as single events may derive from a ship crashing into a mooring line or trying to break it at departure, from installation procedures and operations, and from possible explosions. Impact loads are labeled with their maximum magnitude P_I (as a percentage of the anchor's static capacity) and with the duration t_I of the interval in which the load is above the static working load. Looking at the left side of Fig. 2.41, one can appreciate that for a load to qualify as impact load must have peak magnitude equal or superior to the static working load. Particular consideration has to be devoted to those impact loads whose magnitude is greater than the expected anchor working load, and whose duration is shorter than 1 minute. Furthermore, impact loads do not repeat more than 5 times in the period necessary to dissipate the induced excess pore pressure, otherwise the loading condition would be termed cyclic loading.

In general, for those anchors provided with a fluke, it is observed that they have higher holding capacity when subjected to dynamic impact loads even with magnitudes greater than the allowable static load, and their capacity increases as the duration of the impact diminishes. One explanation to this effect is that the dynamic load causes further lateral penetration of the anchor.

Moreover, snap loads cause negative pore pressure to rapidly develop under the anchor plate contributing to a higher 'undrained' resistance, and then slowly dissipate. Nevertheless, repetitive impacts in a short period may result in a reduction of the soil strength with consequent drop of the anchor capacity and possible liquefaction for cohesionless soils in loose state. In fact, the 'undrained' resistance due to snap loads decreases with lower relative density to the point that loose sands will develop only positive pore pressure undergoing a decline in strength, (Hermann, 1981).

Design for Dynamic/Impact Loading

Hermann (1981) describes that the design of an anchor undergoing dynamic/impact loads can be conducted by using the same approach of a quasi-static loading but introducing new parameters that account for different soil response.

The design is mainly led by the time of occurrence of the impact load; it can occur as a first event or after a series of cyclic loads, and it may happen as a single event or actually may repeat over time and in a period shorter than t_{CD}. All these scenarios relate to the load history of the anchor, and they have effect on the soil properties as well.

Furthermore, the anchor-soil mass system can develop an extra capacity due to its inertia if the impact loading condition lasts less than 0.02 seconds. In this case the increase in capacity is evaluated by an inertial factor; this factor is function of the load duration, the size and the type of anchor. In particular, the shorter the load duration, the higher the inertial factor because higher is the temporary anchor resistance to static capacity ratio. In addition, this new introduced factor already provide for a conservative result, therefore recommendations suggest not using any other FS.

2.4.2.2 *Cyclic Loads*

Cyclic loads generally derive from three major sources:

- oscillation of catenary whose motion is determined by the local current. This loading condition stresses the anchor with high frequencies and low magnitude load resulting in negligible loads for the anchor itself, but representing important scenarios for the fatigue of cable, and mechanical components of the system above it;
- forces coming from buoys or floating ship/platform that once attached to the catenary induce loads at the frequencies of surface waves. Typically, in the range of 0.05 to 0.15 Hz. The surface-wave-induced forces are responsible for a significant loading on the anchor;
- earthquake-induced forces that load the entire soil mass with shear stresses instead of acting on the anchor system.

With reference to the right side of Fig. 2.41, a cyclic load has double amplitude whose magnitude is named P_{cc} and the magnitude of each amplitude must be greater than 5% of

the quasi-static anchor capacity with respect to the apparent average quasi-static load (P_{ave}). In addition, two parameters are necessary and they are the following:

- N_T = total number of cycles during the entire life of anchor. It is useful for estimating the potential cyclic creep;
- N_D = the number of cycles within t_{CD} (defined in 2.4). These cycles are likely to lead to strength loss or liquefaction failure of the soil mass, whereas cycles occurring outside this time frame are negligible.

If during the life period of an anchor many periods of cyclic loading occur and they have almost constant magnitude, the first period will be chosen for the analysis. In contrast, if the magnitude of load increases over time, both earlier periods of smaller magnitude and later periods of higher magnitude should be analyzed to find out which is the most critical, (Hermann, 1981).

Design for Cyclic/Repeated Loading

Possible scenarios are: the anchor undergoes cyclic-loading leading to soil strength loss or liquefaction instability; an earthquake hits the area subjecting the anchor-soil system to cyclic loading and soil strength loss with possible reduction of the holding capacity in all conditions.

Given the nature of soil, particular attention must be paid to loading conditions and possible consequences. During cyclic loading by an earthquake, storm waves and/or wind, loose and fine-grained granular soils are more likely to liquefy and the anchor might fail. The phenomenon occurs because under cyclic loading the soil tends to densify with reduction of the void ratio; still, the duration of each cycle is too short to allow for the induced excess pore pressure to dissipate even though the soil permeability is reasonably high. Hence, the pore pressure buildup over time leads to a significant reduction of the effective stresses until the pore pressure equals the total vertical stress and the absence of effective stresses causes the soil liquefaction. Therefore, the higher the relative density or the permeability of the granular deposit, the lower the chance it could undergo liquefaction because failure occurs if the pore pressure buildup is greater than

dissipation within each load cycle. Once triggered, liquefaction takes much less energy to be re-activated if it is not fully dissipated.

The cyclic loading pattern can be described by both the total number of cycles (see example given in Table 2.3) and the spectral distribution of load magnitude (see Fig. 2.42) as a function of the number of cycles. However, in both cases t_{CD} has to be preliminarily determined from the knowledge of the soil, (Hermann, (1981)).

Table 2.3: Example of critical wave loading analysis, (Hermann, 1981).

Wave Height, H_i (ft)	Number of Waves, N_i	Cumulative Number of Waves	Resulting Cyclic Anchor Load, P_{ui} (% of static capacity)	Analysis for Equivalent Uniform Wave Loading*			
				Load Categories, P_{ui}	Number of Cycles, N_i	N_{if}	ΔN_{eq}
0-5	355	5,000	2	Since these loads are less than 50% of maximum cyclic load, these two-thirds of load cycles can be ignored.			
5-10	525	4,645	5				
10-15	655	4,120	8				
15-20	717	3,465	11				
20-25	725	2,748	13				
25-30	675	2,023	16				
30-35	550	1,348	19	21	930	300,000	6
35-40	380	798	22				
40-45	205	418	25	27	315	25,000	25
45-50	110	213	28				
50-55	60	103	31	33	85	2,000	85
55-60	25	43	34				
60-65	10	18	36	38	15	500	60
65-70	5	8	39				
70-75	2	3	42	44	3	200	30
75-80	1	1	45				
Total	5,000					N'_{eq}	= 206

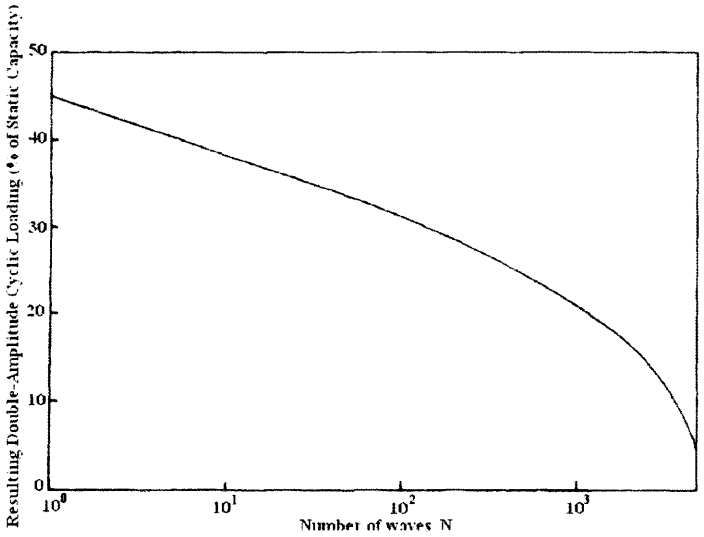

Figure 2.42: Load magnitude as a function of the number of cycles, (Hermann, 1981).

Any type of anchor subjected to cyclic loading will continuously displace upwards, but if the load is kept under a critical value the rate of displacement will decrease over time. For shallow anchors, as the anchor displaces it encounters lower resistance by the weight of the soil wedge upon it, so its rate of movement will increase. On the other hand, deep anchors are sufficiently far from the surface such that the system gets more and more stable unless the load exceeds a critical value and leads the system to failure; in particular, a well-installed anchor, that undergoes cyclic loading with magnitude lower than the initial static capacity, can even experience an increase in capacity (see Fig. 2.43).

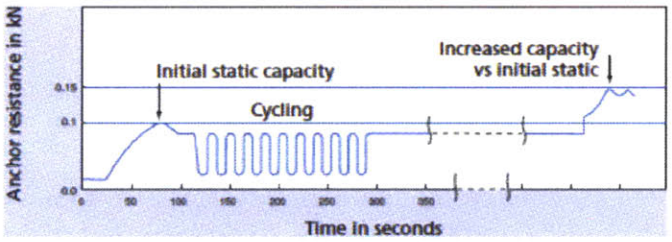

Figure 2.43: Initial and final capacity comparison with the occurrence of cyclic load, (Vryhof Anchors).

When an anchor is subjected to cyclic loading applied in a sinusoidal fashion between zero and a specific peak load P_{cc}, the anchor displacement rate initially slows down and then increases approaching the failure once a critical strain level is reached. A family of hyperbolic curves, shown in Fig. 2.44, can represent the behavior of an anchor system undergoing cyclic loading; varying the number of cycles and the peak magnitude of cyclic load (Q_c) to ultimate anchor capacity (Q_{ult}) ratio, the displacement rate and its value (expressed in fractions of the relative depth λ) change accordingly. If the peak magnitude of load is constant and the number of loading cycles increases, the curves get closer meaning that the displacement rate gets faster: this occurs rapidly when Q_c/Q_{ult} is lower than 30%, but it occurs at a higher number of cycles than for higher values of Q_c/Q_{ult}. Similarly, if the number of cycles is constant and the peak magnitude of load increases, the displacement rate gets faster: in this case, however, the higher the number of cycles, the quicker the displacement increases. Conclusively, a different family of curves can be obtained with respect to the relative depth, the relative density, the anchor size and shape, the installation procedures and the cyclic loading combination.

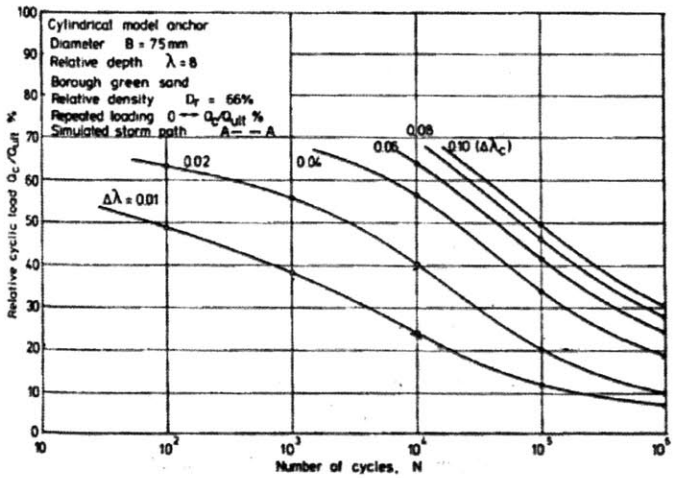

Figure 2.44: Life of anchor for different relative movement limits as function of cyclic load amplitude, adapted from (Andreadis et al., 1981).

Anchors experiencing a total strain lower then the critical value show negligible decline in uplift capacity with respect to their static resistance. In addition, if the anchor system is subjected to a cyclic loading with varying peak load between cycles the resulting capacity reduction results from the cumulative displacements, and during loading the area of the hysteresis loop decreases. Nevertheless, Fig. 2.45 illustrates that the hysteresis loop get smaller during the application of the cyclic loading and their shape stabilizes after only thousands of cycles. However, if the cumulative displacement adds up to the critical value, then the current hysteresis loop will get bigger until the anchor fails and is pulled out of the soil.

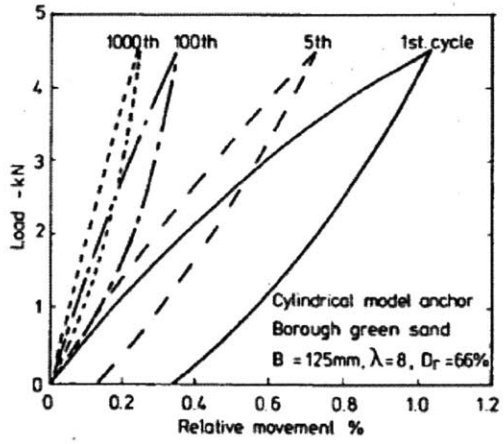

Figure 2.45: Repeated load tests - typical hysteresis loops, (Andreadis et al., 1981).

The relative depth as well as the size of the anchor mainly determines the value of the critical strain before collapse. In fact, the deeper the embedment the larger must be the relative movement of the anchor at each loading cycle to get closer to the surface and start failing. Conversely, the greater the size the greater the initial elastic displacement of the anchor that determines a higher flow of material around its edges towards the cavity below it, and therefore this results in a faster strength reduction.

Nevertheless, as better explained later on in the paper, Clemence and Veesaert (1977) observed how under particular conditions the anchor experiences an increase in the peak capacity before reaching failure (see Fig. 2.46) mainly supported by the inertial force of the soil mass above it, which counteracts the upward movement, and by the enhanced soil strength through dynamic densification.

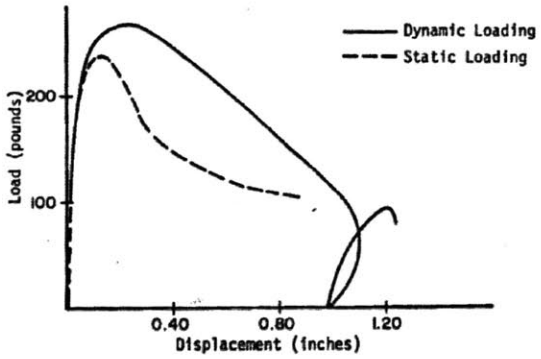

Figure 2.46: Increase in holding capacity of the anchor due to dynamic loading, (Clemence and Veesaert, 1977).

As the cyclic loading is applied, the stresses in the soil follow the same pattern in magnitude and frequencies: they oscillate. It is important to notice that after the initial application of the load during the cyclic loading the horizontal stresses maintain high magnitude within a limited area around the anchor and vertical stresses are lower than the corresponding vertical ones during static loading. In particular, the following Fig. 2.47 shows the distribution of horizontal stresses around the anchor body when it is loaded up to 40% of its ultimate holding capacity either for static or cyclic loading.

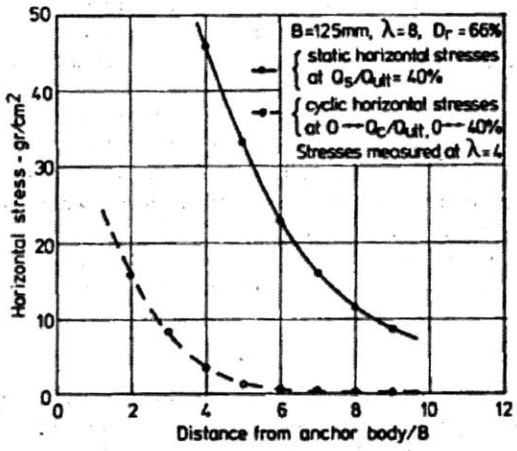

Figure 2.47: Comparison static – cyclic horizontal stresses distribution, (Andreadis et al., 1981).

If a soil-anchor system undergoes a cyclic loading without reaching failure, and then is statically loaded, it will have an increased stiffness compared to that the system would have had if subjected to the sole static load. This improvement derives from the densification of material and it is proved by the progressive reduction in area of the hysteresis loop. For very deep anchors, the enhancement in stiffness after each cyclic movement is lower because larger displacement is required for the system to collapse.

In general, the criteria used for a preliminary design under cyclic loading conditions involve several conservative assumptions so that lower values of FS are legitimate for computing the respective working load.

2.4.2.3 *Cyclic Creep during Loading*

Cyclic creep can be easily appreciated subjecting one anchor to a continuous sinusoidal loading pattern with maximum and minimum magnitude kept constant. As the anchor move upward the portion of soil above its base compresses, and the soil grains are displaced down around the edges. Thus, the anchor tends to move back downward during the unloading portion of each cycle, but the previously displaced matter prevents it from causing cyclic creep. Most importantly, the holding capacity declines, and, with a constant peak magnitude, the cyclic creep rate may even increase over time, (Bemben, Kalajian, and Kupferman, 1973).

2.4.2.4 *Earthquake Loading*

In an area of high seismicity, wherein anchors are supposed to be installed within 100 miles of possible epicenters, the effects of an earthquake should be considered in design.

Earthquakes are source of strong cyclic loads acting directly into the soil mass and subjecting it to shear stresses; these stresses derive from the shear waves that travel out of the epicenter through the soil. The resulting cyclic loads feature a frequency of about 2 Hz, and a number of cycles that ranges from 10 to 30 depending on the quake magnitude. The soil will be subjected to a maximum acceleration, which depends on the distance from the epicenter and the magnitude itself, as shown in Fig. 2.48.

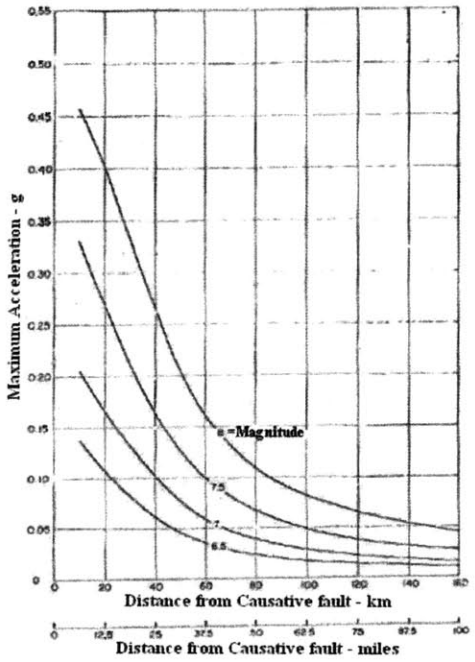

Figure 2.48: Variation of maximum acceleration associated with earthquakes of various magnitudes and different distance from causative fault, (Seed et al., 1969).

Design for Earthquake Loading

In case an earthquake occurs, large shear stresses act within the embedment depth of the anchor and they may reduce the anchor capacity under all types of loads. This scenario is likely to happen for certain categories of soils such as granular soils whose composition indicates clean or relatively clean sand, coarse and uniform silt, with a small percentage

of fines. Nonetheless, a granular soil is less susceptible to experience strength loss if it has high relative density, and it is part of a deep deposit.

Therefore, a liquefaction analysis should be done for the soil zone within the anchor embedment depth up to the mudline. If the site results at risk of liquefaction, the anchor may fail when loaded during the earthquake or after it within a time of 0.2 t_{CD}, whose value can be in the order of minutes for such soils.

A reliable way to evaluate the holding capacity of an anchor and verify its stability under earthquake cyclic conditions is to implement the same approach used for cyclic loading, which considers various factors in order to account for different characteristics of the loading condition with respect to the static one.

2.4.2.5 *Effect of Load History*

The holding capacity of an anchor is a function of the soil properties and particularly of the effective stresses acting among grains. It means that any increase of induced excess pore pressure implies a decrease in capacity as well as its dissipation over time leads to a denser and stronger soil.

This explains why, for those anchors provided with a fluke, it is recommended to start the operation of cable-anchor tensioning after a time of t_{CD} from the end of maximum penetration. In fact, once the drained equilibrium is reached for $t > t_{CD}$, the soil has higher strength than it did during consolidation, so the anchor can be keyed in a shorter distance resulting in larger embedment depth and greater holding capacity.

In summary, to determine the most critical periods of service of the soil-anchor system, either cyclic or impact loading are to be examined, but in a different time frame. Indeed, impact loads have the nature of single events whose damaging effects, if any, can be seen within a period of 0.5 t_{CD}, whilst for cyclic loads the entire period t_{CD} has to be considered.

3 Modelling 1 – Conventional Modelling

In this chapter the static and dynamic capacity of circular anchors in granular soils is investigated through the theory elaborated by Clemence and Veesaert in 1977. The objective is to understand how all the parameters are interrelated. Firstly, a description of their experiences and results is provided. Secondly, using the relationships they proposed, we examine how the variation of the variables affects the anchor capacity at the model scale.

3.1 Static and Dynamic Vertical Uplift Capacity of Circular Anchors

In 1977, S.P. Clemence and C.J. Veesaert investigated on the behavior of embedment anchors in sand under static and dynamic loading. Their research was conducted through a series of laboratory tests, which respected some hypotheses. They are as follows:

- the soil is uniformly graded air dried river sand placed at uniform relative density;
- soil has a Mohr-Coulomb failure criterion;
- the container is a rigid steel box measuring 24"(61 cm) x 24"(61 cm) x 27"(68.5 cm);
- tests are performed with full and half circular anchors (see Fig. 3.1); and,
- the objects of the tests are two flat circular anchors with 3"(5.67 cm) and 5"(12.7 cm) diameter, and equal thickness of 0.125" (32 mm);

Figure 3.1: Typical geometry of a full (left) and half (right) circular anchor.

Moreover, the selected sand had Uniformity Coefficient $C_u=D_{60}/D_{10}=1.39$ and dry density ranging between 14 kN/m^3 and 17 kN/m^3. It was placed in the container at a relative density of 96% for all of the tests.

As shown in Fig. 3.2, the static load was applied by using a turnbuckle and a steel cable at a deflection rate of 0.25" (6.3 mm) per minute. They were associated with a load cell, which measured the actual load transferred to the anchor.

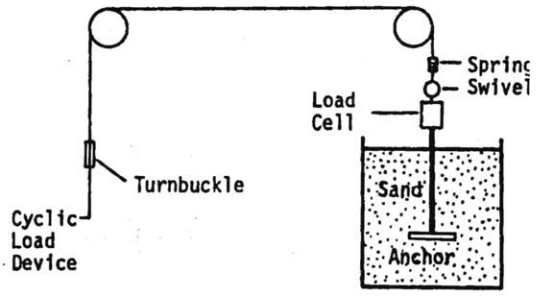

Figure 3.2: Loading system, (Clemence and Veesaert, 1977).

In addition, the dynamic loading was reproduced employing a piston, which simulated linear movements with 1.25" (3.2 cm) displacement amplitude, 3 Hz frequency, and 0.2g acceleration. In particular, to reproduce a real field condition, the dynamic load was applied once the anchor was prestressed to 50% of its ultimate static capacity.

To compare dynamic and static resistance, a series of tests was performed considering multiple values of relative depth (H/B), where H is the embedment depth and B the anchor diameter. The relative depth was chosen equal to 3, 4, 5, 6, 7 for the smaller anchor, and equal to 1, 2, 3 for the bigger one.

Movie filming of the failure movements allowed researchers to define the shape of the rupture surface. This appeared to develop upward from the anchor edges until it reached the surface. Indeed, as illustrated in Fig. 3.3a, C&V (1977) approximated the rupture surface by a truncated cone whose apex angle equals the soil friction angle ϕ. Most importantly, they observed that the failure surface for static and dynamic loading didn't show significant differences (see Fig. 3.3b).

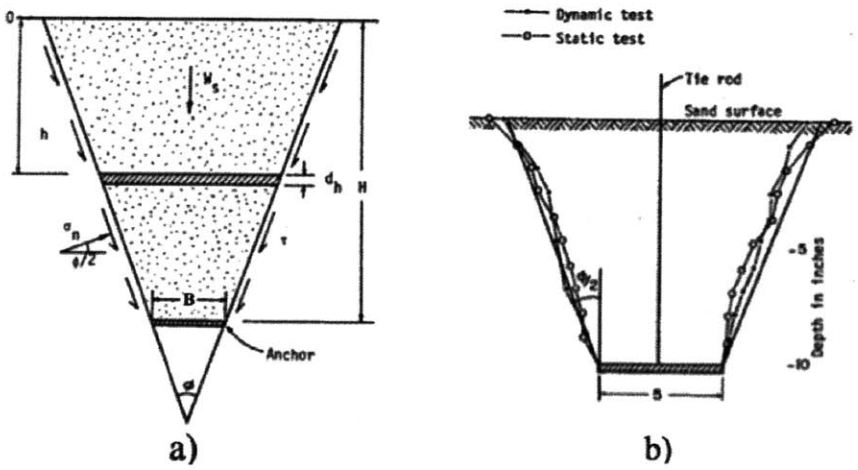

Figure 3.3: a) Rupture surface approximated by a truncated cone; b) Comparison between typical failure surfaces for shallow anchors in static and dynamic lab tests, (Clemence and Veesaert, 1977).

Nevertheless, an interesting finding evolved. As already predicted by other researchers (Balla, 1961 - Baker and Konder, 1965), C&V (1977) noticed that for high relative depth (H/B) the rupture surface didn't follow the same pattern any more. It developed upward with the standard shape for a distance of 2-3 diameters and then "the movement occurred within a vertical column with no well defined failure surface", as shown in Fig. 3.4.

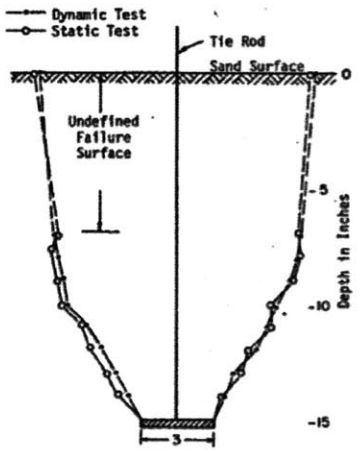

Figure 3.4: Comparison between typical failure surfaces for deep anchor under static and dynamic lab tests, (Clemence and Veesaert, 1977).

They based their theory on the observation of the shape of the failure surface, so they postulated two equations to calculate the uplift resistance of circular anchors under static and dynamic loading.

The static resistance is obtained as the sum of the weight of the soil within the failure surface and the friction that develops along the failure surface itself. Assuming that the normal stress acting along the surface varies linearly with depth, the anchor static resistance can be expressed by:

$$Q_s = \gamma_t V_s + \gamma K_0 \tan(\phi)\cos^2\left(\frac{\phi}{2}\right)\pi\left[\frac{BH^2}{2} + \frac{H^3\tan(\phi/2)}{3}\right] \tag{3.1}$$

In comparison to the static resistance, the dynamic capacity was higher. Researchers attributed this result to two factors:

- the inertial force of the soil mass within the failure surface; and,
- the increase of the shearing resistance along the surface itself due to the enhanced strain rate.

For these reasons, C&V (1977) modified the previous equation and proposed the following expression to compute the dynamic resistance:

$$Q_s = \gamma_t V_s + \gamma K_0 \tan(\phi)\cos^2\left(\frac{\phi}{2}\right)\pi\left[\frac{BH^2}{H} + \frac{H^3\tan(\phi/2)}{3}\right]D_f + V_s\gamma_t a \tag{3.2}$$

In Eqs. (3.1) and (3.2), the parameters represent the following:

Soil Properties

γ_t = total unit weight of soil with S=0%
c = cohesion of the soil
ϕ = friction angle of the soil
ψ = soil dilatancy
K_0 = coefficient of earth pressure at rest

Anchor Properties

B = fluke diameter
R = fluke radius
A = fluke projected area for pullout

Anchor embedment

H = embedment depth of the fluke

H/B = relative depth

Static capacity

B_m = diameter of the larger base of the truncated cone

R_m = radius of the larger base of the truncated cone

V_s = volume of sand within truncated cone failure surface

Q_s = ultimate anchor static capacity

Dynamic capacity

D_f = dynamic strain rate factor

a = acceleration of anchor in units of g

Q_d = ultimate anchor dynamic capacity

Lab tests were performed under specific conditions with different values of the mentioned parameters, specifically:

Table 3.1: Variables' values used for lab tests, (Clemence and Veesaert, 1977).

γ_t =	c =	ϕ =	ψ =	K_0 =	B =	H/B =	D_f =	a =
kN/m^3	kPa	deg	deg	-	cm	-	-	g
17	0	39	0	0.5	5.67	3 to 7	1.1	0.2
17	0	39	0	0.5	12.7	1 to 3	1.1	0.2

For the present analysis, the red line plots the dynamic holding capacity, while the blue line plots the static one. As mentioned, very few tests were performed on the two anchors, and their trends are plotted in Fig. 3.5 with a solid line. However, to compare these lab results with the future theoretical estimates, these lab trends have been extended, with the use of Eqs. (3.1) and (3.2), by increasing the relative depth and keeping unchanged all other variables; the resulting extensions (Qsi, Qdi) have been

denoted by dashed lines. Figure 3.5 shows how keeping B=12.7 cm (B2) both Q_s and Q_d are consistently higher than those for B=5.67 cm (B1).

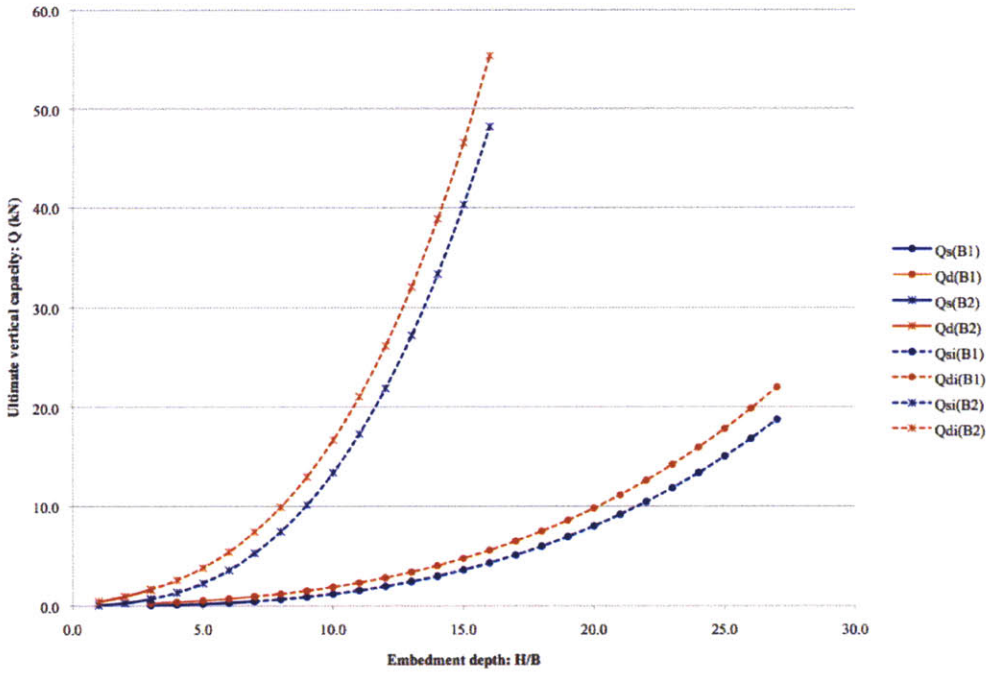

Figure 3.5: Q_s and Q_d curves for actual lab tests, and extension of their trends with variation of H/B.

3.2 Variable Sensitivity

The purpose of this study is to analyze how the variation of variables in Table 1 affects the anchor resistance both under static and dynamic loading. Since Eqs. (3.1) and (3.2) are derived from the mentioned lab tests, multiple computations are performed changing the variables' values, but within a limited range; this provision is necessary in order to use the equations correctly and simulate plausible lab results. In addition, modifications occur taking into account two variables at a time, but one of them is always the relative depth that is used as a basis for comparison.

The proposed variations are indicated in Table 3.2.

Table 3.2: Variables' values used for comparative study.

Variation	γ_t =	c =	ϕ =	ψ =	K_0 =	B =	H/B =	D_f =	a =
-	kN/m	kPa	deg	deg	-	cm	-	-	g
from	17.0	0	39.0	0	0.3	5.67	1	1.1	0.20
to	19.6	0	41.6	0	0.95	18.7	27	3.7	0.46

The analysis results can be plotted and discussed for highlighting some important points.

In the following plots, the light red line and the light blue line plot the theoretical estimates obtained by the use of equation (3.1) and (3.2). In Figure 3.6 the two new curves – $Q_s(B)$ and $Q_d(B)$ – are representative of the increase in Q_s and Q_d with increase in anchor diameter. They start from the bottom curves for B=5.67 cm and move exponentially upward until they intersect the upper curves at B=12.7 cm; further increase in diameter would let Q_s and Q_d increase even faster.

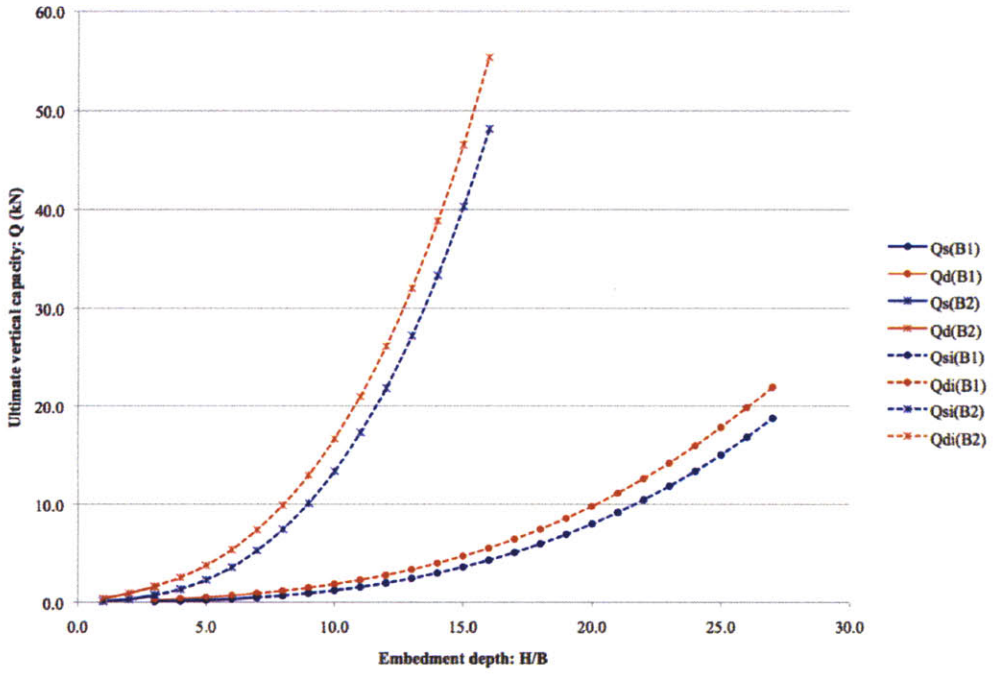

Figure 3.6: Theoretical curves for Q_s and Q_d as functions of the change in B plot with the basic case curves

At first glance, one can appreciate how all trends vary exponentially; still, more important is how the anchor capacity strongly goes up with increase of the anchor diameter. In fact, the diameter governs the anchor capacity because it directly affects the

size of the truncated cone that identifies the rupture surface. Therefore, the bigger the anchor, the heavier the soil plug within the failure surface and the greater the friction that develops along the failure surface itself. In particular, the capacity-diameter relationship is mathematically justified because the volume of the truncated cone shaped surface is a function of R^2 and R_m^2, where R and R_m are respectively the radius of the anchor and the base radius of the cone at the surface.

Fig. 3.7 shows the Q_s and Q_d curves as function of the change in K_0, or ϕ, or γ, and how their trends are much lower than those corresponding to the functions of B. Note that the change of Q_s and Q_d as a function of γ mostly overlaps with the corresponding curves as functions of ϕ, as shown in detail in Fig. 3.8.

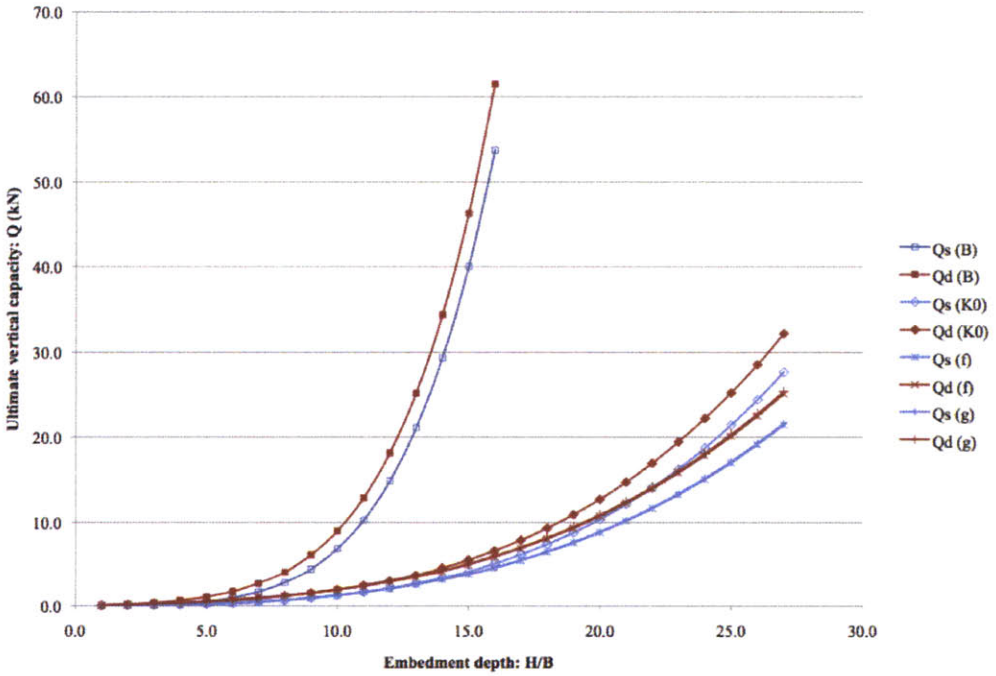

Figure 3.7: Q_s and Q_d, as functions of the change in B, ϕ, γ distinctively, plotted with the basic case curves.

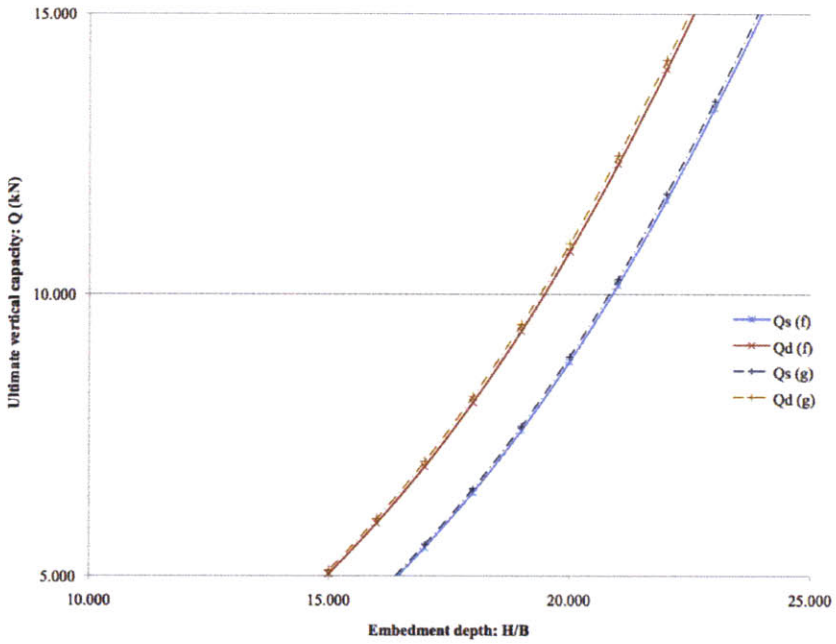

Figure 3.8: Detail of Fig. 7a with Q_s and Q_d, as functions of the change in ϕ, γ.

Finally, Fig. 3.9 shows the Q_s and Q_d curves as functions of the dynamic parameters *a* and D_f. In this case, they are plotted considering the anchor 5.67 cm in diameter, and changing only the relative depth and one of the two dynamic variables at a time. Consequently, both their Q_s curves coincide with the Q_s curve for B=5.67 cm (B1) because the static capacity is not influenced by *a* and D_f.

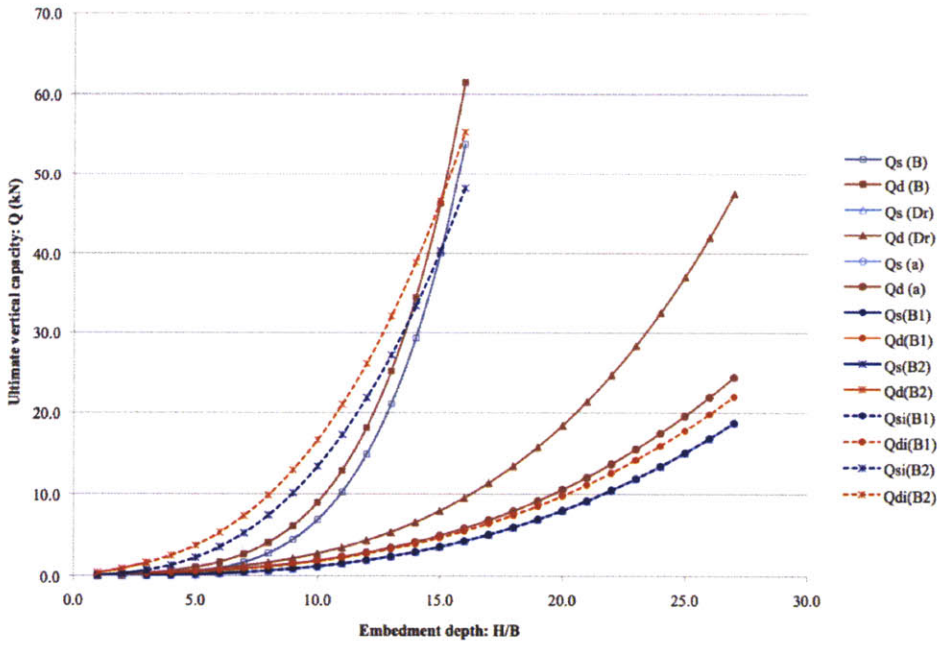

Figure 3.9: Q_s and Q_d, as functions of the change in D_f, *a* distinctively, plot with the basic case curves.

Comparing these trends to those previously examined confirms that B is the leading variable for the anchor loading capacity, and its role is definitely crucial for the anchor resistance.

Moreover, as expected, the dynamic capacity results constantly higher than the static one. For each pair of curves, this difference is remarkable when the independent variable is D_f or a because they only influence the dynamic resistance; particularly, D_f has a higher influence on the resulting capacity since it multiplies the weight of the mobilized soil. When the independent variable is one of B, K_0, ϕ, or γ, the difference between the static and dynamic curves' shapes is less remarkable because both multipliers are kept constant (D_f=1.1, a=0.2), so both static and dynamic capacity increase with the same rate dictated by the common factors.

4 Modelling 2 – Modelling-of-Models

The purpose of this chapter is to ascertain that the model predictions, discussed in chapter 3, can adequately simulate the prototype conditions. This is necessary in order to eventually extrapolate results from the model to the prototype scale. At first, the chapter presents the concepts of the modelling-of-models followed by the proper dimensional analysis for the case study. This analysis discusses the variable selection and the determination of the dimensionless products. Secondly, the dimensionless products are used to express the relationship between the model and the prototype. This goal is achieved by use of past centrifugal tests. Finally, after introducing the prototype conditions, we propose a first anchor design. In accordance to the theories under discussion, this design is developed for the simplified case of dry soil.

4.1 Introduction to the Modelling-of-Models and Dimensional Analysis

The modelling-of-models is a powerful resource, which helps control the correctness of the modelling procedure and finally establish if data can be extrapolated to the prototype scale. However, as Taylor (1995) warns, the modelling-of-models does not represent a sound guarantee for the aforementioned goal because the variables involved in model tests may only be varied within a limited range of values and, therefore, they always differ from the prototype's by at least an order of magnitude.

The modelling-of-models can take advantage of a powerful tool, such as the centrifuge. Its usefulness comes from the possibility to reproduce at a small scale the same stress state and distribution acting on the prototype, a fundamental principle when it comes to soil behavior. In particular, the high gravitational acceleration generated allows experimenters to simulate field conditions with the same material provided there is a minimum value of the model width to mean grain diameter ratio, (Iglesia, Einstein, and Whitman).

When the acceleration of gravity is scaled up by a factor of N, and the model's main dimension is N-times smaller than the prototype's, the grain size should not be scaled. In fact, the centripetal force leads an increase in the specific unit weights from $\gamma=\rho g$ at rest to $\gamma=\rho(V/R^2)=\rho Ng$ at speed, where R=radius of the centrifuge and V=velocity of rotation. Hence, the model will experience the same stress state distribution as the prototype at real scale, (Dickin and Leung, 1983).

In essence, a series of tests consists of varying the acceleration of gravity g and the model size (diameter) according to proper scaling laws with the desired target of obtaining identical results in dimensionless or normalized spaces, (Iglesia, Einstein, and Whitman).

Additionally, to further validate the results, other tests may be performed using a material different from the one present in situ and scaling the grain size properly by 1/N. The intent of this is to investigate slight differences due to the grain size and comprehend the extent of its influence to achieve a reasonable similitude. However, it is generally preferable to use the real material because it may not be exhaustively known or the alternative one (for example, glass beads) may not have the same properties, (Fuglsang and Ovesen, 1988; Iglesia, Einstein, and Whitman).

In conclusion, size effects in granular soils may affect centrifugal experiments. To avoid scale errors and set up correct tests, experimenters should make use of the dimensional analysis and of the chart proposed by Christensen and Bagge (1977).

This chart plots the main dimension of the model (for instance, diameter or width) on the horizontal axis and the gravitational scale factor N on the vertical axis, both on the logarithmic scale. Since these two parameters must satisfy the following similarity:

$$B_p=N \times B_m \tag{4.1}$$

where B stands for the dimension of the device to be tested, and the subscripts p and m indicate the prototype and the model respectively, different tests for the same prototype should align on a 45° ascending line. Fig. 4.1 illustrates how tests performed by Ovesen (1981) for the uplift capacity of anchors in sand complied with equation (1), so they didn't show any scale error, (Fuglsang and Ovesen, 1988).

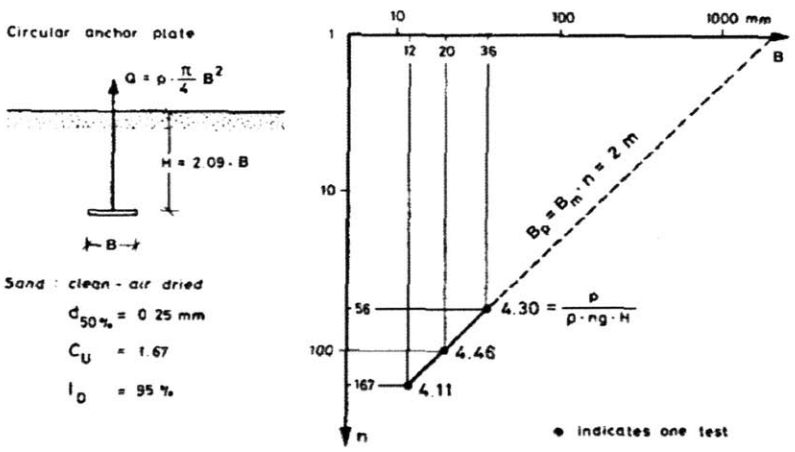

Figure 4.1: Tests results reported by Ovesen (1981) on the Christensen and Bagge's chart, (Fuglsang and Ovesen, 1988).

Most importantly, in order to extrapolate information from the model to the prototype, the experimenter must ascertain that the model will reproduce the actual phenomenon. For this reason, the dimensional analysis helps set criteria that, if entirely complied with by the model, indicate the success of simulation. Nevertheless, the model may not include some of the laws that regulate the phenomenon at real scale, therefore the experimenter should:

- identify those variables and laws whose compliance is crucial for the simulation, and adequately set the test; and,
- prove insignificant and/or be aware of the effects that non-reproduced conditions have on the results.

As thoroughly discussed by Langhaar (1951), while the dimensional analysis helps derive the model laws, this is correctly achieved only with a sound knowledge of the phenomenon; then, once all independent variables have been defined, experimental evidence is necessary to prove the goodness of the selection, (Fuglsang and Ovesen, 1988; Langhaar, 1951; Ovesen, 1981).

The application of the dimensional analysis to a natural phenomenon suggests to go through the following steps:

- select the independent variables for the model study;
- sort variables and form dimensionless products; and,

- evaluate the correctness of modelling by comparing dimensionless products for the model and the prototype.

This procedure will be examined in the following paragraphs.

DIMENSIONAL VARIABLES SELECTION

The prototype considered here is a horizontal circular plate anchor embedded in a sand-gravelly deposit with an average grain size ranging between 0.53 mm and 21.3 mm, as shown in Table 4.1.

Table 4.1: Grain size characteristics of the Coastal Plain Deposit of the Sicilian shore, (Jamiolkowski and Lo Presti, 2003).

	Gravel (%)		Sand (%)		Fines (%)		D50 (mm)		D60/D10		D_{max} (mm)		No. of tests
	Mean	St. dev.	Mean	St. dev.	Mean	St. dev.	From	To	From	To	Mean	St. dev	
Tower foundation													
Holocene(CPD)													
BH	58.0	22.1	34.4	18.4	8.6	6.7	0.53	9.60	3.4	223.7	47.0	17.1	46
LPT	65.5	22.5	31.7	21.6	2.8	2.2	0.60	21.30	2.1	126.9	57.9	24.1	73
SPT	59.6	17.4	36.4	16.7	4.0	2.1	0.60	15.00	3.1	103.3	30.1	8.1	103

Despite its complex stress-strain behavior, due to the dependence on density, stress level, stress path, and strain rate, soil generally acts as a continuum; therefore, high gravity and proper scaling allow one to reproduce identical stresses and strains at corresponding points in the model and the prototype.

Ovesen (1981) performed a few tests on either circular or square vertical anchors with the objective of examining their uplift holding capacity in granular soil. Ovesen (1981) used air-dried sand with 1.25 mm mean grain diameter that was accurately layered in the centrifuge box in order to obtain a uniform distribution. At the same time, the anchor model was being embedded in it, and subjected to a vertical pullout force once the system was set up.

With the background information provided in chapter 2 and the support of Ovesen's (1981) experiences, independent variables to describe the vertical resistance of a circular

anchor have been defined and reported in Table 4.2 with their symbols and their dimensions in terms of force (F), and length (L), (Ovesen, 1981).

Table 4.2: Independent variables for dimensional analysis, adapted from (Ovesen, 1981).

Variables	Symbols	Dimensional Units
Diameter	B	L
Embedment depth	H	L
Unit weight	γ	F/L^3
Void ratio	e	dimensionless
Soil friction angle	ϕ	dimensionless
Soil cohesion	c	F/L^2
Crushing strength of grains	σ_g	F/L^2
Modulus of Elasticity of grains	E_g	F/L^2
Mean grain diameter	d_{50}	L

A discussion about the selected variables follows:

The diameter of the anchor (B) is crucial because it governs the anchor capacity. It influences the size of the rupture surface, so the larger the anchor, the heavier the soil plug within the failure surface and the greater the friction force that develops along the failure surface itself between the mobilized soil and the one that rests in place.

The embedment depth (H) is also an obvious parameter, similar to the diameter, because it has a direct impact on the uplift resistance of the anchor. The deeper the anchor, the greater the volume of soil within the shearing surface and the higher the pullout resistance of the anchor for a given diameter and soil properties.

The unit weight (γ) and the void ratio (e) of soil are two material parameters that one must consider. The former determines the weight of the soil plug within the failure surface, the latter influences the relative density of the material; therefore, they act as fundamental variables in determining the counter-force to the external pullout.

The soil friction angle (ϕ) and the crushing strength (σ_g) of the grain material (which relates to the angle of dilatancy) are two other independent variables involved in the system failure mechanism. In particular, Rowe and Davis (1982) demonstrate how the uplift resistance of vertical axis anchors depends on them through the bearing capacity factor N_q.

The soil cohesion (c) and soil modulus of elasticity of grains (E) are significant quantities, as well. They are directly related to the stress-strain-strength behavior of the material, therefore model and prototype should be properly scaled.

The mean grain diameter (d_{50}) is the last of the independent variables to consider. It is important because the anchor diameter to d_{50} ratio may cause scale effects if not maintained above a certain value.

The acceleration of gravity (g) is very important for the model and prototype similitude. It is not included in the set of variables, but it is known that it is responsible for the stresses acting between soil grains and on any buried structure; indeed, the gravitational acceleration is the main feature of the model test apparatus (centrifuge) because it allows one to reproduce in the model the same distribution of stresses as in the prototype, and all scaling factors used in a centrifuge model test relate to its magnitude. In this particular case, Ovesen (1981) managed to obtain some important results thanks to the innovative characteristics of the centrifugal system.

Finally, another potential variable for the model study might be the earth pressure coefficient at rest (K_0). However, as argued by Rowe and Davis (1982), its influence on the holding capacity of vertical-axis anchors is negligible.

DETERMINATION OF DIMENSIONLESS PRODUCTS

The uplift capacity of a circular anchor in granular soil can be expressed as a function of the preceding nine variables

$$Q = f(B, e, \phi, c, \sigma_g, E_g, d_{50}, H, \gamma) \tag{4.2}$$

This equation has to be dimensionally homogeneous. According to Buckingham's Theorem (1914), this condition is satisfied if the equation can be rewritten in terms of dimensionless products; therefore, f has to be formulated as a function of those dimensionless products associated with independent variables and Q has to be normalized with respect to one or more of these variables in order to obtain also a dimensionless ratio. Each variable has dimensional units given by some combination of the basic system units considered in the study, which are force (F), and length (L).

Dimensionless products can be derived via Langhaar's (1951) procedure, which states that, given **n** independent variables whose units are a combination of **p** basic dimensions, the maximum associated number of dimensionless products can be **n-p**. To determine these products one can use the following procedure:

1) Each variable can be written as a function of the basic dimensions F, and L, as already presented in Table 4.2.
2) Numerical relations between independent variables and basic dimensions can be arranged in matrix form, as illustrated in Matrix (4.1). In particular, as Langhaar (1951) suggests, the order of variables should follow from left to right reporting at the very left the easiest variable to regulate during the test, and at the very right the most difficult one.

Matrix (4.1)

	B	e	ϕ	c	σ_g	E_g	d_{50}	H	γ
F	0	0	0	1	1	1	0	0	1
L	1	0	0	2	2	2	1	1	3

3) The rank **r** – order of the greatest non-zero determinant – of Matrix (4.1) is determined, and the number of dimensionless products to obtain is **n-r**. In particular, looking at the 8th and 9th columns the resulting matrix (shown below) has a non-zero determinant; therefore, the rank of the matrix is 2, and the number of dimensionless products to be determined is 9-2=7.

$$\begin{vmatrix} 0 & 1 \\ 1 & 3 \end{vmatrix}$$

4) Each dimensionless product can be written as a product of powers of the independent variables.

$$\Pi_i = B^{k_1} e^{k_2} \phi^{k_3} c^{k_4} \sigma_g^{\ k_5} E_g^{\ k_6} d_{50}^{\ k_7} H^{k_8} \gamma^{k_9} \tag{4.3}$$

or $$\Pi_i = [L]^{k_1} [F^0 L^0]^{k_2} [F^0 L^0]^{k_3} [FL^{-2}]^{k_4} [FL^{-2}]^{k_5} [FL^{-2}]^{k_6} [L]^{k_7} [L]^{k_8} [FL^{-3}]^{k_9} \tag{4.4}$$

or $$\Pi_i = [F]^{k_4+k_5+k_6+k_9} [L]^{k_1-2k_4-2k_5-2k_6+k_7+k_8-3k_9} \tag{4.5}$$

5) In order to have Π_i dimensionless, exponents of the powers in eq. (4.5) must satisfy the following **n-r** homogeneous equations:

$$k_4 + k_5 + k_6 + k_9 = 0 \tag{4.6}$$

$$k_1 - 2k_4 - 2k_5 - 2k_6 + k_7 + k_8 - 3k_9 = 0 \tag{4.7}$$

These equations can also be expressed in the following matrix form:

$$\begin{vmatrix} 0 & 0 & 0 & 1 & 1 & 1 & 0 & 0 & 1 \\ 1 & 0 & 0 & -2 & -2 & -2 & 1 & 1 & -3 \end{vmatrix} \begin{vmatrix} k_1 \\ \dots \\ k_9 \end{vmatrix} = 0 \tag{4.8}$$

6) Only **r** equations can be used to identify independent dimensionless products. Since r=2, both Eq. (4.6) and (4.7) can be used.

7) The number of unknowns, **n**=9, is greater than the number of available equations, **r**=2; therefore, the system of equations is indeterminate and the value of n-r=7

unknowns must be fixed. This can be achieved by assigning zero to each of the seven unknowns except for one that is considered equal to unity.

8) **r**=2 unknowns must be selected in order to have explicit values for them Eqs. (4.6) and (4.7). These variables may appear in more than one dimensionless product; hence, the dimensionless products will be dependent on these variables, but independent on each other. A set of solutions is possible if H and γ are the two chosen variables; they represent the basic units length (L) and force (F) respectively, and their product, γH, allows one to express the specific anchor uplift capacity, p [kPa], in a dimensionless fashion, p/γH. Consequently, the dimensionless products can be determined as mentioned in step 7.:

First, Eqs. (4.6) and (4.7) can be rewritten as

$$k_9 = -k_4 - k_5 - k_6 \tag{4.9}$$

$$k_8 = -k_1 - k_7 - k_4 - k_5 - k_6 \tag{4.10}$$

Then, assigning the values k_1=1 and k_4, k_5, k_6, k_7=0, and operating with Eqs. (4.9) and (4.10), one gets k_8=-1 and k_9=0. Thus, the first dimensionless product is:

$$\Pi_1 = H^1 D^{-1} = H/D$$

The second and third dimensionless products are determined by the dimensionless independent variables as follows:

$$\Pi_2 = e \quad \Pi_3 = \phi$$

The fourth dimensionless product can be formed using the same equations as for Π_1, but assigning values k_4=1 and k_1, k_5, k_6, k_7=0. From Eq. (4.9) and (4.10) it results that k_8=-1 and k_9=-1, so the second dimensionless product is:

$$\Pi_4 = c^1 H^{-1} \gamma^{-1} = c/H\gamma$$

The process continues in the same manner, so replacing k_5=1 and k_1, k_4, k_6, k_7=0 in Eqs. (4.9) and (4.10) one obtains k_8=-1 and k_9=-1, so the fifth dimensionless product is:

$$\Pi_5 = \sigma_g^{\ 1} H^{-1} \gamma^{-1} = \sigma_g / H\gamma$$

With k_6=1 and k_1, k_4, k_5, k_7=0, Eqs. (4.9) and (4.10) return k_8=-1 and k_9=-1, hence the sixth dimensionless product is:

$$\Pi_6 = E_g^{\ 1} H^{-1} \gamma^{-1} = E_g / H\gamma$$

Substituting k_7=1 and k_1, k_4, k_5, k_6=0, Eqs. (4.9) and (4.10) give back k_8=-1 and k_9=0; as a result the seventh dimensionless product:

$$\Pi_7 = d_{50}^{\ 1} H^{-1} = d_{50} / H$$

In summary, the seven dimensionless products are as follows:

$$\Pi_1 = H/D \qquad \Pi_2 = e \qquad \Pi_3 = \phi \qquad \Pi_4 = c/H\gamma$$

$$\Pi_5 = \sigma_g / H\gamma \qquad \Pi_6 = E_g / H\gamma \qquad \Pi_7 = d_{50} / H$$

These products represent all independent products that can be determined through dimensional analysis for the present model study; eventually, other dimensionless, but dependent, products may be derived trough a product of their powers, but one should ascertain that they are independent of each other, (Langhaar, 1951; Ovesen, 1981).

Although many sets of independent dimensionless products may be obtained from the same group of variables, the products presented here come from a specific selection; in fact, the experimenter does not have the control of all variables, so few of them (**r**=2), will be part of every dimensionless product, whereas each of the other independent variables, that can be experimentally regulated, will be part of only one dimensionless product in order to guarantee sound control of the experiment. In such a model study, H

and γ are the most difficult variables to control during model tests, so they have been selected as the variables to hold constant and to form the majority of the dimensionless products.

Conclusively, with Q=pA (p=anchor capacity per unit area of the anchor fluke, A=area of the anchor fluke), the dimensionless specific anchor uplift capacity can be expressed as an unknown function of these seven products (Langhaar, 1951):

$$\frac{p}{\gamma H} = f\left(\frac{H}{D}, e, \phi, \frac{c}{\gamma H}, \frac{\sigma_g}{\gamma H}, \frac{E_g}{\gamma H}, \frac{d_{50}}{\gamma H}\right) \tag{4.11}$$

4.2 Use of Dimensionless Products

After the dimensional analysis, a perfect simulation would require that all dimensionless products be identical for both the model and the prototype as stated below:

$$\Pi_{i\ model} = \Pi_{i\ prototype} \quad \text{for} \quad i=1,..,7 \tag{4.12}$$

Unfortunately, such a degree of similarity is almost never possible to achieve and the inequality of few dimensionless products must be justified as a secondary influence on the simulation, (Fuglsang and Ovesen, 1988; Ovesen, 1981).

As mentioned before, Ovesen (1981) investigated on the vertical uplift capacity of square and circular anchors in dry sand with the specific purpose to discover which scale errors affect the predictions derived from conventional model. In particular, he performed tests on shallow embedded anchors (H/B≤3.5) and reproduced a circular anchor by testing a square anchor slab with equivalent width B_e, which implies the same fluke area (see Fig. 4.2).

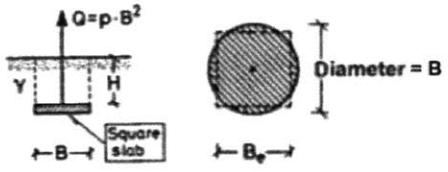

Figure 4.2: Ovesen (1981) – Test setting and definition of circular anchor, (Ovesen, 1981).

Departing from the condition of complete similarity, according to which all seven dimensionless products have same value in both the model and the prototype, he pointed out that conventional models fail to satisfy four out of the seven equalities. In particular, the problem concerns products Π_4, Π_5, Π_6, Π_7, because conventional models forfeit the chance to reproduce the same stress-strain soil behavior of the prototype since the gravitational acceleration remains unvaried, whereas the geometry is scaled down by a factor of N.

On the other hand, centrifugal tests comply with six out of seven products: only product Π_7 is still different from the prototype, because the material in use is as that in situ and consequently the average grain size to embedment depth ratio can not be replicated. Table 4.3 summarizes which similitude requirements are and are not satisfied by conventional and centrifugal models with respect to the prototype conditions; the Table also reports θ, angle of inclination of the anchor, which is not taken into consideration as the present case study focuses on vertical-axis anchor.

Table 4.3: Conventional model and centrifugal model comparison of similitude requirements, (Ovesen, 1981).

	Prototype Scale: 1:1 Gravity: g	Conventional Model Scale: 1:n Gravity: g		Centrifugal Model Scale: 1:n Gravity: ng	
1	$B_e/H = \frac{1}{B_e/H}$	B_e/H	similar	B_e/H	similar
2	θ	θ	similar	θ	similar
3	e	e	similar	e	similar
4	ϕ_μ	ϕ_μ	similar	ϕ_μ	similar
5	$\frac{\sigma_c}{\gamma \cdot H}$	$\frac{\sigma_c}{\gamma \cdot H/n}$	not similar	$\frac{\sigma_c}{\gamma n \cdot H/n}$	similar
6	$\frac{\sigma_g}{\gamma \cdot H}$	$\frac{\sigma_g}{\gamma \cdot H/n}$	not similar	$\frac{\sigma_g}{\gamma n \cdot H/n}$	similar
7	$\frac{E_g}{\gamma \cdot H}$	$\frac{E_g}{\gamma \cdot H/n}$	not similar	$\frac{E_g}{\gamma n \cdot H/n}$	similar
8	$\frac{d_g}{H}$	$\frac{d_g}{H/n}$	not similar	$\frac{d_g}{H/n}$	not similar

Ovesen (1981) performed dozens of tests about the uplift capacity of circular anchors in dry sand either in conventional models or with the centrifuge. He not only compared his own results to the prototypes, but also compared others' conventional model results with the corresponding ones he obtained from centrifugal models. An interesting and expected result evolved: as illustrated in Fig. 4.3, the uplift resistance predicted by conventional

models appeared overestimated compared to that anticipated by centrifugal models both in loose and dense sand.

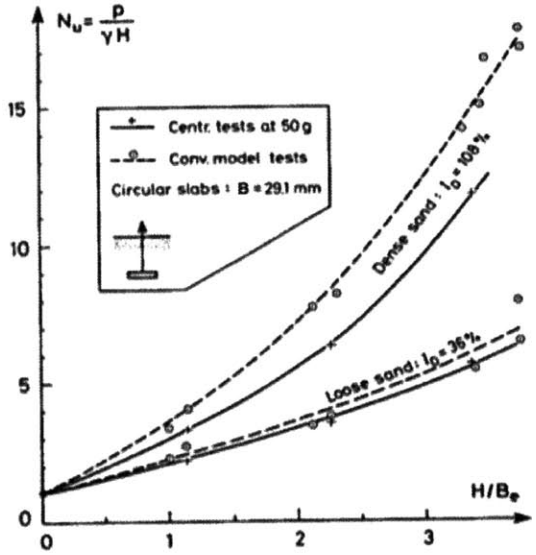

Figure 4.3: Ovesen (1981) – Comparison between conventional and centrifugal test results, (Ovesen, 1981).

The tested material was always the same type of sand, yet varying the relative density (D_r), the experimenter could vary the soil friction angle, which reached 37.7° for a dense sand (D_r=108%) and 29.5° for a loose sand (D_r=38%). However, since difficulties were encountered in defining the friction angle through triaxial tests, Ovesen (1981) decided to estimate ϕ by means of the material properties via an empirical expression in accordance with the Danish Code of Practice for Foundation Engineering 1977:

$$\phi_{tr} = 30^{\circ} - \frac{3}{C_u} + \left(14 - \frac{4}{C_u}\right) D_r \tag{4.13}$$

where $C_u = D_{60}/D_{10}$ = uniformity coefficient of soil.

As a matter of fact, scale errors affect the results of conventional models; therefore the use of the centrifuge apparatus and of proper scaling laws lead to a more reliable and correct way to extrapolate model results to the prototype scale. Being aware of this fact, Ovesen (1981) summarized all his results of the centrifuge model tests performed on circular anchors, plotted them on a normalized space (see Fig. 4.4), and looked for a new expression that could fit his data.

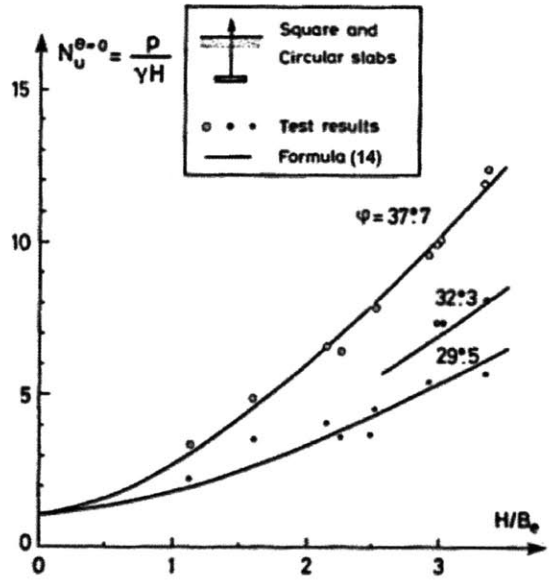

Figure 4.4: Ovesen (1981) – Summary of test results for the vertical uplift capacity of circular anchors, (Ovesen, 1981).

Finally, he succeeded in his data regression analysis and proposed the following new formula for the dimensionless vertical uplift capacity of circular anchor in sand

$$\frac{p}{\gamma H} = 1 + (4.32 \cdot \tan\phi - 1.58)\left(\frac{H}{B_e}\right)^{3/2} \tag{4.14}$$

The presented Eq. (4.14) can be used to predict the real anchor uplift capacity, but, because of the actual test conditions, one has to comply with the following two conditions:

- the anchor is embedded at shallow depth, or $0 \leq H/B \leq 3.5$; and,
- the soil friction angle ϕ falls in the range between 29° and 42°.

Few field tests have been run by Matsuo (1968) to verify the validity of Eq. (4.14); as shown in Table 4.4, the reproduced conditions account for medium-dense sand with high friction angle and embedment ratios H/B always lower than 3.5, and even lower than 1. The uplift capacity factors ($p/\gamma H$), or the dimensionless specific anchor uplift capacities, obtained from the field tests and Eq. (4.14), are in good agreement, especially for the second test where H/B reaches the lowest value of 0.55. Overall, they demonstrated the great accuracy of Eq. (4.14) with errors rarely higher than 5%, (Ovesen, 1981).

Table 4.4: Field test data and comparison with Eq. (4.14), adapted from (Ovesen, 1981).

H m	B_e m	γ kN/m^3	ϕ	$\frac{p}{\gamma H}$ test by Matsuo	$\frac{p}{\gamma H}$ formula (14)	Performed by
1.10	1.60	15.0	36°	1.78	1.89	(I-5)
1.10	2.00	16.0	35°	1.59	1.59	Matsuo (III-2)
1.10	1.60	16.0	35°	1.88	1.83	(1968) (I-2)
1.10	1.20	16.0	35°	2.20	2.27	(IV-2)

4.3 Prototype Conditions

The prototype in object is a circular anchor embedded in the uppermost layer of the Messina Strait, which is the coastal plain deposit (CPD).

As Fig. 4.5 suggests, the prototype conditions require more than one anchor subjected to a vertical uplift load in a tension-leg fashion to keep in place a floating structure. This consists of three connected floating platforms with an upside-down tripod structure supporting a horizontal-axis marine current turbine.

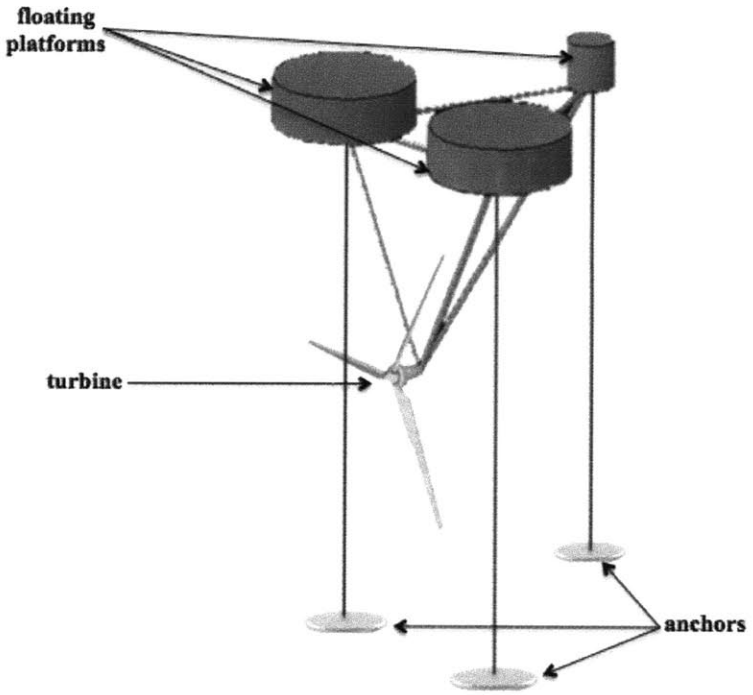

Figure 4.5: Three-platforms floating structure supporting a horizontal-axis marine current turbine.

Three circular anchors would be employed for this project, and they have the following characteristics:

- two anchors tie down the two front platforms counteracting the big drag force acting on the structure. For the geometry and the loading pattern of the problem, they would withstand the same pulling force, so they would be identical; and,
- one anchor on the back ties down the third small floating platform avoiding it to pop out of the water. The pullout force acting on the anchor is much smaller compared to the other two, so the anchor is likely to have a smaller size and/or a smaller embedment ratio H/D.

In particular, the reactions coming from the floating structure have been computed through a structural analysis that takes into account the dead weight and buoyancy force, the drag force of wind and marine current, and the impact of waves with their dynamic spectrum. As a result, the magnitude of the reactions in terms of total dynamic load transferred to the anchors is presented in Table 4.5.

Table 4.5: Structural reactions – total dynamic vertical pullout force for the anchors.

	Front platform	Back platform
Reaction	1,192 t 11,688 kN	320 t 3,138 kN

A perfect simulation of the prototype conditions assumes that all similarity requirements between model and prototype are satisfied. As already discussed, this is very difficult, if not impossible, to satisfy with any model test; however, centrifuge model tests provide a much better similitude than conventional tests, and six dimensionless products (with the exception of d_{50}/H) are likely to be identical to the field conditions for a hypothetical centrifuge model test that uses the coastal plain deposit as material.

For this reason, Eq. (4.14) is a strong candidate for the design of circular anchors for the present case study.

Nevertheless, with reference to Clemence and Veesaert (1977), their theory provides an additional tool to assess the uplift capacity of a circular anchor during dynamic loading. This tool may be used to evaluate the anchor performance under seismic loading, yet great attention should be devoted to the final result since it is a product of conventional model tests. Eventually, Ovesen's (1981) theory could be extended to estimate also the dynamic anchor capacity: first, a preliminary comparison between C&V's (1977) theory and Ovesen's (1981) theory about the static anchor resistance should be run to appreciate the gap between the two predictions; second, the evaluation of the anchor performance under dynamic loading could follow from C&V's (1977) theory by correcting the output with the error found in step 1.

However, an initial evaluation of the model tests run by C&V (1977) can be done on the basis of the dimensionless products. Table 4.6 and Table 4.7 report respectively the values of the fundamental parameters controlled during the tests and the corresponding values for the prototype.

Table 4.6: Variables' values used for lab tests (Clemence and Veesaert, 1977).

γ_t =	c =	ϕ =	ψ =	K_0 =	D_r =	C_u =	B =	h/B =
kN/m^3	kPa	deg	deg	-	%	-	cm	-
17	0	39	0	0.5	96	1.39	5.67	3 to 7
17	0	39	0	0.5	96	1.39	12.7	1 to 3

Table 4.7: Variables' values for the prototype conditions, (Jamiolkowski and Lo Presti, 2003).

γ_t =	c =	ϕ =	ψ =	K_0 =	D_r =	C_u =
kN/m^3	kPa	deg	deg	-	%	-
18.6 to 19.6	0	36 to 47	0	0.4	50	2 to 223

A brief discussion about the similitude of dimensionless products follows:

$$\Pi_1 = H/D \qquad \Pi_2 = e \qquad \Pi_3 = \phi \qquad \Pi_4 = c/H\gamma$$

$$\Pi_5 = \sigma_g/H\gamma \qquad \Pi_6 = E_g/H\gamma \qquad \Pi_7 = d_{50}/H$$

Π_1 : it is the anchor relative depth or embedment ratio. Since different embedment ratios were explored during the tests and the real anchor will probably feature one of these values, this dimensionless product might meet the similarity requirement and assume the same value for the prototype conditions as for the tests. Moreover, given the relative density of the material in situ, its composition, and its mechanical characteristics, it appears more convenient to install the anchor at shallow depth (as during most of the tests) from the mudline and eventually enlarge its diameter to obtain the required capacity at low embedment ratio.

Π_2 : it is the soil void ratio. This dimensionless product certainly misrepresents the prototype conditions because the two materials have a significant difference in terms of relative density and composition. The soil employed for the lab tests is uniform sand accurately layered in order to obtain a uniform distribution, whereas the material at the site does not only contain sand, but also gravel and silt. In addition, its composition allows for a non-uniform distribution in space, therefore, this dimensionless product will not have the same value for conventional tests as for the prototype.

Π_3 : the friction angle of the material used for the tests falls within the range of the measured values of the soil friction angle in situ; therefore, Π_3 satisfies the similitude requirement. Indeed, although the prototype material has a different composition than the material used during the conventional model tests, the friction angle is still equal.

Finally, Π_4 , Π_5 , Π_6 , Π_7 do not meet the similitude requirements for reasons already mentioned.

4.4 Anchor Design

After the dimensional analysis and the brief overview on the prototype conditions, the following section will apply the discussed theories with the purpose to obtain a design for the foundations in question. As already mentioned, the first step to accomplish consists of designing the anchors for the static loads. The basic loading condition is the so-called "short-term quasi-static" load; it derives from the thrust generated by waves, wind, and

current on the floater in addition to the structural buoyancy, and it accounts for 50% to 90% of the total dynamic load as shown in Fig. 4.6.

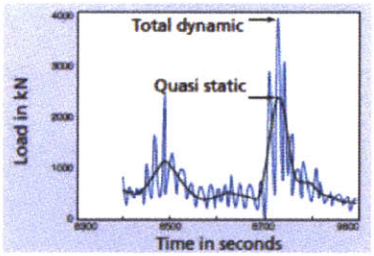

Figure 4.6: Difference between quasi-static load and total dynamic load, (Vryhof Anchors).

As for the quasi-static loading condition, to evaluate the required anchor ultimate holding capacity (UHC), it is sufficient to multiply the quasi-static load by a proper factor of safety (FS): API standard API-RP2SK suggests the value of FS to use for permanent and temporary moorings both for intact and damaged conditions (see Tables 4.8 and 4.9 analogous to Tables 2.1 and 2.2), so we can assume to extend the validity of these FS to our tension-leg anchor system.

Table 4.8: FS for permanent mooring, (Vryhof Anchors).

Permanent mooring	Quasi-static load	Total dynamic load
Intact load condition	1.8	1.5
Damaged condition	1.2	1.0

Table 4.9: FS for temporary mooring, (Vryhof Anchors).

Temporary mooring	Quasi-static load	Total dynamic load
Intact load condition	1.0	0.8
Damaged condition	Not required	Not required

Considering the extent of the quasi-static load is 90% of the total dynamic load, the magnitude of the reactions to take into account for the present analysis is reported in Table 4.10. Moreover, given the anchor system working as a permanent installation, and the corresponding FS=1.8 for intact load condition, the required UHC for the anchors employed to tie down the front and back platforms are presented in the following Table 4.11.

Table 4.10: Structural reactions – quasi-static vertical pullout force for the anchors.

	Front platform	Back platform
Reaction	1,073 t	288 t
	10,519 kN	2,824 kN

Table 4.11: Required static ultimate holding capacity (UHC) for the anchors.

	Front platform	Back platform
Required Ultimate Uplift Resistance	1,931 t 18,934 kN	518 t 5,084 kN

Once the UHC has been calculated, C&V's (1977) theory and Ovesen's (1981) theory can be used to evaluate the dimensions of those circular anchors to be installed to sustain such vertical uplift loads. First, two assumptions must be made about the relative depth H/B and the soil coefficient of uniformity C_u: as previously described, C&V (1977) and Ovesen (1981) performed conventional tests within a limited range of H/B and C_u values. In particular, C&V (1977) ran tests with H/B from 1 to 7 and C_u=1.39, while Ovesen's (1981) tests had H/B always lower than 3.5 and C_u=1.67. To adequately take advantage of these past results, we assume to design the anchor for an embedment ratio H/B=3, which implies the failure mechanism to be well known and developed up to the surface, and for C_u=1.67 because it is sufficiently close to both the C_u of sand used in the conventional model tests and the lowest C_u value of the prototype granular soil; therefore, a higher C_u in situ can only result in better anchor performance.

As already explained in this thesis (in the previous and present chapters), according to C&V's (1977) and Ovesen's (1981) theories, the equations to use for the design of circular anchors under static loading are respectively:

$$Q_s = \gamma_t V_s + \gamma K_0 \tan(\phi) \cos^2\left(\frac{\phi}{2}\right) \pi \left[\frac{BH^2}{2} + \frac{H^3 \tan(\phi/2)}{3}\right] \tag{3.1}$$

$$\frac{p}{\gamma H} = 1 + (4.32 \cdot \tan\phi - 1.58)\left(\frac{H}{B_e}\right)^{3/2} \tag{4.14}$$

Searching for the anchor dimensions that satisfy the UHC requirements, one obtains the results presented in the following Tables 4.12, 4.13, and 4.14:

Table 4.12: Anchor diameter (B) according to C&V's (1977) and Ovesen's (1981) theories for static loading.

	Front platform	Front platform	Back platform	Back platform
	C&V (1977)	Ovesen (1981)	C&V (1977)	Ovesen (1981)
B (m)	3.705	**3.712**	2.390	**2.395**
B (ft)	12.16	**12.18**	7.84	**7.86**

Table 4.13: Anchor fluke area (A) according to C&V's (1977) and Ovesen's (1981) theories for static loading.

	Front platform	Front platform	Back platform	Back platform
	C&V (1977)	Ovesen (1981)	C&V (1977)	Ovesen (1981)
A (m^2)	10.78	**10.82**	4.487	**4.505**
A (ft^2)	116.04	**116.50**	48.30	**48.49**

Table 4.14: Anchor fluke embedment depth (H) according to C&V's (1977) and Ovesen's (1981) theories for static loading.

	Front platform	Front platform	Back platform	Back platform
	C&V (1977)	Ovesen (1981)	C&V (1977)	Ovesen (1981)
H (m)	11.11	**11.14**	7.17	**7.18**
H (ft)	36.47	**36.54**	23.53	**23.57**

From the illustrated results, one can appreciate how C&V's (1977) theory, based on conventional model tests, slightly overestimates the anchor capacity. In fact, for the same UHC this theory leads to smaller anchors than those expected to be installed using Ovesen's (1981) theory: specifically, the anchor fluke area estimated by Ovesen (1981) is 0.4% larger than that computed by C&V (1977), whereas the anchor fluke diameter is 0.2% larger. In other words, for a certain anchor fluke diameter C&V (1977) overestimates the anchor uplift capacity by 0.59% with respect to Ovesen's (1981)

theory. As a consequence, Ovesen (1981)'s results are accepted as somewhat more reliable and more conservative, therefore, these dimensions represent the first output of the present analysis.

Based on this difference between the two approaches, one can try to predict the dynamic holding capacity of the circular anchors. Even though, C&V (1977) are the only ones who suggested a formula to evaluate this resistance, the comparison with Ovesen's (1981) theory allows one to make a rough estimate of the dynamic capacity from a centrifugal model test perspective. Indeed, knowing the final anchor dimensions and the 0.59% difference for the static holding capacity, one can calculate the dynamic uplift resistance through the following C&V's (1977) Eq. (3.2) and then correct it by the same percentage.

$$Q_s = \gamma_t V_s + \gamma K_0 \tan(\phi) \cos^2\left(\frac{\phi}{2}\right)\pi \left[\frac{BH^2}{H} + \frac{H^3 \tan(\phi/2)}{3}\right] D_f + V_s \gamma_t a \qquad (3.2)$$

Specifically, the values of D_f and a must be defined:

- in the second term, D_f accounts for the increase in shear force along the failure surface due to dynamic loading. According to what Casagrande and Shannon (1948) and Seed and Lundgren (1954) observed in sand, this increase ranges from 10% to 20%, therefore, an average value of 1.15 is assumed for D_f;
- in the third term, which accounts for the soil mass inertial force, a represents the acceleration of the anchor in units of g (acceleration of gravity). Considering that the anchor follows the ground motion, a can be assumed equal to 0.36g from what the horizontal peak ground acceleration map of southern Italy shows in Fig. 2.8.

As expected and shown in Table 4.15, the dynamic capacity of circular anchors is higher than the static one. It has been calculated by using formula (3.2), and correcting the output with the difference previously found (0.59%) from the comparison between C&V's (1977) and Ovesen's (1981) theory about the static UHC.

Table 4.15: Anchor dynamic UHC according to C&V's (1977) theory with a correction of 0.59%.

	Front platform	Back platform
	C&V (1977) corrected	C&V (1977) corrected
Q_d (t)	1,973.17	545.10
Q_d (kN)	19,350.86	5,345.83

In addition, according to the same API standard API-RP2SK, the ultimate holding capacity of anchors for dynamic loading is determined by accounting for a lower FS. As Table 4.8 suggests, FS equals 1.5 for the total dynamic load and for an anchor operating as a permanent installation and in intact conditions. Consequently, the anchor dynamic UHC reported in Table 4.15 must be at least equal or superior to the holding capacity requirements presented in Table 4.16: these latter values result from multiplying the reactions reported in Table 4.5 by the new FS=1.5. Tables 4.15 and 4.16 illustrate that this requirement is satisfied for both the back and the front anchors.

Table 4.16: Anchor total dynamic UHC requirements for FS=1.5.

	Front platform	Back platform
Q_d (t)	1,787.63	480.00
Q_d (kN)	17,531.24	4,707.36

A step further is the comparison of the present solution with that initially adopted to stabilize the floating structure. As Fig. 4.7 illustrates, the initial solution for anchoring the floating structure consisted of two mooring drag embedment anchors connected to the front platforms and one suction caisson connected to the back platform in tension-leg fashion. The two drag anchors counteract the large drag force acting on the structure by tying down the two front platforms with catenary mooring systems departing from each platform. Each drag anchor weighs 9.5 metric tons, and, when tensioned to the maximum design load, it responds by dragging for about 12.6 m and penetrating for 3.2 m below the

mudline (see Fig. 4.8). The suction anchor on the back will tie down the third smaller platform in tension-leg fashion avoiding it to pop out of the water, so its holding capacity will be exploited in the pure vertical direction; with reference to Fig. 4.9 this suction anchor has a 12 m diameter (D) and a 5.5 m length (L), with a wall 35 mm thick (t1) and a top lid 50 mm thick (t2).

Figure 4.7: Three-platform floating structure bearing a horizontal-axis turbine.

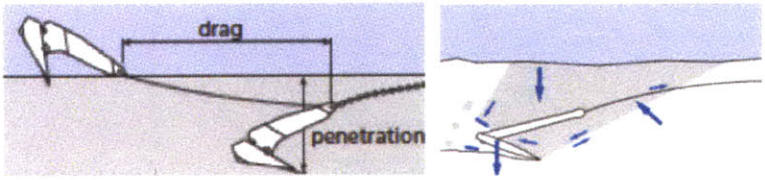

Figure 4.8: Left – Drag embedment anchor during installation; Right – Resistant mechanisms, (Vryhof Anchors).

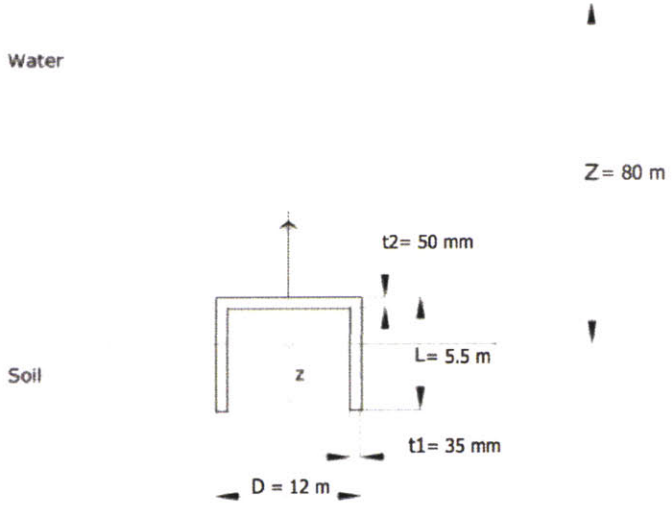

Figure 4.9: Geometry of a suction anchor, (Bakker et al., 2006).

Table 4.17 presents the comparison between the new and the old anchor designs. In particular, it compares the volume (V) and the weight (W) of anchors assuming that:

- all anchors are made of steel (with unit weight γ=77 kN/m^3) and the amount of steel used is directly related to the anchor dimensions and shape, and
- the circular anchors in the new design have a plate thickness (t) equal to 3% of the anchor diameter, as Fig. 4.10 illustrates.

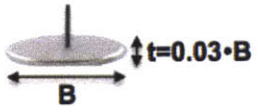

Figure 4.10: Geometry of a new circular anchor.

Table 4.17: Anchors volume and weight for the two discussed solutions.

NEW DESIGN

	Front platform	Back platform
	circular anchors	
t (cm)	11.14	7.18
t (in)	4.38	2.83
V (m^3)	1.205	0.324
V (ft^3)	42.57	11.43
W (kN)	92.81	24.92
W (T)	10.43	2.80

OLD DESIGN

Front platform	Back platform
drag anchor	*suction anchor*
-	-
-	-
1.21	15.36
42.74	542.60
93.17	1,182.71
10.47	132.94

In conclusion, this new solution with circular anchors is expected to have the advantages of reducing the overall dimensions of the anchors, reducing the material necessary for their manufacture, and minimizing the duration and cost of installation.

5 Final Design

This chapter addresses the problem of installing the circular anchors in the real context of the Messina Strait. The analyses conducted in the previous chapter led to a first version of the new anchor design, which considered the soil in dry conditions. Now, additional aspects are taken into consideration because the offshore reality certainly involves both soil and water. Therefore, we propose a second version of the new anchor design. It accounts for the effect of water on the soil unit weight and, subsequently, on the anchor uplift resistance. We compare the two versions for highlighting the changes and we verify the efficiency of the new designed anchors for the real prototype requirements. Secondly, given the high seismicity of the area, a sensitivity analysis allows one to understand what can be the dynamic soil response and how it would impact the soil-anchor interaction. An experimental study by Elgamal et al. (2005) is the principal means of this analysis. Finally, a solution is proposed for minimizing either the potential liquefaction or the scour phenomenon in the area of influence of the anchors, and two options for the anchor installation are suggested.

5.1 New Anchor Design for Saturated Material

In contrast to the dry material used in either conventional or centrifugal tests, the discussed circular anchors have to be installed in the seabed of the Messina Strait. This scenario is different and the presence of pore pressure causes the effective stresses to be lower. Assuming from the tests that the distribution of pore pressure is hydrostatic, the vertical effective stress acting on a generic soil element is determined by the buoyant unit weight of soil times the embedment depth from the mudline. Having lower effective stresses than the dry case results in lower shear strength of the granular soil and, also, in lower weight of the soil plug that, when mobilized by the shearing failure of the soil mass above the anchor, prevent the anchor to be pulled out.

In order to account for the decrease of the effective stress, the new anchor design should be revised. In fact, the size of the anchors should be defined to withstand the static and total ultimate pullout forces in the actual scenario of lower soil strength and lower soil unit weight. Specifically, these circumstances will lead towards a second version of the new anchor design with bigger anchors and/or larger embedment depth.

The procedure consists in applying again the theories by Clemence and Veesaert (1977) and Ovesen (1981). We take into account the buoyant unit weight of soil while keeping unchanged the soil friction angle since it was determined through the empirical correlation in Eq. (2.1) after field tests and we assume a drained soil response. As a first analysis, we examine the static loading conditions and we compare the results with the design version obtained in dry soil in the previous chapter 4. Since we are dealing with salt water, its average unit weight in the Mediterranean Sea is 10.1 kN/m^3 for a buoyant unit weight of CPD equal to 12.9 kN/m^3 assuming that the saturated unit weight of soil averages 23 kN/m^3.

Applying the equations (3.1) and (4.14) discussed earlier in chapters 3 and 4, and searching for the anchor dimensions that satisfy the UHC requirements in Table 5.1 (corresponding to Table 4.11), one obtains the results presented in the following Tables 5.2, 5.3, and 5.4:

$$Q_s = \gamma_t V_s + \gamma K_0 \tan(\phi)\cos^2\left(\frac{\phi}{2}\right)\pi\left[\frac{BH^2}{2} + \frac{H^3\tan(\phi/2)}{3}\right] \tag{3.1}$$

$$\frac{p}{\gamma H} = 1 + (4.32\cdot\tan\phi - 1.58)\left(\frac{H}{B_e}\right)^{3/2} \tag{4.14}$$

Table 5.1: Required static ultimate holding capacity (UHC) for the anchors.

	Front platform	Back platform
Required Ultimate Uplift Resistance	1,931 t 18,934 kN	518 t 5,084 kN

Table 5.2: Anchor diameter (B) according to C&V's (1977) and Ovesen's (1981) theories for static loading, saturated conditions.

	Front platform	Front platform	Back platform	Back platform
	C&V (1977)	Ovesen (1981)	C&V (1977)	Ovesen (1981)
B (m)	4.215	**4.224**	2.719	**2.725**
B (ft)	13.83	**13.86**	8.92	**8.94**

Table 5.3: Anchor fluke area (A) according to C&V's (1977) and Ovesen's (1981) theories for static loading, saturated conditions.

	Front platform	Front platform	Back platform	Back platform
	C&V (1977)	Ovesen (1981)	C&V (1977)	Ovesen (1981)
A (m^2)	13.96	**14.01**	5.81	**5.83**
A (ft^2)	150.21	**150.81**	62.52	**62.77**

Table 5.4: Anchor fluke embedment depth (H) according to C&V's (1977) and Ovesen's (1981) theories, saturated conditions.

	Front platform	Front platform	Back platform	Back platform
	C&V (1977)	Ovesen (1981)	C&V (1977)	Ovesen (1981)
H (m)	12.65	**12.67**	8.16	**8.17**
H (ft)	41.49	**41.57**	26.77	**26.82**

As already observed in chapter 4, C&V (1977) slightly overestimates the anchor resistance by 0.59% yielding smaller anchor dimensions; therefore, Ovesen's (1981) results are accepted as somewhat more reliable and more conservative.

In comparison to what obtained for the anchor design in dry soil, the new anchors have a larger diameter and heavier weight to properly withstand the same pullout force in saturated granular soil. In particular, their diameter (B), fluke area (A), and embedment depth (H) have increased as shown in Table 5.5. Moreover, Fig. 5.1 and Fig. 5.2 illustrate

the anchors' dimensions as for the first (in dry soil) and the second (in saturated soil) versions of the new design for both the front and the back platforms.

Table 5.5: Comparison between the dimensions of the circular anchors designed for dry soil and those designed for saturated soil according to Ovesen's (1981) theory.

	Front platform	Front platform	Back platform	Back platform	Percentage increase
	Dry soil	Saturated soil	Dry soil	Saturated soil	
B (m)	3.712	**4.224**	2.395	**2.725**	13.78%
A (m^2)	10.82	**14.01**	4.50	**5.83**	29.45%
H (m)	11.14	**12.67**	7.18	**8.17**	13.78%

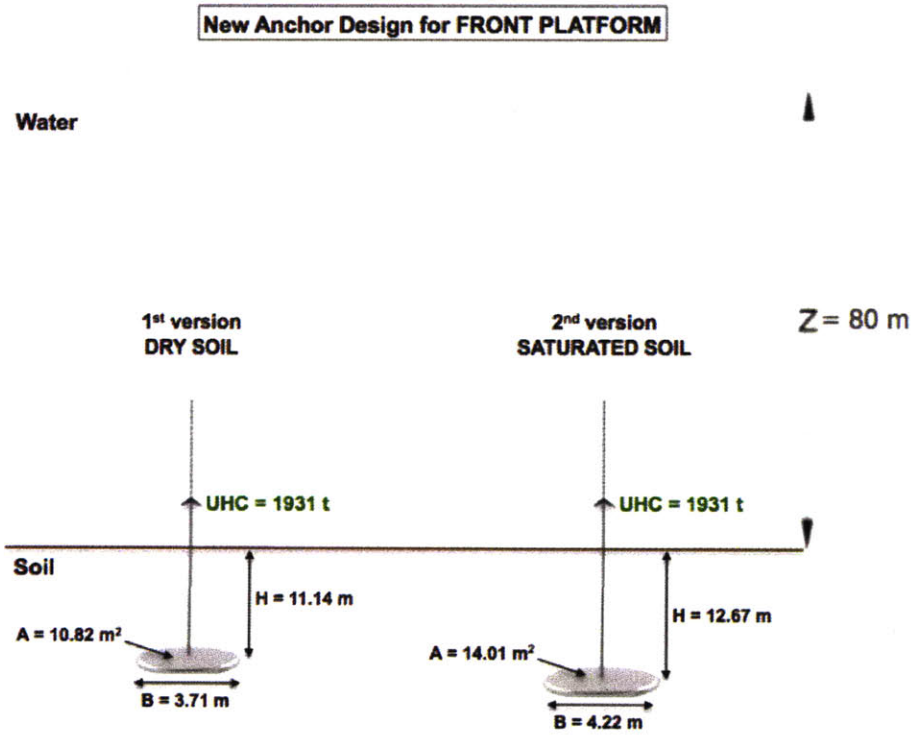

Figure 5.1: Dimensions of the circular anchors for the front platform resulting from the first version (in dry soil) and second version (in saturated soil) of the new design.

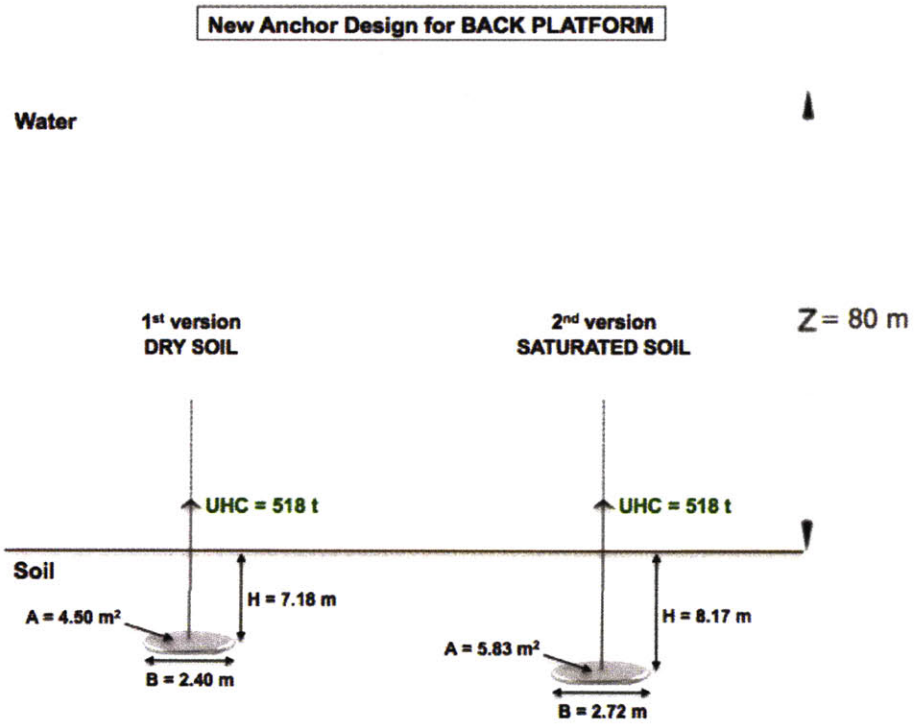

Figure 5.2: Dimensions of the circular anchors for the back platform resulting from the first version (in dry soil) and second version (in saturated soil) of the new design.

A step further is to predict the dynamic holding capacity of the new designed circular anchors with the same approach used in chapter 4. It consists of calculating the dynamic uplift resistance through equation (3.2) by C&V (1977) based on the new anchor dimensions and, then, correcting it by the difference between C&V's (1977) and Ovesen's (1981) theory for the static holding capacity. This computation yields the results presented in the following Tables 5.6 and 5.7.

$$Q_s = \gamma_t V_s + \gamma K_0 \tan(\phi)\cos^2\left(\frac{\phi}{2}\right)\pi\left[\frac{BH^2}{H} + \frac{H^3\tan(\phi/2)}{3}\right]D_f + V_s\gamma_t a \qquad (3.2)$$

Table 5.6: Anchor dynamic UHC according to C&V's (1977) theory with a correction of 0.59%.

	C&V (1977) corrected	
	Front platform	Back platform
	Saturated soil	Saturated soil
Q_d (t)	**1,960.61**	**539.88**
Q_d (kN)	**19,227.66**	**5,294.58**

Table 5.7: Comparison between the dynamic UHCs of the circular anchors designed for dry soil and those of the circular anchors designed for saturated soil according to C&V's (1977) theory with a correction of 0.59%.

	C&V (1977) corrected			
	Front platform		Back platform	
	Dry soil	Saturated soil	Dry soil	Saturated soil
Q_d (t)	1,973.17	**1,960.61**	545.10	**539.88**
Q_d (kN)	19,350.86	**19,227.66**	5,345.83	**5,294.58**

Therefore, another important finding is that, although the anchor size is increased, the dynamic capacity of the circular anchors is slightly lower than that calculated for the first version (dry soil) of the new anchor design. This occurs because the unit weight of the soil has a great impact on the dynamic resistance of the anchors according to Eq. (3.2); particularly, the buoyant unit weight of the soil leads to a much lower weight and inertial force of the soil plug that mobilizes within the rupture surface and tends to inhibit the pullout of the anchor. Nevertheless, the anchors' capacity is still sufficient to withstand the ultimate total dynamic pullout force presented in Table 5.8 (analogous to Table 4.16).

Table 5.8: Anchor total dynamic UHC requirements for FS=1.5.

	Front platform	Back platform
Q_d (t)	1,787.63	480.00
Q_d (kN)	17,531.24	4,707.36

5.2 Soil Dynamic Response

As discussed in the second chapter, the Messina Strait is the most seismic area of the Italian peninsula. To complete a satisfactory project, we must consider the effect that the ground motion has on the stiffness and strength of the saturated material. This is necessary in order to evaluate if the foundation system has been efficiently and safely designed, or, due to potential decrease in capacity caused by an eventual seismic event, if it would be better to consider an additional factor of safety in the anchor design.

Given the nature of the material in the uppermost geological layer, it is interesting to look at how saturated dense sand behaves when it is subjected to an earthquake-shaking event. In particular, Elgamal et al. (2005) investigated the dynamic response of this material by performing some centrifugal tests. They considered saturated dense sand with the characteristics reported in the following Table 5.9:

Table 5.9: Characteristics of the saturated sand employed by Elgamal et al. (2005).

γ_t =	soil total unit weight	20.3	kN/m^3
D_r =	soil relative density	100	%
γ_{fluid} =	fluid unit weight	9.8	kN/m^3

They simulated the propagation of vertical shear waves by exciting the material along the longitudinal direction and they replicated 27 shaking events for which the centrifugal acceleration ranged from 9.2g to 37.3g and the peak acceleration at the surface of the sand mass ranged from 0.03g to 1.7g. The soil volume within the container measured 1651 x 787 x 553 mm. By varying the applied centrifugal acceleration, the same soil volume reproduced a prototype thickness between 5.1 m and 20.6 m. As Fig. 5.3 shows, even though the soil reacts to shaking with an undrained response, Elgamal et al. (2005) observed that at the peaks in acceleration correspond decreases in pore pressure. Lambe and Whitman (1969) already had pointed out that this phenomenon is caused by the dilative tendency of the soil at large shear strains (γ). Vucetic (1986) and Matasovic and Vucetic (1993) demonstrated that this dilation leads to increase in confinement or to decrease in pore pressure with subsequent increase in shearing resistance.

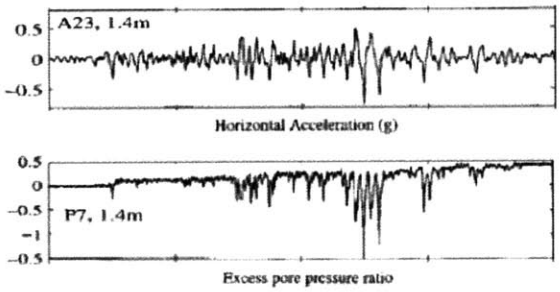

Figure 5.3: Acceleration and pore pressure time history for one shaking event at 1.4 m from the surface in prototype scale, (Elgamal et al., 2005).

In contrast to the observed undrained response, a drained one would not affect the confinement to the same extent and the shear modulus would always decrease with shear strain.

Focusing on three shaking events, representative of different earthquake magnitudes (weak, moderate, strong), Elgamal et al. (2005) noticed how the dynamic response of the material changes. In particular, it is interesting to identify what is the maximum shear strain and the relation that defines the shear stress-strain response, the shear stiffness, and the degree of damping. The following Table 5.10 lists these four factors and how they change for each of the events represented in Fig. 5.4.

Table 5.10: Soil response to three different shaking events, adapted from (Elgamal et al., 2005).

	Weak event	**Moderate event**	**Strong event**
Maximum shear strain (γ_{max})	0.01%	0.20%	0.50%
Shear stress-strain response	linear	non-linear	non-linear
Shear stiffness	constant	decrease with γ	initial decrease with γ, for γ>0.3% regain in stiffness due to soil dilation as already proven by (Ishihara, 1985)
Damping	minimal	significant	significant

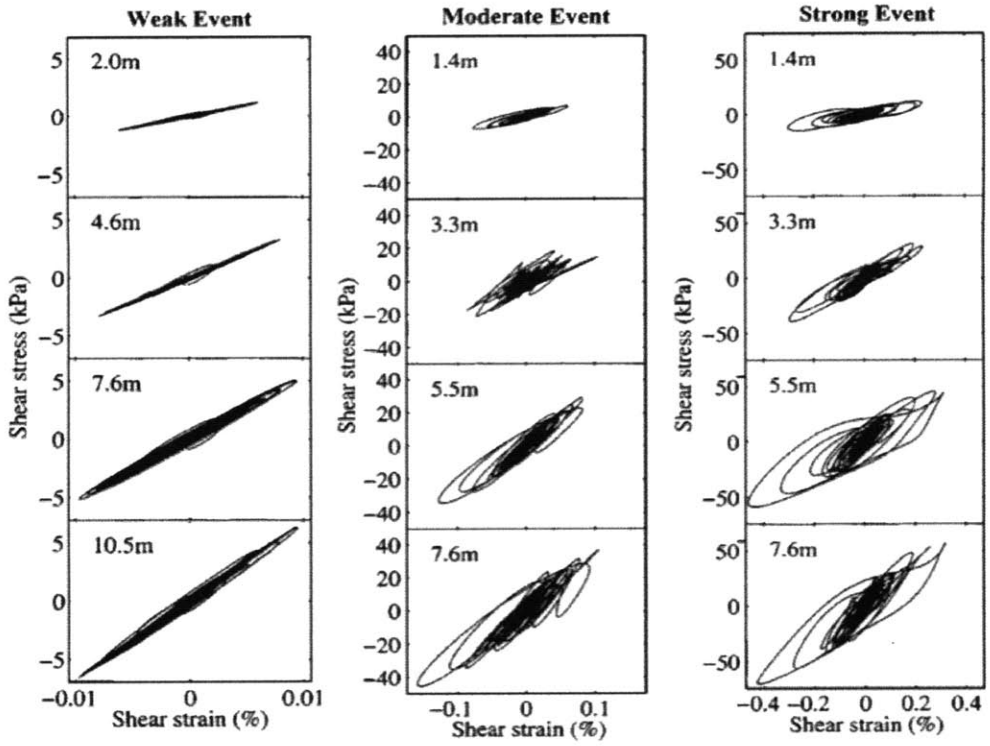

Figure 5.4: Shear stress-shear strain histories for three shaking events, (Elgamal et al., 2005).

Fig. 5.4 shows that the shear stress-strain response of soil changes according to both the magnitude of the shaking event and the degree of confinement due to depth. For the weak event, the soil has always a linear response meaning that the shearing stiffness does not change and the damping ratio, represented by the area within the loops, is negligible. As the soil response at very low shear strain does not have visible loops, the soil responds with its highest shear modulus G_0 (low strain shear modulus), which increases with confinement as the steeper slope of the response indicates, and with a damping that slightly develops at great depth. In contrast, for the moderate and the strong shaking events, the shear stress-strain response is visibly non-linear. In both events, the soil response indicates the tendency of the soil stiffness to decrease with shear strain, but the initial shear stiffness is also higher as the depth increases. In addition, during a strong shaking event, the soil response describes S-shaped loops: the shear stiffness decreases with shear strain, but when $\gamma \geq 0.3\%$ the soil dilation leads to a regain in stiffness. The dynamic soil response is characterized by loops whose area gets larger as the confinement increases; however, at large shear strains the S-shape of the loops becomes

more noticeable as the confinement increases and the area within them no longer increases resulting in a limit for the damping ratio.

Elgamal et al. (2005) concluded that the earthquake shaking causes the relative density to further increase with subsequent slight increases of G_0. In addition, G_0 increases with depth or confinement and the damping ratio also starts increasing with depth, but, then, it reaches an upper limit.

With regard to the Messina Strait, Fig. 5.5 (corresponding to Fig. 2.3) illustrates how the shear modulus G decreases up to a minimum value of 20% of its initial value G_0, according to Ismes (1985); from what is learnt by Elgamal et al. 's (2005) experience, the reason why G does not decrease further may be the undrained soil response, which causes the confinement stress to increase preventing the shear modulus to reach lower values.

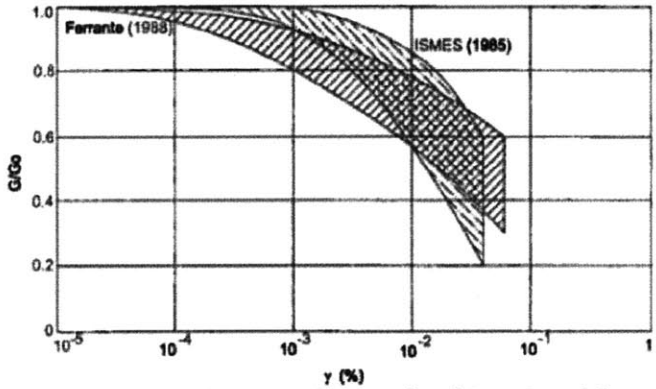

Figure 5.5: Shear modulus decay vs. shear strain of CPD from laboratory tests, (Jamiolkowski and Lo Presti, 2003).

Similarly, as shown in Fig. 5.6 (analogous to Fig. 2.4), the change of damping ratio is such that it reaches the highest value at about 7% according to Ferrante (1968). This low value of damping at large shear strain may be due to soil dilation and to the non-linear soil response; in fact, for strong shaking events the shear stress-strain response displays S-shaped loops which, together with the soil undrained response, produce an upper limit of the damping ratio.

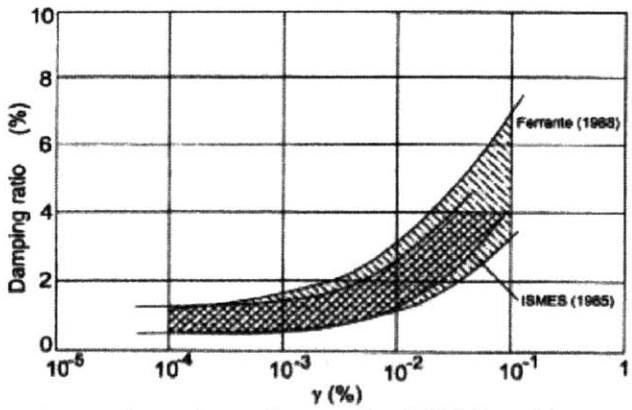

Figure 5.6: Damping ratio vs. shear strain of CPD from laboratory tests, (Jamiolkowski and Lo Presti, 2003).

In conclusion, the earthquake-induced large shear strains in a dense saturated granular soil lead to an increase in confinement and shear strength. Nevertheless, as explained in the previous paragraph, the dynamic capacity of the circular anchors is lower, but still sufficient, than that calculated for the first version (in dry soil) of our new design. As a result, the procedure adopted to obtain the design for circular anchors in saturated granular soil does not need to include an extra factor of safety. The dynamic holding capacity of the anchors will not be subjected to any decrease during earthquake shaking events and, therefore, the design is likely to be effective.

5.3 Countermeasures against Liquefaction and Scour

As observed by Jamiolkowski and Lo Presti (2003) and reported in the second chapter of this thesis, the Coastal Plain Deposit (CPD) may incur liquefaction. For the particular case study, soil liquefaction may be caused by the rocking of the floating structure that, subjected to the action of waves, transfers significant dynamic loading to the embedded anchors. In this condition, it may eventually be advisable to further help the soil to dissipate the induced pore pressure; one solution to achieve this is to place an apron of graded rock around the anchor location in order to have the water flowing radially away without contributing to the pore pressure buildup, (Gerwick, 1999).

Given the shape and way-of-work of the anchors, they should not be subjected to any scour effect. Nevertheless, the Messina Strait has a steady current velocity that averages 2.5 m/s and, therefore, it may remove the most superficial granular material on the seabed; moreover, the presence of the steel cables, which connect the anchors to the floating platforms in pairs, may cause scour to be locally stronger, so that part of the material overlying each anchor may be permanently removed. This scenario would result in a lower embedment depth for each anchor and, therefore, it would expose each anchor to the risk of being more easily pulled out of the ground under the static and dynamic actions transferred by the steel cables. Consequently, it may be advisable to place rock blocks of proper size or mat segments (see Fig. 5.7) in the area of influence of each anchor, so they would not only prevent the scour phenomenon, but also act as an extra load to increase the anchor holding capacity, (Gerwick, 1999).

Figure 5.7: Series of mat segments to employ offshore for scour prevention, (Flexmat Gravity Anchor).

5.4 Installation Method

The designed circular anchors could be installed following the procedure illustrated in Fig. 2.24 for the jetting-in driven anchors. A pile follower would be driven with the anchor connected sideways to it, so that when the proper depth is reached the anchor is released, the pile is retrieved, and then the anchor is keyed by chain/cable tensioning to adjust it to the correct position. In addition, a second easier option may be practically viable: given the size and the weight, each anchor might penetrate into the seabed under its own weight provided that the penetration occurs with the anchor orientated such that its side faces down (see Fig. 5.8).

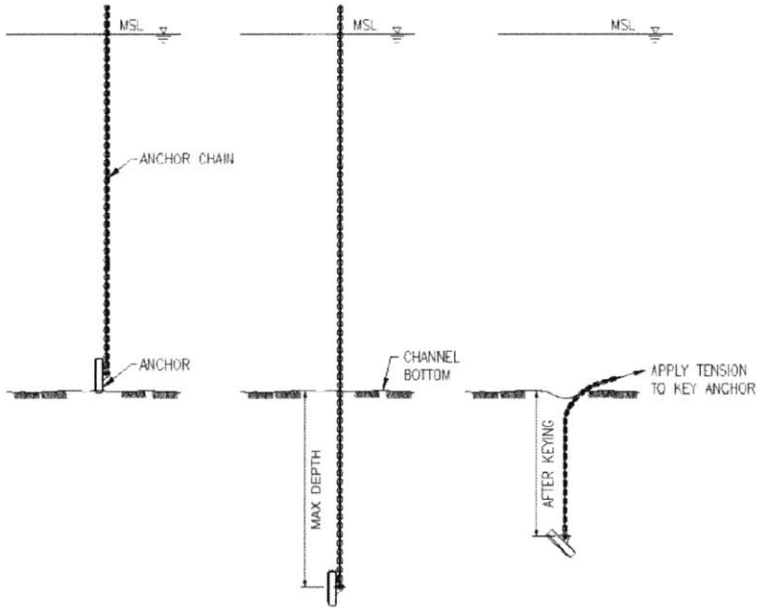

Figure 5.8: Anchor self-weight penetration and subsequent keying, adapted from (Safaqah and Gerin, 2004): left – the anchor sinks and reaches the seabed; middle – the anchor penetrates into the seabed under his own self-weight; right – the anchor is keyed by applying tension to the chain/cable that connects it to the floater.

However, given the nature of the soil in situ, it might be necessary to install the anchor using a pile follower in order to have proof that the prescribed depth is reached. In this case, the installation is more likely to occur with a submergible pile hammer pounding on the pile follower at depth close to 80 m rather than using a dry hammer pounding on a pile more than 80 m long.

6 Summary and Conclusions

This section presents summary and conclusions about the design of the circular anchors discussed in the previous chapters. In addition, some comments and recommendations are made with regard to the real employment of such anchors in the Messina Strait.

6.1 Circular Anchors Design

The project study consists of a three-platform floating structure carrying a horizontal-axis turbine by use of a tripod structure. To keep the floating structure in place, the initial design consisted of two mooring anchors connected to the front floating platforms by a catenary system and one suction caisson connected at the back platform in a tension-leg fashion. Examining past theories and tests, and using a specific dimensional analysis, we determined that circular plate anchors subjected to a vertical uplift load in a tension-leg fashion represent a good alternative (see Fig. 6.1).

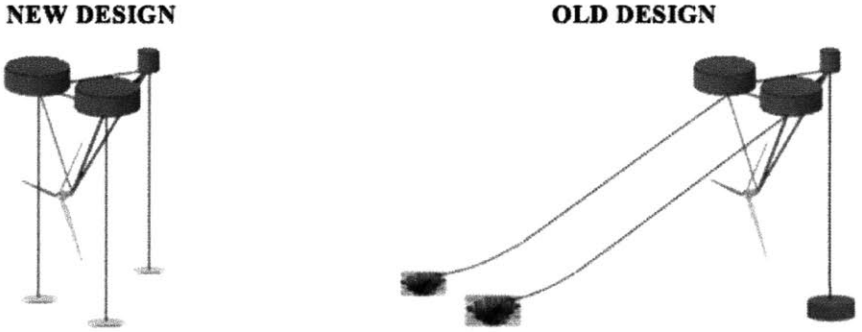

Figure 6.1: New and Old design for the anchor system that keeps the floating structure stationary.

Conventional and centrifugal model tests show that a few soil and anchor parameters affect the soil-anchor response during both static and dynamic loading. The static uplift capacity of circular anchors is a function of the diameter and embedment depth of the anchor as well as the unit weight, the friction angle, and the state of stress of the soil. This relationship has been observed by Clemence and Veesaert (1977) through numerous conventional model tests. In particular, the diameter governs the anchor capacity because it directly affects the size and weight of the soil plug within the failure surface, and it

influences the friction that develops along the same failure surface. In comparison to the static resistance, the dynamic capacity is higher. This occurs because under dynamic conditions the soil mass within the failure surface develops an inertial force and the shearing resistance along the failure surface increases due to the higher strain rate.

However, conventional model tests cannot enable one to reproduce the stress-strain soil behavior of the prototype. In contrast, the modelling-of-models approach solves this problem by taking advantage of the centrifuge and reproducing at a small scale the same stress state and distribution acting on the prototype. This approach was adopted by Ovesen (1981) who performed several centrifugal tests and succeeded in determining a more accurate equation for the vertical uplift capacity of circular anchors in sand.

The design of the circular anchors for the floating structure of the project case study has considered both theories, Clemence's and Veesaert's (1977) based on conventional tests and Ovesen's (1981) based on centrifugal tests. As expected, the theory by Clemence and Veesaert (1977) slightly overestimates the anchor capacity. In fact, this theory leads to smaller anchors than those obtained using Ovesen's (1981); therefore, the design obtained through the application of this second theory is believed to be more reliable and conservative. To meet the capacity requirements for static load (listed in Table 6.1) imposed by the structural reactions coming from the floating structure and the factor of safety suggested by API standard API-RP2SK, the first version (Version 1) of our new design led to the following anchor dimensions and embedment depth in dry soil: the circular anchors have a diameter of 3.71 m and 2.40 m for a depth of 11.14 m and 7.18 m from the mudline for the front and the back platform respectively.

Table 6.1: Required static ultimate holding capacity (UHC) for the anchors.

	Static UHC requirements	
	Front platform	Back platform
Q_d (t)	1,931	518
Q_d (kN)	18,934	5,084

To reproduce the real scenario of the Messina Strait, the anchor design has been refined to account for the presence of water, which has a significant effect on the soil unit weight (Version 2). In comparison to what was obtained for the anchor design in dry material, the new anchors have larger diameter and deeper embedment to properly withstand the same pullout force in saturated granular soil. In particular, according to this second version of our new anchor design, the circular anchors have a diameter of 4.22 m and 2.72 m for a depth of 12.67 m and 8.17 m from the mudline, respectively, for the front and the back platform.

With regard to the anchor dynamic uplift capacity, one can calculate the dynamic uplift resistance as proposed by Clemence and Veesaert (1977) and, then, correct it with the difference obtained from a comparison between Clemence's and Veesaert's (1977) theory and Ovesen's (1981) theory about the static anchor resistance. Although the anchor size increases considering the presence of water, the dynamic capacity of the circular anchors is lower than that calculated for the design version in dry soil. This occurs because the unit weight of the soil has a great impact on the dynamic resistance of the anchors: in fact, it directly influences the inertial force of the soil mass within the failure surface and the increase of the shearing resistance along the same surface due to the enhanced strain rate.

Furthermore, the effect of the ground motion on the stiffness and strength of the saturated material influences the anchor design in a positive way. The earthquake shaking causes the relative density to further increase with subsequent slight increase of G_0 (low strain shear modulus), which also increases with depth or confinement. The dilative tendency that the soil experiences at large shear strains (γ) leads to an increase in confinement or to a decrease in pore pressure with a subsequent increase in shearing resistance; however, this effect is counterbalanced by the soil buoyant unit weight that has a greater influence on the whole soil-anchor system leading to a lower capacity in dynamic conditions than under static loading.

In conclusion, Tables 6.2 and 6.3 summarize the main characteristics of the circular anchors designed according to Version 2. In addition, Table 6.2 provides a comparison

between the dimensions of these new anchors and those of the anchors belonging to the initial design.

Table 6.2:: Comparison between the volume and weight of the anchors for new design (Version 2) and the initial old design.

	NEW DESIGN		OLD DESIGN	
	Front platform	Back platform	Front platform	Back platform
	circular anchors		*drag anchor*	*suction anchor*
t (cm)	12.67	8.17	-	-
t (in)	4.99	3.22	-	-
V (m^3)	1.775	0.477	1.21	15.36
V (ft^3)	62.69	16.83	42.74	542.60
W (kN)	136.70	36.70	93.17	1,182.71
W (T)	15.36	4.13	10.47	132.94

Table 6.3: Dynamic Ultimate Holding Capacity (UHC) and corresponding requirements for the circular anchors of the new design in Version 2.

	Dynamic UHC		Dynamic UHC requirements	
	Front platform	Back platform	Front platform	Back platform
Q_d (t)	**1,960.61**	**539.88**	1,787.63	480.00
Q_d (kN)	**19,227.66**	**5,294.58**	17,531.24	4,707.36

Therefore, this new solution with circular anchors (as designed in Version 2 for saturated soil) is satisfactory for the following reasons:

- all three anchors meet the ultimate holding capacity requirements both for the static and dynamic conditions;
- the overall dimensions of the anchors are smaller than those of the drag and suction anchors developed in the initial (old) design;

- the volume of material used for producing all three anchors is much less than the volume used for the anchors provided by the initial (old) solution. The circular anchors for the front platforms are heavier than the previously assumed drag anchors, but there is an enormous saving of material for the anchor that ties the back platform;
- the transportation and installation of the anchors should be easier and faster. Their shape should allow one to transport them as a stack taking up a minimum space for several anchors, and all three anchors can be installed with the same procedure;
- the cost of purchase and installation for production on a large scale is much lower with these anchors than with the previous ones given the savings in material, transportation, and installation; and,
- the anchor system allows the floating structure to be kept in place independently of the current direction. The old solution with drag anchors relied on the most frequent current direction with possible failure of the system if the current changes direction; in fact, the drag anchors work successfully only if pulled horizontally and if the anchor fluke defines the failure wedge in the pulling direction (see Fig. 6.2).

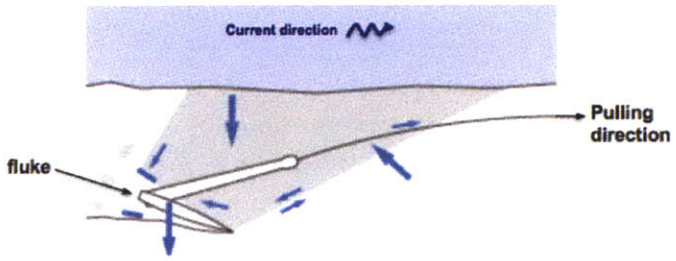

Figure 6.2: Drag anchor resistant mechanisms, (Vryhof Anchors)

6.2 Recommendations

The aim of this study has been to find, and evaluate, an alternative to the foundations employed for the floating structure located in the Messina Strait that carries a horizontal-axis marine current turbine. We predicted the vertical uplift capacity of circular anchors for this specific application through a multistep procedure. However, to prove the design

reliability, it is recommended to perform some tests and analyses before employing the designed anchor system at the real scale. Specifically:

- some centrifugal tests should be run to simulate the actual prototype conditions. These tests should consider the same non-uniform material as the material in-situ or, if run with uniform sand, the soil coefficient of uniformity should be changed from test to test to cover the range of values it can have in the field. Moreover, tests should be run using equipment to monitor the soil stresses and pore pressures during load application for both static and dynamic loading;
- few field tests should be performed accounting for the size and depth of the anchors as defined by the design. This would allow one to prove that the installation procedure works, and, then, monitor the anchor behavior in the real environment. The tests ought to apply the load both statically and dynamically stressing few anchors up to failure and few anchors up to the working load in order to verify their compliance with the safety factors used in the design requirements; and,
- additional centrifugal tests could be performed to test only the soil or the whole soil-anchor system by subjecting it to shaking events of different magnitudes. In particular, the model should be excited by the earthquake time history that is likely to hit the Messina Strait. This would allow one to confirm the anticipated dynamic soil response and eventually prove the soundness of the anchor design as a whole.

7 References

Abdellaoui Maane M., Larrecq G., Manno A., Pereira-Mosqueira F. (2010), "M.I.T. C.E.E. H.P.S. Master of Engineering Project 2010 – Marine Turbine Project," 2010.

Andreadis A., Harvey R. C., Eldon B. (1981), "Embedded Anchor Response to Uplift Loading," Journal of Geotechnical Engineering Division, Vol. 107, No. 1, 59-78, 1981.

Baker W. H., Konder T. W. (1972), "Pullout Load Capacity of a Circular Earth Anchor Buried in Sand," National Academy of Sciences, Highway Research Board, No. 108, 1-10, 1972.

Bakker T. B., De Heer M. A., Heerema A. E., Smeets P. (2006), "Suction Anchors," Offshore Enginnering, TU Delft, 2006, Web Picture. <http://www.offshoremoorings.org/moorings/2006/Groep7/index_bestanden/Page729.htm>.

Balla A. (1961), "The Resistance of Breaking-out of Mushroom Foundations for Pylons," Proceedings – Fifth International Conference on Soil Mechanics and Foundation Engineering, Paris, France, Vol. 1, 569-576, 1961.

Beard R. M. (1980), "Holding Capacity of Plate Anchors," Civil Engineering Laboratory, Technical Report No. R-882 – Port Hueneme, California, October 1980.

Bemben S. M., Kalajian E.H., Kupferman M. (1973), "The Vertical Holding Capacity of Marine Anchors in Sand and Clay Subjected to Static and Cyclic Loading," Preprints – Offshore Technology Conference, No. OTC 1912, 871-880, 1973.

Bemben S. M., Kupferman M. (1975), "The Vertical Holding Capacity of Marine Anchor Flukes Subjected to Static and Cyclic Loading," Proceedings – Offshore Technology Conference, No. OTC 2185, 363-374, 1975.

Bolton M. D. (1986), "The Strength and Dilatancy of Sands," Geotechnique, 36 (1), 65-67, 1986.

Bouazza A., Finlay T.W. (1991), "uplift capacity of plate anchors buried in two layered sand" - Geotechnique 41, No. 1, 169-170, 1991.

Buckingham E. (1914), "On Physically Similar Systems; Illustrations of the Use of Dimensional Equations," Phys. Rev., Vol. IV, no. 4, p. 345, 1914.

C&C technologies Survey Services, Web picture. <http://www.cctechnol.com/piclib/361.png>.

Clemence S. P., Veesaert C. J. (1977), "Dynamic Pullout Resistance of Anchors in Sand," Proceedings of the International Symposium on Soil-Structure Interaction, Roorkee, India, 389-397, 1977.

CNR – National Research Council, Italy

Dickin E. A., Leung C. F. (1983), "Centrifugal Model Tests on Vertical Anchor Plates," Journal of Geotechnical Engineering Division, ASCE, Vol. 109, No. 2, pp 1503-1525, 1983.

Elgamal A., Yang Z., Lai T., Kutter B. L., Wilson D. W. (2005), "Dynamic Response of Saturated Dense Sand in Laminated Centrifuge Container," Journal of Geotechnical and Geoenvironmental Engineering, Vol. 131, No. 5, pp. 598-609, ASCE, May 1, 2005.

Faccioli E. (1994), "Seismic ground amplification, stability analyses and 3-Dimensional SSI studies for the 3300 m one-span suspension bridge across the Messina Strait," 10th ECEE, Wien 28th August 1994, Balkeme, Vol. 3, pp. 1769-1779, (1994).

Ferrante G. (1988), "Comportamento in Colonna Risonante di Sabbie Frantumabili e della Ghiaia di Messina," Politecnico di Torino, Department of Structural and Geotechnical Engineering, pp. 251, (in Italian).

Flexmat Gravity Anchor, Web picture. <www.marecon.com/resources/Information%20 Document%20for%20Offshore%20Application.pdf>.

Fuglsang L. D., Ovesen N. Krebs (1988), "The Application of the Theory of Modelling to Centrifuge Studies," Centrifuge in Soil Mechanics, pp. 119-138, 1988.

Gerwick Jr. Ben. C. (1999), "Construction of Marine and Offshore Structures," 2nd Ed., 1999.

Hanna A., Ayadat T., Sabry M. (2007), "Pullout Resistance of Single Vertical Shallow Helical and Plate Anchors in Sand," Geotech Geol Eng (2007) 25: 559-573.

Hermann H. G. (1981), "Design Procedures for Embedment Anchors Subjected to Dynamic Loading Conditions," Naval Facilities Engineering Command, Alexandria, Virginia 22332 – Naval Civil Engineering Laboratory, Port Hueneme, California 93043 - Technical Report R-888, November 1981.

Houlsby G. T., Byrne B. W. (2005), "Design Procedures for Installation of Suction Caissons in Clay and Other Materials" – Proceedings of the Institution of Civil Engineers, Geotechnical Engineering 158, April 2005 Issue GE2, pages 75-82.

Hunt for the Hood, Web picture. <www.channel4.com/history/microsites/H/hood/images/ bgpictures/Dynamic_positioning_small.gif>.

Iglesia G. R., Einstein H. H., Whitman R. V., "Validation of Centrifuge Model Scaling for Soil Systems Via Trapdoor Tests."

Ismes (1985), "Indagini Geotecniche 1984-Giugno 1985 svolte in concomitanza con lo studio della fagliazione di superficie. Relazioni, tabelle e Figure riassuntive estratte dai rapporti Ismes 2685 del 15.4.85 e 2690 del 12.6.85, 1985, (in Italian).

Jamiolkowski M., Lo Presti D. C. F. (2003), "Geotechnical Characterization of Holocene and Pleistocene Messina Sand Gravel Deposits," Dpt. Of Structural and Geotechnical Engineering, Technical University of Turin, Italy – Tan M. T. S., Phoon K. K., Hight D. W., Leroueil S., "Characterisation and Engineering Properties of Natural Soil" – Vol. 2, 2003.

Lambe T. W., Whitman R. V. (1969), "Soil Mechanics," Wiley, New York, 1969.

Langhaar H. L. (1951), "Dimensional Analysis and Theory of Models," 1951.

Lee H. (2009), "How to Install Super Strength Pile or SS Pile," March 16, 2009, Web picture "Sketch for Pile Driving". <http://pile-driving.com/tag/pile/>.

Marine Sciences at UNC Chapel Hill, UNC College of Arts and Sciences, Web picture. <http://marine.unc.edu/Research/bane35>.

Matasovic N., Vucetic M. (1993), "Cyclic Characterization of Liquefiable Sands," J. Geotech. Eng., 119(11), 1805-1822, 1993.

Matsuo M. (1968), "Study of the Uplift Resistance of Footing (II)," Soils & Foundations, VIII, No. 1, March, Tokyo, 1968.

Menck, Menck Products, Web picture. <www.menck.com>.

Moore B. (2000), "Mobil Offshore Drilling Unit," Wikimedia, August, 2000, Web picture. <http://upload.wikimedia.org/wikipedia/commons/7/75/Mobile-offshore-drilling-unit.gif>.

Navarre G. (2008), "Floating Production Advances Multicolumn Floater Offers Deepwater Options," E&P magazine, September 1, 2008, Web picture. <http://www.epmag.com/Images/September/Floating-Multi-column-AGR1.jpg>.

NGI, "Suction anchor.ppt," Picture from Web presentation. <www.ead.anl.gov/new /newsdocs/Lunne_lect6_suction_anchor.pdf>.

OAC Offshore Aquaculture Consortium, "...Deploy of a Single Point Buoy (SPB) System," Web picture, 2002. <www.masgc.org>.

Ovesen N. Krebs (1981), "Centrifuge Tests of the Uplift Capacity of Anchors," Proceeding of the 10th International Conference on Soil Mechanics and Foundation Engineering, Vol. 1, pp. 717-722, 1981.

Peruzza L. (1996), "Attenuazione dell'Intensita' Macrosismica," rapporto sintetico per il GdL "Rischio Sismico," Maggio 1996. Web Map. <http://emidius.mi.ingv.it/ GNDT/PS.html>, (in Italian).

Pino N. A., Piatanesi A., Valensise G., Boschi E. (2009), "The 28 December 1908 Messina Straits Earthquake (Mw 7.1): A Great Earthquake throughout a Century of Seismology," Historical Seismologists, March/April 2009, Web picture. <www.seismosoc.org /publications/SRL/SRL_80/srl_80-2_hs.htm>, (in Italian).

Ponniah D. A., Finlay T.W. (1988), "Cyclic behavior of plate anchors," Canadian Geotechnical Journal, Vol. 25, 374-381, 1988.

Riemers M. E. (2004), "Development of The Deepwater Suction Embedded Anchor (SEA)," Marine Construction Amsterdam Conference, 10-11 March 2004.

Riemers M. E., Kirstein A. A. (1999), Moorings & Anchors Conference, "Development and Capabilities of The Suction Embedded Anchor (SEA)," Suction Pile Technology bv Paper Suction Embedded Anchor (SEA), Moorings & Anchors Conference, 22-23 November, 1999.

Roadtraffic-technology.com, "Woodrow Wilson Bridge Project, DC, USA," Web picture. <http://www.roadtraffic-technology.com/projects/woodrow_wilson/>.

Rowe R. K., Davis E. H. (1982), "The Behavior of Anchor Plates in Sand," Geotechnique 32, No. 1, 25-41, 1982.

Safaqah O. A., Gerin M. (2004), (Gerwick B. C., Inc., Oakland, CA), "Mooring Bridge Caissons During Construction Using Jetted-in Driven Plate Anchors," Geotechnical Special Publication, n. 126 II, pp 1309-1316, 2004, Geotechnical Engineering for Transportation Projects: Proceedings of Geo-Trans 2004.

Seed H. B., Idriss I. M., Kiefer F. W. (1969), "Characteristics of Rock Motions during Earthquakes," Journal of the Soil Mechanics and Foundations Division, ASCE, Vol. 95, No. SM5, pp. 1199-1218, paper No. 6783, September 1969.

Seed H. B., Tokimatsu K., Harder L. F., e Chung R. M. (1985), "The Influence of SPT procedures in soil liquefaction resistance evaluations, Journal of Geotechnical Engineering, ASCE, 111 (12), 1425-1445, 1985.

Sigh S.P., Ramaswaymy S.V. (2002), "Response of plate anchors to sustained-cyclic loading," Indian Geotechnical Journal 32, No. 2, 161-172, 2002.

Slejko D., Peruzza L., and A. Rebez with the contribution of Stucchi M., Scandone P., and Faccioli E., and collaboration of Albarello D., Bobbio M., Camassi R., Meletti C., Monachesi G., and Zerga A. (1996), in "Pericolosità Sismica del Territorio Nazionale" a cura di Dario Slejko (Osservatorio Geofisico Sperimentale di Trieste) documento consegnato al Sottosegretario per il Coordinamento della Protezione Civile il 15.07.1996 "Modalità di Attenuazione dell' Intensità Macrosismica" a cura di L. Peruzza, rapporto sintetico per il GdL "Rischio Sismico", Maggio 1996, (in Italian).

SPT Offshore, Products, Web picture. <http://www.sptoffshore.com/>.

True D. G. (1975), "Penetration of Projectiles into Seafloor Soils," Civil Engineering Laboratory, Technical Report No. R-882 – Port Hueneme, California, May 1975.

TTI Tension Technology International, Services - Mooring, Web picture, 2003. <http://www.tensiontech.com/services/mooring.html>.

U.S. Department of Transportation – Federal Highway Administration, "Begin Pile Driving," Web picture. <http://www.fhwa.dot.gov/infrastructure/tccc/tutorial/piles/pile10.htm>.

Vryhof Anchors, Web picture. <www.vryhof.com>.

Vucetic M. (1986), "Pore Pressure Buildup and Liquefaction of Level Sandy Sites During Earthquakes," PhD Thesis, Rensselaer Polytechnic Institute, Troy, N.Y., 1986.

Wikipedia, "1908 Messina Earthquake," Web picture. <http://en.wikipedia.org/wiki/1908_Messina_earthquake>.

8 Appendixes

8.1 Geological Cross-Section of the Messina Strait

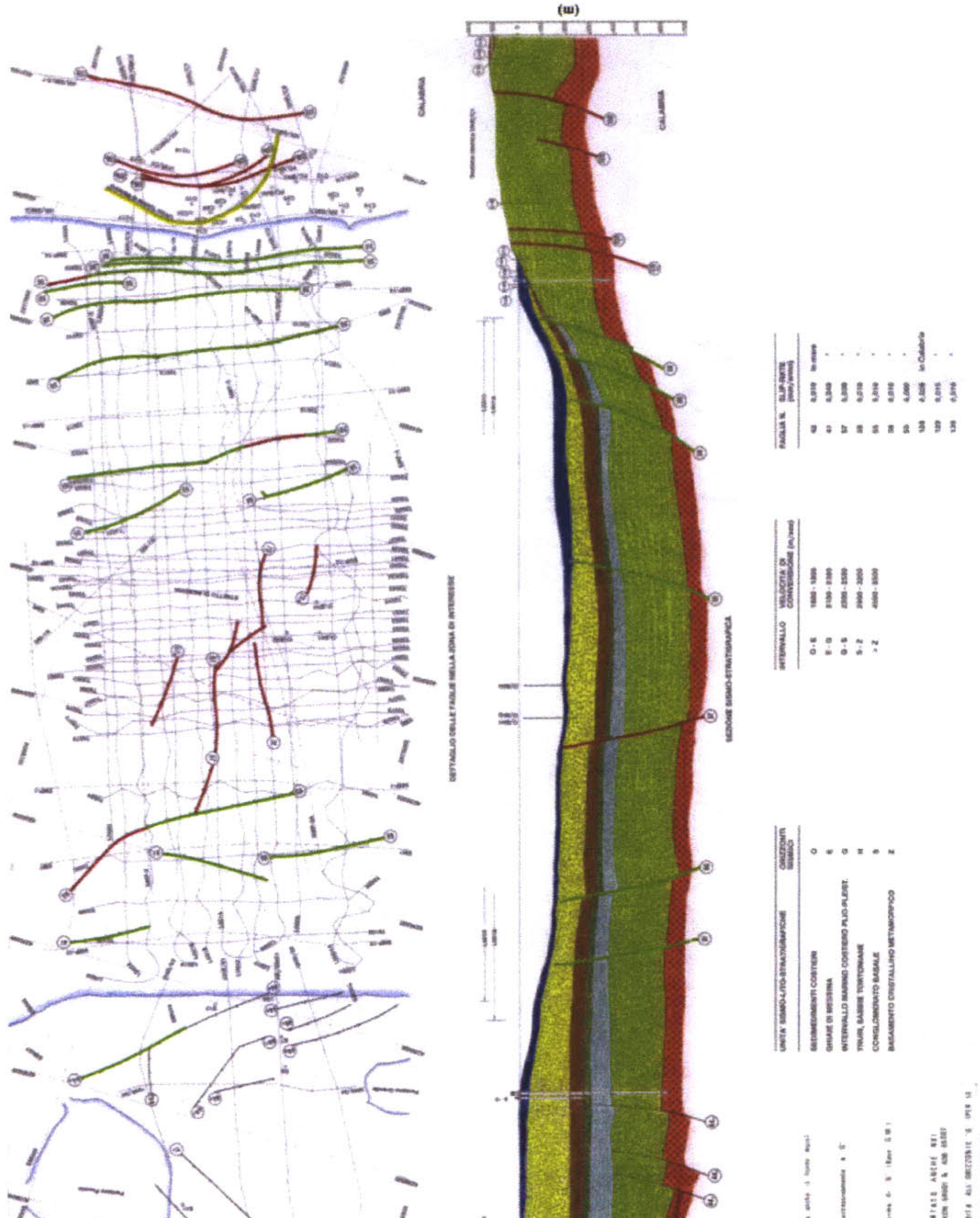

Figure 8.1: Seismic-stratigraphic cross-section and identification of faults of the Messina Strait.

8.2 Spreadsheets supporting the Conventional Modelling

S.P. Clemence & C.J. Veesaert

"Pullout Resistance of Circular Anchors in Dry Sand under Static and Cyclic Loading"

Hypotheses:

- container was 24"(61cm) x 24"(61cm) x 27"(68.5cm).
- tests were performed with half circular anchors 3"(5.67cm) and 5"(12.7cm) in diameter
- soil has a Mohr-Coulomb failure criterion

Soil Properties		Starting values	
γ_t =	soil total unit weight	17.0 kN/m3	108.2 pcf
c =	soil cohesion	0.0 kPa	0.0 psi
ϕ =	soil friction angle	39.0 °	0.7 rad
ψ =	soil dilatancy	0.0 °	0.0 rad
K_0 =	coefficient of earth pressure at rest	0.5	
D_r =	soil relative density	96%	
C_u =	coefficient of uniformity	1.39	
Anchor Properties			
B =	fluke diameter	0.057 m	0.19 ft
R =	fluke radius = B/2	0.029 m	0.09 ft
A =	fluke projected area for pullout = π*B^2/4	0.003 m2	0.027 ft2
H/B =	relative depth	(variable)	
H =	embedment depth at the fluke = H/B*B	(variable)	

Anchor static capacity

D_m = diameter of the major base of the truncated cone = B+2H*tan(ϕ/2)

R_m = radius of the major base of the truncated cone = D_m/2

V_s = volume of sand in truncated cone = (π*H/3)*(R^2+R_m^2+R*R_m)

Q_s = ultimate anchor static capacity → (see formula below)

$$Q_s = \gamma_t V_s + \gamma K_0 \tan(\phi)\cos^2\left(\frac{\phi}{2}\right)\pi\left[\frac{BH^2}{2} + \frac{H^3\tan(\phi/2)}{3}\right]$$

Anchor dynamic capacity

D_f = dynamic strain rate factor

a = accelaration of anchor in unit of g

Q_d = ultimate anchor dynamic capacity = (see formula below)

$$Q_d = \gamma_t V_s + \gamma K_0 \tan(\phi)\cos^2\left(\frac{\phi}{2}\right)\pi\left[\frac{BH^2}{H} + \frac{H^3\tan(\phi/2)}{3}\right]D_f + V_s\gamma_t a$$

Changing B and H/B

Soil Properties					*Anchor Properties*			*Anchor embedment depth*	
γ_t =	c =	ϕ =	ψ =	K_0 =	B =	R =	A =	H/B =	H =
(kN/m^3)	(kPa)	(°)	(°)	-	(m)	(m)	(m^2)	-	(m)
17	0.000	39.000	0.000	0.500	0.057	0.028	0.003	1.000	0.057
17	0.000	39.000	0.000	0.500	0.062	0.031	0.003	2.000	0.123
17	0.000	39.000	0.000	0.500	0.067	0.033	0.003	3.000	0.200
17	0.000	39.000	0.000	0.500	0.072	0.036	0.004	4.000	0.287
17	0.000	39.000	0.000	0.500	0.077	0.038	0.005	5.000	0.384
17	0.000	39.000	0.000	0.500	0.082	0.041	0.005	6.000	0.490
17	0.000	39.000	0.000	0.500	0.087	0.043	0.006	7.000	0.607
17	0.000	39.000	0.000	0.500	0.092	0.046	0.007	8.000	0.734
17	0.000	39.000	0.000	0.500	0.097	0.048	0.007	9.000	0.870
17	0.000	39.000	0.000	0.500	0.102	0.051	0.008	10.000	1.017
17	0.000	39.000	0.000	0.500	0.107	0.053	0.009	11.000	1.174
17	0.000	39.000	0.000	0.500	0.112	0.056	0.010	12.000	1.340
17	0.000	39.000	0.000	0.500	0.117	0.058	0.011	13.000	1.517
17	0.000	39.000	0.000	0.500	0.122	0.061	0.012	14.000	1.704
17	0.000	39.000	0.000	0.500	0.127	0.063	0.013	15.000	1.901
17	0.000	39.000	0.000	0.500	0.132	0.066	0.014	16.000	2.107
17	0.000	39.000	0.000	0.500	0.137	0.068	0.015	17.000	2.324
17	0.000	39.000	0.000	0.500	0.142	0.071	0.016	18.000	2.551
17	0.000	39.000	0.000	0.500	0.147	0.073	0.017	19.000	2.787
17	0.000	39.000	0.000	0.500	0.152	0.076	0.018	20.000	3.034
17	0.000	39.000	0.000	0.500	0.157	0.078	0.019	21.000	3.291
17	0.000	39.000	0.000	0.500	0.162	0.081	0.021	22.000	3.557
17	0.000	39.000	0.000	0.500	0.167	0.083	0.022	23.000	3.834
17	0.000	39.000	0.000	0.500	0.172	0.086	0.023	24.000	4.121
17	0.000	39.000	0.000	0.500	0.177	0.088	0.025	25.000	4.418
17	0.000	39.000	0.000	0.500	0.182	0.091	0.026	26.000	4.724
17	0.000	39.000	0.000	0.500	0.187	0.093	0.027	27.000	5.041

Changing B and H/B

Anchor static capacity					*Anchor dynamic capacity*			
D_m = (m)	R_m = (m)	V_s = (m^3)	Q_s = (kN)	Q_s = (t)	D_f = -	a = (g)	Q_d = (kN)	Q_d = (t)
0.097	0.048	0.000	0.007	**0.001**	1.100	0.200	0.074	**0.008**
0.149	0.075	0.001	0.033	**0.003**	1.100	0.200	0.189	**0.019**
0.208	0.104	0.003	0.099	**0.010**	1.100	0.200	0.368	**0.038**
0.275	0.137	0.008	0.238	**0.024**	1.100	0.200	0.647	**0.066**
0.348	0.174	0.015	0.499	**0.051**	1.100	0.200	1.078	**0.110**
0.429	0.214	0.029	0.948	**0.097**	1.100	0.200	1.731	**0.176**
0.517	0.258	0.051	1.676	**0.171**	1.100	0.200	2.704	**0.276**
0.611	0.306	0.084	2.800	**0.285**	1.100	0.200	4.123	**0.420**
0.713	0.357	0.134	4.472	**0.456**	1.100	0.200	6.151	**0.627**
0.822	0.411	0.205	6.880	**0.701**	1.100	0.200	8.990	**0.916**
0.938	0.469	0.305	10.257	**1.046**	1.100	0.200	12.894	**1.314**
1.061	0.531	0.441	14.887	**1.518**	1.100	0.200	18.170	**1.852**
1.191	0.596	0.624	21.111	**2.152**	1.100	0.200	25.187	**2.567**
1.328	0.664	0.866	29.331	**2.990**	1.100	0.200	34.385	**3.505**
1.473	0.736	1.180	40.025	**4.080**	1.100	0.200	46.286	**4.718**
1.624	0.812	1.583	53.745	**5.479**	1.100	0.200	61.496	**6.269**
1.783	0.891	2.093	71.136	**7.251**	1.100	0.200	80.720	**8.228**
1.948	0.974	2.732	92.934	**9.473**	1.100	0.200	104.769	**10.680**
2.121	1.060	3.525	119.985	**12.231**	1.100	0.200	134.573	**13.718**
2.300	1.150	4.499	153.245	**15.621**	1.100	0.200	171.188	**17.450**
2.487	1.244	5.687	193.798	**19.755**	1.100	0.200	215.811	**21.999**
2.681	1.341	7.123	242.861	**24.756**	1.100	0.200	269.789	**27.501**
2.882	1.441	8.848	301.798	**30.764**	1.100	0.200	334.631	**34.111**
3.090	1.545	10.906	372.128	**37.934**	1.100	0.200	412.023	**42.000**
3.305	1.653	13.347	455.539	**46.436**	1.100	0.200	503.840	**51.360**
3.528	1.764	16.224	553.899	**56.463**	1.100	0.200	612.156	**62.401**
3.757	1.878	19.598	669.267	**68.223**	1.100	0.200	739.266	**75.358**

Changing K_0 and H/B

Soil Properties					*Anchor Properties*			*Anchor embedment depth*	
γ_t =	c =	ϕ =	ψ =	K_0 =	B =	R =	A =	H/B =	H =
(kN/m^3)	(kPa)	(°)	(°)	-	(m)	(m)	(m^2)	-	(m)
17	0.000	39.000	0.000	0.300	0.057	0.029	0.003	1.000	0.057
17	0.000	39.000	0.000	0.325	0.057	0.029	0.003	2.000	0.114
17	0.000	39.000	0.000	0.350	0.057	0.029	0.003	3.000	0.171
17	0.000	39.000	0.000	0.375	0.057	0.029	0.003	4.000	0.228
17	0.000	39.000	0.000	0.400	0.057	0.029	0.003	5.000	0.285
17	0.000	39.000	0.000	0.425	0.057	0.029	0.003	6.000	0.342
17	0.000	39.000	0.000	0.450	0.057	0.029	0.003	7.000	0.399
17	0.000	39.000	0.000	0.475	0.057	0.029	0.003	8.000	0.456
17	0.000	39.000	0.000	0.500	0.057	0.029	0.003	9.000	0.513
17	0.000	39.000	0.000	0.525	0.057	0.029	0.003	10.000	0.570
17	0.000	39.000	0.000	0.550	0.057	0.029	0.003	11.000	0.627
17	0.000	39.000	0.000	0.575	0.057	0.029	0.003	12.000	0.684
17	0.000	39.000	0.000	0.600	0.057	0.029	0.003	13.000	0.741
17	0.000	39.000	0.000	0.625	0.057	0.029	0.003	14.000	0.798
17	0.000	39.000	0.000	0.650	0.057	0.029	0.003	15.000	0.855
17	0.000	39.000	0.000	0.675	0.057	0.029	0.003	16.000	0.912
17	0.000	39.000	0.000	0.700	0.057	0.029	0.003	17.000	0.969
17	0.000	39.000	0.000	0.725	0.057	0.029	0.003	18.000	1.026
17	0.000	39.000	0.000	0.750	0.057	0.029	0.003	19.000	1.083
17	0.000	39.000	0.000	0.775	0.057	0.029	0.003	20.000	1.140
17	0.000	39.000	0.000	0.800	0.057	0.029	0.003	21.000	1.197
17	0.000	39.000	0.000	0.825	0.057	0.029	0.003	22.000	1.254
17	0.000	39.000	0.000	0.850	0.057	0.029	0.003	23.000	1.311
17	0.000	39.000	0.000	0.875	0.057	0.029	0.003	24.000	1.368
17	0.000	39.000	0.000	0.900	0.057	0.029	0.003	25.000	1.425
17	0.000	39.000	0.000	0.925	0.057	0.029	0.003	26.000	1.482
17	0.000	39.000	0.000	0.950	0.057	0.029	0.003	27.000	1.539

Changing K_0 and H/B

Anchor static capacity					*Anchor dynamic capacity*			
D_m = (m)	R_m = (m)	V_s = (m^3)	Q_s = (kN)	Q_s = (t)	D_f = -	a = (g)	Q_d = (kN)	Q_d = (t)
0.097	0.049	0.000	0.006	**0.001**	1.100	0.200	0.047	**0.005**
0.138	0.069	0.001	0.022	**0.002**	1.100	0.200	0.110	**0.011**
0.178	0.089	0.002	0.053	**0.005**	1.100	0.200	0.194	**0.020**
0.218	0.109	0.004	0.106	**0.011**	1.100	0.200	0.305	**0.031**
0.259	0.129	0.006	0.185	**0.019**	1.100	0.200	0.450	**0.046**
0.299	0.150	0.010	0.299	**0.030**	1.100	0.200	0.636	**0.065**
0.340	0.170	0.014	0.453	**0.046**	1.100	0.200	0.869	**0.089**
0.380	0.190	0.020	0.656	**0.067**	1.100	0.200	1.159	**0.118**
0.420	0.210	0.027	0.916	**0.093**	1.100	0.200	1.513	**0.154**
0.461	0.230	0.036	1.241	**0.127**	1.100	0.200	1.942	**0.198**
0.501	0.251	0.046	1.641	**0.167**	1.100	0.200	2.455	**0.250**
0.541	0.271	0.059	2.126	**0.217**	1.100	0.200	3.061	**0.312**
0.582	0.291	0.073	2.705	**0.276**	1.100	0.200	3.773	**0.385**
0.622	0.311	0.089	3.389	**0.345**	1.100	0.200	4.601	**0.469**
0.663	0.331	0.107	4.190	**0.427**	1.100	0.200	5.558	**0.567**
0.703	0.351	0.128	5.119	**0.522**	1.100	0.200	6.656	**0.678**
0.743	0.372	0.152	6.188	**0.631**	1.100	0.200	7.908	**0.806**
0.784	0.392	0.178	7.411	**0.755**	1.100	0.200	9.327	**0.951**
0.824	0.412	0.207	8.800	**0.897**	1.100	0.200	10.929	**1.114**
0.864	0.432	0.239	10.369	**1.057**	1.100	0.200	12.727	**1.297**
0.905	0.452	0.274	12.132	**1.237**	1.100	0.200	14.737	**1.502**
0.945	0.473	0.312	14.105	**1.438**	1.100	0.200	16.975	**1.730**
0.985	0.493	0.354	16.301	**1.662**	1.100	0.200	19.458	**1.983**
1.026	0.513	0.399	18.738	**1.910**	1.100	0.200	22.202	**2.263**
1.066	0.533	0.448	21.431	**2.185**	1.100	0.200	25.224	**2.571**
1.107	0.553	0.501	24.397	**2.487**	1.100	0.200	28.544	**2.910**
1.147	0.573	0.558	27.654	**2.819**	1.100	0.200	32.179	**3.280**

Changing ϕ and H/B

Soil Properties					*Anchor Properties*			*Anchor embedment depth*	
γ_t =	c =	ϕ =	ψ =	K_0 =	B =	R =	A =	H/B =	H =
(kN/m^3)	(kPa)	(°)	(°)	-	(m)	(m)	(m^2)	-	(m)
17	0.000	39.000	0.000	0.500	0.057	0.028	0.003	1.000	0.057
17	0.000	39.100	0.000	0.500	0.057	0.028	0.003	2.000	0.113
17	0.000	39.200	0.000	0.500	0.057	0.028	0.003	3.000	0.170
17	0.000	39.300	0.000	0.500	0.057	0.028	0.003	4.000	0.227
17	0.000	39.400	0.000	0.500	0.057	0.028	0.003	5.000	0.284
17	0.000	39.500	0.000	0.500	0.057	0.028	0.003	6.000	0.340
17	0.000	39.600	0.000	0.500	0.057	0.028	0.003	7.000	0.397
17	0.000	39.700	0.000	0.500	0.057	0.028	0.003	8.000	0.454
17	0.000	39.800	0.000	0.500	0.057	0.028	0.003	9.000	0.510
17	0.000	39.900	0.000	0.500	0.057	0.028	0.003	10.000	0.567
17	0.000	40.000	0.000	0.500	0.057	0.028	0.003	11.000	0.624
17	0.000	40.100	0.000	0.500	0.057	0.028	0.003	12.000	0.680
17	0.000	40.200	0.000	0.500	0.057	0.028	0.003	13.000	0.737
17	0.000	40.300	0.000	0.500	0.057	0.028	0.003	14.000	0.794
17	0.000	40.400	0.000	0.500	0.057	0.028	0.003	15.000	0.851
17	0.000	40.500	0.000	0.500	0.057	0.028	0.003	16.000	0.907
17	0.000	40.600	0.000	0.500	0.057	0.028	0.003	17.000	0.964
17	0.000	40.700	0.000	0.500	0.057	0.028	0.003	18.000	1.021
17	0.000	40.800	0.000	0.500	0.057	0.028	0.003	19.000	1.077
17	0.000	40.900	0.000	0.500	0.057	0.028	0.003	20.000	1.134
17	0.000	41.000	0.000	0.500	0.057	0.028	0.003	21.000	1.191
17	0.000	41.100	0.000	0.500	0.057	0.028	0.003	22.000	1.247
17	0.000	41.200	0.000	0.500	0.057	0.028	0.003	23.000	1.304
17	0.000	41.300	0.000	0.500	0.057	0.028	0.003	24.000	1.361
17	0.000	41.400	0.000	0.500	0.057	0.028	0.003	25.000	1.418
17	0.000	41.500	0.000	0.500	0.057	0.028	0.003	26.000	1.474
17	0.000	41.600	0.000	0.500	0.057	0.028	0.003	27.000	1.531

Changing ϕ and H/B

Anchor static capacity					*Anchor dynamic capacity*			
D_m = (m)	R_m = (m)	V_s = (m^3)	Q_s = (kN)	Q_s = (t)	D_f = -	a = (g)	Q_d = (kN)	Q_d = (t)
0.097	0.048	0.000	0.007	**0.001**	1.100	0.200	0.074	**0.008**
0.137	0.069	0.001	0.025	**0.003**	1.100	0.200	0.158	**0.016**
0.178	0.089	0.002	0.061	**0.006**	1.100	0.200	0.258	**0.026**
0.219	0.109	0.004	0.119	**0.012**	1.100	0.200	0.381	**0.039**
0.260	0.130	0.006	0.205	**0.021**	1.100	0.200	0.531	**0.054**
0.301	0.150	0.010	0.324	**0.033**	1.100	0.200	0.716	**0.073**
0.342	0.171	0.015	0.481	**0.049**	1.100	0.200	0.942	**0.096**
0.384	0.192	0.020	0.683	**0.070**	1.100	0.200	1.215	**0.124**
0.426	0.213	0.028	0.935	**0.095**	1.100	0.200	1.543	**0.157**
0.468	0.234	0.037	1.244	**0.127**	1.100	0.200	1.931	**0.197**
0.511	0.255	0.048	1.614	**0.165**	1.100	0.200	2.386	**0.243**
0.553	0.277	0.061	2.053	**0.209**	1.100	0.200	2.917	**0.297**
0.596	0.298	0.076	2.566	**0.262**	1.100	0.200	3.529	**0.360**
0.639	0.320	0.093	3.161	**0.322**	1.100	0.200	4.231	**0.431**
0.683	0.341	0.113	3.843	**0.392**	1.100	0.200	5.030	**0.513**
0.726	0.363	0.136	4.619	**0.471**	1.100	0.200	5.933	**0.605**
0.770	0.385	0.161	5.497	**0.560**	1.100	0.200	6.948	**0.708**
0.814	0.407	0.190	6.482	**0.661**	1.100	0.200	8.083	**0.824**
0.858	0.429	0.222	7.583	**0.773**	1.100	0.200	9.347	**0.953**
0.902	0.451	0.258	8.806	**0.898**	1.100	0.200	10.747	**1.095**
0.947	0.474	0.297	10.158	**1.035**	1.100	0.200	12.291	**1.253**
0.992	0.496	0.341	11.648	**1.187**	1.100	0.200	13.990	**1.426**
1.037	0.519	0.388	13.282	**1.354**	1.100	0.200	15.850	**1.616**
1.082	0.541	0.440	15.068	**1.536**	1.100	0.200	17.880	**1.823**
1.128	0.564	0.497	17.014	**1.734**	1.100	0.200	20.091	**2.048**
1.174	0.587	0.559	19.129	**1.950**	1.100	0.200	22.491	**2.293**
1.220	0.610	0.625	21.420	**2.183**	1.100	0.200	25.089	**2.557**

Changing γ and H/B

Soil Properties					*Anchor Properties*			*Anchor embedment depth*	
γ_t =	c =	ϕ =	ψ =	K_0 =	B =	R =	A =	H/B =	H =
(kN/m^3)	(kPa)	(°)	(°)	-	(m)	(m)	(m^2)	-	(m)
17	0.000	39.000	0.000	0.500	0.057	0.028	0.003	1.000	0.057
17.1	0.000	39.000	0.000	0.500	0.057	0.028	0.003	2.000	0.113
17.2	1.000	39.000	0.000	0.500	0.057	0.028	0.003	3.000	0.170
17.3	2.000	39.000	0.000	0.500	0.057	0.028	0.003	4.000	0.227
17.4	3.000	39.000	0.000	0.500	0.057	0.028	0.003	5.000	0.284
17.5	4.000	39.000	0.000	0.500	0.057	0.028	0.003	6.000	0.340
17.6	5.000	39.000	0.000	0.500	0.057	0.028	0.003	7.000	0.397
17.7	6.000	39.000	0.000	0.500	0.057	0.028	0.003	8.000	0.454
17.8	7.000	39.000	0.000	0.500	0.057	0.028	0.003	9.000	0.510
17.9	8.000	39.000	0.000	0.500	0.057	0.028	0.003	10.000	0.567
18	9.000	39.000	0.000	0.500	0.057	0.028	0.003	11.000	0.624
18.1	10.000	39.000	0.000	0.500	0.057	0.028	0.003	12.000	0.680
18.2	11.000	39.000	0.000	0.500	0.057	0.028	0.003	13.000	0.737
18.3	12.000	39.000	0.000	0.500	0.057	0.028	0.003	14.000	0.794
18.4	13.000	39.000	0.000	0.500	0.057	0.028	0.003	15.000	0.851
18.5	14.000	39.000	0.000	0.500	0.057	0.028	0.003	16.000	0.907
18.6	15.000	39.000	0.000	0.500	0.057	0.028	0.003	17.000	0.964
18.7	16.000	39.000	0.000	0.500	0.057	0.028	0.003	18.000	1.021
18.8	17.000	39.000	0.000	0.500	0.057	0.028	0.003	19.000	1.077
18.9	18.000	39.000	0.000	0.500	0.057	0.028	0.003	20.000	1.134
19	19.000	39.000	0.000	0.500	0.057	0.028	0.003	21.000	1.191
19.1	20.000	39.000	0.000	0.500	0.057	0.028	0.003	22.000	1.247
19.2	21.000	39.000	0.000	0.500	0.057	0.028	0.003	23.000	1.304
19.3	22.000	39.000	0.000	0.500	0.057	0.028	0.003	24.000	1.361
19.4	23.000	39.000	0.000	0.500	0.057	0.028	0.003	25.000	1.418
19.5	24.000	39.000	0.000	0.500	0.057	0.028	0.003	26.000	1.474
19.6	25.000	39.000	0.000	0.500	0.057	0.028	0.003	27.000	1.531

Changing γ and H/B

Anchor static capacity					*Anchor dynamic capacity*			
D_m = (m)	R_m = (m)	V_s = (m^3)	Q_s = (kN)	Q_s = (t)	D_f = -	a = (g)	Q_d = (kN)	Q_d = (t)
0.097	0.048	0.000	0.007	**0.001**	1.100	0.200	0.074	**0.008**
0.137	0.069	0.001	0.025	**0.003**	1.100	0.200	0.158	**0.016**
0.177	0.089	0.002	0.061	**0.006**	1.100	0.200	0.260	**0.026**
0.217	0.109	0.004	0.120	**0.012**	1.100	0.200	0.384	**0.039**
0.257	0.129	0.006	0.206	**0.021**	1.100	0.200	0.536	**0.055**
0.298	0.149	0.010	0.326	**0.033**	1.100	0.200	0.724	**0.074**
0.338	0.169	0.014	0.485	**0.049**	1.100	0.200	0.953	**0.097**
0.378	0.189	0.020	0.689	**0.070**	1.100	0.200	1.231	**0.125**
0.418	0.209	0.027	0.944	**0.096**	1.100	0.200	1.563	**0.159**
0.458	0.229	0.036	1.255	**0.128**	1.100	0.200	1.957	**0.199**
0.498	0.249	0.046	1.630	**0.166**	1.100	0.200	2.420	**0.247**
0.539	0.269	0.058	2.073	**0.211**	1.100	0.200	2.958	**0.302**
0.579	0.289	0.072	2.592	**0.264**	1.100	0.200	3.579	**0.365**
0.619	0.309	0.088	3.193	**0.325**	1.100	0.200	4.290	**0.437**
0.659	0.330	0.106	3.883	**0.396**	1.100	0.200	5.099	**0.520**
0.699	0.350	0.126	4.667	**0.476**	1.100	0.200	6.014	**0.613**
0.739	0.370	0.149	5.554	**0.566**	1.100	0.200	7.042	**0.718**
0.780	0.390	0.175	6.550	**0.668**	1.100	0.200	8.191	**0.835**
0.820	0.410	0.204	7.661	**0.781**	1.100	0.200	9.469	**0.965**
0.860	0.430	0.235	8.896	**0.907**	1.100	0.200	10.884	**1.109**
0.900	0.450	0.269	10.261	**1.046**	1.100	0.200	12.444	**1.269**
0.940	0.470	0.307	11.764	**1.199**	1.100	0.200	14.159	**1.443**
0.980	0.490	0.348	13.413	**1.367**	1.100	0.200	16.036	**1.635**
1.020	0.510	0.393	15.214	**1.551**	1.100	0.200	18.085	**1.844**
1.061	0.530	0.441	17.176	**1.751**	1.100	0.200	20.314	**2.071**
1.101	0.550	0.493	19.306	**1.968**	1.100	0.200	22.731	**2.317**
1.141	0.570	0.549	21.613	**2.203**	1.100	0.200	25.347	**2.584**

Changing D_f and H/B

Soil Properties					*Anchor Properties*			*Anchor embedment depth*	
γ_t =	c =	ϕ =	ψ =	K_0 =	B =	R =	A =	H/B =	H =
(kN/m^3)	(kPa)	(°)	(°)	-	(m)	(m)	(m^2)	-	(m)
17	0.000	39.000	0.000	0.500	0.057	0.028	0.003	1.000	0.057
17	0.000	39.000	0.000	0.500	0.057	0.028	0.003	2.000	0.113
17	0.000	39.000	0.000	0.500	0.057	0.028	0.003	3.000	0.170
17	0.000	39.000	0.000	0.500	0.057	0.028	0.003	4.000	0.227
17	0.000	39.000	0.000	0.500	0.057	0.028	0.003	5.000	0.284
17	0.000	39.000	0.000	0.500	0.057	0.028	0.003	6.000	0.340
17	0.000	39.000	0.000	0.500	0.057	0.028	0.003	7.000	0.397
17	0.000	39.000	0.000	0.500	0.057	0.028	0.003	8.000	0.454
17	0.000	39.000	0.000	0.500	0.057	0.028	0.003	9.000	0.510
17	0.000	39.000	0.000	0.500	0.057	0.028	0.003	10.000	0.567
17	0.000	39.000	0.000	0.500	0.057	0.028	0.003	11.000	0.624
17	0.000	39.000	0.000	0.500	0.057	0.028	0.003	12.000	0.680
17	0.000	39.000	0.000	0.500	0.057	0.028	0.003	13.000	0.737
17	0.000	39.000	0.000	0.500	0.057	0.028	0.003	14.000	0.794
17	0.000	39.000	0.000	0.500	0.057	0.028	0.003	15.000	0.851
17	0.000	39.000	0.000	0.500	0.057	0.028	0.003	16.000	0.907
17	0.000	39.000	0.000	0.500	0.057	0.028	0.003	17.000	0.964
17	0.000	39.000	0.000	0.500	0.057	0.028	0.003	18.000	1.021
17	0.000	39.000	0.000	0.500	0.057	0.028	0.003	19.000	1.077
17	0.000	39.000	0.000	0.500	0.057	0.028	0.003	20.000	1.134
17	0.000	39.000	0.000	0.500	0.057	0.028	0.003	21.000	1.191
17	0.000	39.000	0.000	0.500	0.057	0.028	0.003	22.000	1.247
17	0.000	39.000	0.000	0.500	0.057	0.028	0.003	23.000	1.304
17	0.000	39.000	0.000	0.500	0.057	0.028	0.003	24.000	1.361
17	0.000	39.000	0.000	0.500	0.057	0.028	0.003	25.000	1.418
17	0.000	39.000	0.000	0.500	0.057	0.028	0.003	26.000	1.474
17	0.000	39.000	0.000	0.500	0.057	0.028	0.003	27.000	1.531

Changing D_f and H/B

Anchor static capacity					*Anchor dynamic capacity*			
D_m = (m)	R_m = (m)	V_s = (m^3)	Q_s = (kN)	Q_s = (t)	D_f = -	a = (g)	Q_d = (kN)	Q_d = (t)
0.097	0.048	0.000	0.007	**0.001**	1.100	0.200	0.074	**0.008**
0.137	0.069	0.001	0.025	**0.003**	1.200	0.200	0.170	**0.017**
0.177	0.089	0.002	0.061	**0.006**	1.300	0.200	0.296	**0.030**
0.217	0.109	0.004	0.118	**0.012**	1.400	0.200	0.459	**0.047**
0.257	0.129	0.006	0.202	**0.021**	1.500	0.200	0.668	**0.068**
0.298	0.149	0.010	0.317	**0.032**	1.600	0.200	0.933	**0.095**
0.338	0.169	0.014	0.469	**0.048**	1.700	0.200	1.265	**0.129**
0.378	0.189	0.020	0.662	**0.067**	1.800	0.200	1.676	**0.171**
0.418	0.209	0.027	0.901	**0.092**	1.900	0.200	2.179	**0.222**
0.458	0.229	0.036	1.192	**0.122**	2.000	0.200	2.787	**0.284**
0.498	0.249	0.046	1.539	**0.157**	2.100	0.200	3.515	**0.358**
0.539	0.269	0.058	1.947	**0.198**	2.200	0.200	4.379	**0.446**
0.579	0.289	0.072	2.421	**0.247**	2.300	0.200	5.397	**0.550**
0.619	0.309	0.088	2.966	**0.302**	2.400	0.200	6.585	**0.671**
0.659	0.330	0.106	3.587	**0.366**	2.500	0.200	7.962	**0.812**
0.699	0.350	0.126	4.289	**0.437**	2.600	0.200	9.549	**0.973**
0.739	0.370	0.149	5.076	**0.517**	2.700	0.200	11.366	**1.159**
0.780	0.390	0.175	5.954	**0.607**	2.800	0.200	13.435	**1.370**
0.820	0.410	0.204	6.928	**0.706**	2.900	0.200	15.779	**1.608**
0.860	0.430	0.235	8.002	**0.816**	3.000	0.200	18.421	**1.878**
0.900	0.450	0.269	9.181	**0.936**	3.100	0.200	21.387	**2.180**
0.940	0.470	0.307	10.471	**1.067**	3.200	0.200	24.701	**2.518**
0.980	0.490	0.348	11.876	**1.211**	3.300	0.200	28.391	**2.894**
1.020	0.510	0.393	13.401	**1.366**	3.400	0.200	32.485	**3.311**
1.061	0.530	0.441	15.051	**1.534**	3.500	0.200	37.011	**3.773**
1.101	0.550	0.493	16.831	**1.716**	3.600	0.200	41.998	**4.281**
1.141	0.570	0.549	18.746	**1.911**	3.700	0.200	47.479	**4.840**

Changing *a* and H/B

Soil Properties					*Anchor Properties*			*Anchor embedment depth*	
γ_t =	c =	ϕ =	ψ =	K_0 =	B =	R =	A =	H/B =	H =
(kN/m^3)	(kPa)	(°)	(°)	-	(m)	(m)	(m^2)	-	(m)
17	0.000	39.000	0.000	0.500	0.057	0.028	0.003	1.000	0.057
17	0.000	39.000	0.000	0.500	0.057	0.028	0.003	2.000	0.113
17	0.000	39.000	0.000	0.500	0.057	0.028	0.003	3.000	0.170
17	0.000	39.000	0.000	0.500	0.057	0.028	0.003	4.000	0.227
17	0.000	39.000	0.000	0.500	0.057	0.028	0.003	5.000	0.284
17	0.000	39.000	0.000	0.500	0.057	0.028	0.003	6.000	0.340
17	0.000	39.000	0.000	0.500	0.057	0.028	0.003	7.000	0.397
17	0.000	39.000	0.000	0.500	0.057	0.028	0.003	8.000	0.454
17	0.000	39.000	0.000	0.500	0.057	0.028	0.003	9.000	0.510
17	0.000	39.000	0.000	0.500	0.057	0.028	0.003	10.000	0.567
17	0.000	39.000	0.000	0.500	0.057	0.028	0.003	11.000	0.624
17	0.000	39.000	0.000	0.500	0.057	0.028	0.003	12.000	0.680
17	0.000	39.000	0.000	0.500	0.057	0.028	0.003	13.000	0.737
17	0.000	39.000	0.000	0.500	0.057	0.028	0.003	14.000	0.794
17	0.000	39.000	0.000	0.500	0.057	0.028	0.003	15.000	0.851
17	0.000	39.000	0.000	0.500	0.057	0.028	0.003	16.000	0.907
17	0.000	39.000	0.000	0.500	0.057	0.028	0.003	17.000	0.964
17	0.000	39.000	0.000	0.500	0.057	0.028	0.003	18.000	1.021
17	0.000	39.000	0.000	0.500	0.057	0.028	0.003	19.000	1.077
17	0.000	39.000	0.000	0.500	0.057	0.028	0.003	20.000	1.134
17	0.000	39.000	0.000	0.500	0.057	0.028	0.003	21.000	1.191
17	0.000	39.000	0.000	0.500	0.057	0.028	0.003	22.000	1.247
17	0.000	39.000	0.000	0.500	0.057	0.028	0.003	23.000	1.304
17	0.000	39.000	0.000	0.500	0.057	0.028	0.003	24.000	1.361
17	0.000	39.000	0.000	0.500	0.057	0.028	0.003	25.000	1.418
17	0.000	39.000	0.000	0.500	0.057	0.028	0.003	26.000	1.474
17	0.000	39.000	0.000	0.500	0.057	0.028	0.003	27.000	1.531

Changing *a* and H/B

Anchor static capacity					*Anchor dynamic capacity*			
D_m = (m)	R_m = (m)	V_s = (m^3)	Q_s = (kN)	Q_s = (t)	D_f = -	a = (g)	Q_d = (kN)	Q_d = (t)
0.097	0.048	0.000	0.007	**0.001**	1.100	0.200	0.074	**0.008**
0.137	0.069	0.001	0.025	**0.003**	1.100	0.210	0.158	**0.016**
0.177	0.089	0.002	0.061	**0.006**	1.100	0.220	0.257	**0.026**
0.217	0.109	0.004	0.118	**0.012**	1.100	0.230	0.379	**0.039**
0.257	0.129	0.006	0.202	**0.021**	1.100	0.240	0.528	**0.054**
0.298	0.149	0.010	0.317	**0.032**	1.100	0.250	0.712	**0.073**
0.338	0.169	0.014	0.469	**0.048**	1.100	0.260	0.935	**0.095**
0.378	0.189	0.020	0.662	**0.067**	1.100	0.270	1.206	**0.123**
0.418	0.209	0.027	0.901	**0.092**	1.100	0.280	1.530	**0.156**
0.458	0.229	0.036	1.192	**0.122**	1.100	0.290	1.913	**0.195**
0.498	0.249	0.046	1.539	**0.157**	1.100	0.300	2.363	**0.241**
0.539	0.269	0.058	1.947	**0.198**	1.100	0.310	2.886	**0.294**
0.579	0.289	0.072	2.421	**0.247**	1.100	0.320	3.489	**0.356**
0.619	0.309	0.088	2.966	**0.302**	1.100	0.330	4.179	**0.426**
0.659	0.330	0.106	3.587	**0.366**	1.100	0.340	4.963	**0.506**
0.699	0.350	0.126	4.289	**0.437**	1.100	0.350	5.848	**0.596**
0.739	0.370	0.149	5.076	**0.517**	1.100	0.360	6.842	**0.697**
0.780	0.390	0.175	5.954	**0.607**	1.100	0.370	7.952	**0.811**
0.820	0.410	0.204	6.928	**0.706**	1.100	0.380	9.185	**0.936**
0.860	0.430	0.235	8.002	**0.816**	1.100	0.390	10.548	**1.075**
0.900	0.450	0.269	9.181	**0.936**	1.100	0.400	12.051	**1.228**
0.940	0.470	0.307	10.471	**1.067**	1.100	0.410	13.699	**1.396**
0.980	0.490	0.348	11.876	**1.211**	1.100	0.420	15.501	**1.580**
1.020	0.510	0.393	13.401	**1.366**	1.100	0.430	17.465	**1.780**
1.061	0.530	0.441	15.051	**1.534**	1.100	0.440	19.600	**1.998**
1.101	0.550	0.493	16.831	**1.716**	1.100	0.450	21.912	**2.234**
1.141	0.570	0.549	18.746	**1.911**	1.100	0.460	24.411	**2.488**

BASIC CASE B1=5.67 cm

Soil Properties					*Anchor Properties*			*Anchor embedment depth*	
γ_t =	c =	ϕ =	ψ =	K_0 =	B =	R =	A =	H/B =	H =
(kN/m^3)	(kPa)	(°)	(°)	-	(m)	(m)	(m^2)	-	(m)
17	0.000	39.000	0.000	0.500	0.057	0.028	0.003	3.000	0.170
17	0.000	39.000	0.000	0.500	0.057	0.028	0.003	4.000	0.227
17	0.000	39.000	0.000	0.500	0.057	0.028	0.003	5.000	0.284
17	0.000	39.000	0.000	0.500	0.057	0.028	0.003	6.000	0.340
17	0.000	39.000	0.000	0.500	0.057	0.028	0.003	7.000	0.397
17	0.000	39.000	0.000	0.500	0.057	0.028	0.003	8.000	0.454
17	0.000	39.000	0.000	0.500	0.057	0.028	0.003	9.000	0.510
17	0.000	39.000	0.000	0.500	0.057	0.028	0.003	10.000	0.567
17	0.000	39.000	0.000	0.500	0.057	0.028	0.003	11.000	0.624
17	0.000	39.000	0.000	0.500	0.057	0.028	0.003	12.000	0.680
17	0.000	39.000	0.000	0.500	0.057	0.028	0.003	13.000	0.737
17	0.000	39.000	0.000	0.500	0.057	0.028	0.003	14.000	0.794
17	0.000	39.000	0.000	0.500	0.057	0.028	0.003	15.000	0.851
17	0.000	39.000	0.000	0.500	0.057	0.028	0.003	16.000	0.907
17	0.000	39.000	0.000	0.500	0.057	0.028	0.003	17.000	0.964
17	0.000	39.000	0.000	0.500	0.057	0.028	0.003	18.000	1.021
17	0.000	39.000	0.000	0.500	0.057	0.028	0.003	19.000	1.077
17	0.000	39.000	0.000	0.500	0.057	0.028	0.003	20.000	1.134
17	0.000	39.000	0.000	0.500	0.057	0.028	0.003	21.000	1.191
17	0.000	39.000	0.000	0.500	0.057	0.028	0.003	22.000	1.247
17	0.000	39.000	0.000	0.500	0.057	0.028	0.003	23.000	1.304
17	0.000	39.000	0.000	0.500	0.057	0.028	0.003	24.000	1.361
17	0.000	39.000	0.000	0.500	0.057	0.028	0.003	25.000	1.418
17	0.000	39.000	0.000	0.500	0.057	0.028	0.003	26.000	1.474
17	0.000	39.000	0.000	0.500	0.057	0.028	0.003	27.000	1.531

BASIC CASE B1=5.67 cm								
Anchor static capacity					*Anchor dynamic capacity*			
D_m = (m)	R_m = (m)	V_s = (m^3)	Q_s = (kN)	Q_s = (t)	D_f = -	a = (g)	Q_d = (kN)	Q_d = (t)
0.177	0.089	0.002	0.061	**0.01**	1.100	0.200	0.257	**0.03**
0.217	0.109	0.004	0.118	**0.01**	1.100	0.200	0.377	**0.04**
0.257	0.129	0.006	0.202	**0.02**	1.100	0.200	0.524	**0.05**
0.298	0.149	0.010	0.317	**0.03**	1.100	0.200	0.703	**0.07**
0.338	0.169	0.014	0.469	**0.05**	1.100	0.200	0.921	**0.09**
0.378	0.189	0.020	0.662	**0.07**	1.100	0.200	1.182	**0.12**
0.418	0.209	0.027	0.901	**0.09**	1.100	0.200	1.493	**0.15**
0.458	0.229	0.036	1.192	**0.12**	1.100	0.200	1.859	**0.19**
0.498	0.249	0.046	1.539	**0.16**	1.100	0.200	2.285	**0.23**
0.539	0.269	0.058	1.947	**0.20**	1.100	0.200	2.778	**0.28**
0.579	0.289	0.072	2.421	**0.25**	1.100	0.200	3.343	**0.34**
0.619	0.309	0.088	2.966	**0.30**	1.100	0.200	3.985	**0.41**
0.659	0.330	0.106	3.587	**0.37**	1.100	0.200	4.711	**0.48**
0.699	0.350	0.126	4.289	**0.44**	1.100	0.200	5.526	**0.56**
0.739	0.370	0.149	5.076	**0.52**	1.100	0.200	6.436	**0.66**
0.780	0.390	0.175	5.954	**0.61**	1.100	0.200	7.446	**0.76**
0.820	0.410	0.204	6.928	**0.71**	1.100	0.200	8.562	**0.87**
0.860	0.430	0.235	8.002	**0.82**	1.100	0.200	9.790	**1.00**
0.900	0.450	0.269	9.181	**0.94**	1.100	0.200	11.135	**1.14**
0.940	0.470	0.307	10.471	**1.07**	1.100	0.200	12.602	**1.28**
0.980	0.490	0.348	11.876	**1.21**	1.100	0.200	14.199	**1.45**
1.020	0.510	0.393	13.401	**1.37**	1.100	0.200	15.930	**1.62**
1.061	0.530	0.441	15.051	**1.53**	1.100	0.200	17.800	**1.81**
1.101	0.550	0.493	16.831	**1.72**	1.100	0.200	19.817	**2.02**
1.141	0.570	0.549	18.746	**1.91**	1.100	0.200	21.984	**2.24**

BASIC CASE B2=12.7 cm

Soil Properties					*Anchor Properties*			*Anchor embedment depth*	
γ_t =	c =	ϕ =	ψ =	K_0 =	B =	R =	A =	H/B =	H =
(kN/m^3)	(kPa)	(°)	(°)	-	(m)	(m)	(m^2)	-	(m)
17	0.000	39.000	0.000	0.500	0.127	0.064	0.013	1.000	0.127
17	0.000	39.000	0.000	0.500	0.127	0.064	0.013	2.000	0.254
17	0.000	39.000	0.000	0.500	0.127	0.064	0.013	3.000	0.381
17	0.000	39.000	0.000	0.500	0.127	0.064	0.013	4.000	0.508
17	0.000	39.000	0.000	0.500	0.127	0.064	0.013	5.000	0.635
17	0.000	39.000	0.000	0.500	0.127	0.064	0.013	6.000	0.762
17	0.000	39.000	0.000	0.500	0.127	0.064	0.013	7.000	0.889
17	0.000	39.000	0.000	0.500	0.127	0.064	0.013	8.000	1.016
17	0.000	39.000	0.000	0.500	0.127	0.064	0.013	9.000	1.143
17	0.000	39.000	0.000	0.500	0.127	0.064	0.013	10.000	1.270
17	0.000	39.000	0.000	0.500	0.127	0.064	0.013	11.000	1.397
17	0.000	39.000	0.000	0.500	0.127	0.064	0.013	12.000	1.524
17	0.000	39.000	0.000	0.500	0.127	0.064	0.013	13.000	1.651
17	0.000	39.000	0.000	0.500	0.127	0.064	0.013	14.000	1.778
17	0.000	39.000	0.000	0.500	0.127	0.064	0.013	15.000	1.905
17	0.000	39.000	0.000	0.500	0.127	0.064	0.013	16.000	2.032
17	0.000	39.000	0.000	0.500	0.127	0.064	0.013	17.000	2.159
17	0.000	39.000	0.000	0.500	0.127	0.064	0.013	18.000	2.286
17	0.000	39.000	0.000	0.500	0.127	0.064	0.013	19.000	2.413
17	0.000	39.000	0.000	0.500	0.127	0.064	0.013	20.000	2.540
17	0.000	39.000	0.000	0.500	0.127	0.064	0.013	21.000	2.667
17	0.000	39.000	0.000	0.500	0.127	0.064	0.013	22.000	2.794
17	0.000	39.000	0.000	0.500	0.127	0.064	0.013	23.000	2.921
17	0.000	39.000	0.000	0.500	0.127	0.064	0.013	24.000	3.048
17	0.000	39.000	0.000	0.500	0.127	0.064	0.013	25.000	3.175
17	0.000	39.000	0.000	0.500	0.127	0.064	0.013	26.000	3.302
17	0.000	39.000	0.000	0.500	0.127	0.064	0.013	27.000	3.429

BASIC CASE B2=12.7 cm

Anchor static capacity					*Anchor dynamic capacity*			
D_m = (m)	R_m = (m)	V_s = (m^3)	Q_s = (kN)	Q_s = (t)	D_f = -	a = (g)	Q_d = (kN)	Q_d = (t)
0.217	0.108	0.003	0.076	**0.01**	1.100	0.200	0.408	**0.04**
0.307	0.153	0.010	0.285	**0.03**	1.100	0.200	0.925	**0.09**
0.397	0.198	0.022	0.682	**0.07**	1.100	0.200	1.617	**0.16**
0.487	0.243	0.042	1.324	**0.13**	1.100	0.200	2.545	**0.26**
0.577	0.288	0.070	2.265	**0.23**	1.100	0.200	3.774	**0.38**
0.667	0.333	0.109	3.561	**0.36**	1.100	0.200	5.368	**0.55**
0.757	0.378	0.159	5.267	**0.54**	1.100	0.200	7.390	**0.75**
0.847	0.423	0.224	7.438	**0.76**	1.100	0.200	9.904	**1.01**
0.937	0.468	0.303	10.130	**1.03**	1.100	0.200	12.972	**1.32**
1.026	0.513	0.399	13.397	**1.37**	1.100	0.200	16.660	**1.70**
1.116	0.558	0.514	17.296	**1.76**	1.100	0.200	21.029	**2.14**
1.206	0.603	0.648	21.881	**2.23**	1.100	0.200	26.145	**2.67**
1.296	0.648	0.804	27.208	**2.77**	1.100	0.200	32.070	**3.27**
1.386	0.693	0.984	33.333	**3.40**	1.100	0.200	38.869	**3.96**
1.476	0.738	1.188	40.310	**4.11**	1.100	0.200	46.604	**4.75**
1.566	0.783	1.419	48.194	**4.91**	1.100	0.200	55.339	**5.64**
1.656	0.828	1.678	57.042	**5.81**	1.100	0.200	65.138	**6.64**
1.746	0.873	1.967	66.908	**6.82**	1.100	0.200	76.065	**7.75**
1.836	0.918	2.287	77.848	**7.94**	1.100	0.200	88.183	**8.99**
1.926	0.963	2.640	89.917	**9.17**	1.100	0.200	101.555	**10.35**
2.016	1.008	3.027	103.170	**10.52**	1.100	0.200	116.246	**11.85**
2.106	1.053	3.451	117.663	**11.99**	1.100	0.200	132.318	**13.49**
2.196	1.098	3.913	133.451	**13.60**	1.100	0.200	149.836	**15.27**
2.286	1.143	4.413	150.589	**15.35**	1.100	0.200	168.863	**17.21**
2.376	1.188	4.955	169.132	**17.24**	1.100	0.200	189.463	**19.31**
2.466	1.233	5.540	189.137	**19.28**	1.100	0.200	211.698	**21.58**
2.556	1.278	6.169	210.658	**21.47**	1.100	0.200	235.634	**24.02**

8.3 Spreadsheets supporting the Modelling-of-Models and Final Design

PRELIMINARY PROTOTYPE ANCHOR DESIGN in DRY SOIL - Back Platform

Q =	required anchor total dynamic capacity =	320.0 t	3138.2 kN
Q' =	required anchor static capacity = 90%*Q	288.0 t	2824.4 kN
FS_s =	factor of safety recommended by API RP2SK for quasi-static load =	1.8	
Q_{rs} =	required ultimate anchor static capacity = Q'*FS_s	518.4 t	5083.9 kN
FS_d =	factor of safety recommended by API RP2SK for total dynamic load =	1.5	
Q_{rd} =	required ultimate anchor static capacity = Q*FS_d	480.0 t	4707.4 kN

Soil Properties

γ_t =	soil total unit weight	19.0 kN/m3	120.9 pcf
c =	soil cohesion	0.0 kPa	0.0 psi
ϕ =	soil friction angle	39.0 °	0.7 rad
ψ =	soil dilatancy	0.0 °	0.0 rad
K_0 =	coefficient of earth pressure at rest	0.5	
D_r =	soil relative density	55%	
C_u =	coefficient of uniformity	1.67	
ϕ_{tr} =	estimated friction angle through triaxial tests for Ovesen (1981) = (see formula below)	34.6 °	0.6 rad

$$\phi_{tr} = 30^{\circ} - \frac{3}{C_u} + \left(14 - \frac{4}{C_u}\right) D_r$$

ANCHOR STATIC CAPACITY

Clemence S.P. & Veesaert C.J. (1977)

Anchor Properties

A =	fluke projected area for pullout = (result of "goal seek" operation)	4.487 m2	48.30 ft2
B =	fluke diameter = $\sqrt{(4A/\pi)}$	2.39 m	7.84 ft
R =	fluke radius = B/2	1.20 m	3.92 ft
H/B =	relative depth = (input)	3.0	
H =	embedment depth at the fluke = H/B*B	7.17 m	23.53 ft

Anchor static capacity

D_m =	diameter of the major base of the truncated cone = B+2H*tan(ϕ/2)	7.47 m	24.50 ft
R_m =	radius of the major base of the truncated cone = D_m/2	3.73 m	12.25 ft
V_s =	volume of sand in truncated cone = (π*H/3)*(R^2+$R_m{}^2$+R*R_m)	148.94 m3	5259.87 ft3
Q_s =	ultimate anchor static capacity → (see formula below) = Q_{rs}	5084.0 kN	518.4 t

$$Q_s = \gamma_t V_s + \gamma K_0 \tan(\phi) \cos^2\left(\frac{\phi}{2}\right) \pi \left[\frac{BH^2}{2} + \frac{H^3 \tan(\phi/2)}{3}\right]$$

Ovesen N. Kribs (1981)

Anchor Properties

A =	fluke projected area for pullout = (result of "goal seek" operation)	4.505 m2	48.49 ft2
B_e =	equivalent fluke diameter for Ovesen (1981) = $\sqrt{A}$	2.12 m	6.96 ft
B =	fluke diameter for C&V (1977), fluke width for Ovesen (1981) == $\sqrt{(4A/\pi)}$	2.39 m	7.86 ft
H/B =	relative depth = (input)	3.0	
H =	embedment depth at the fluke = H/B*B	7.18 m	23.57 ft

Anchor static capacity

p =	specific ultimate anchor static capacity = (see formula below)	1128.6 kPa	163.7 psi
Q_s =	ultimate anchor static capacity ➔ p*A = Q_{rs}	5084.0 kN	518.4 t

$$\frac{p}{\gamma H} = 1 + (4.32 \cdot \tan\phi - 1.58)\left(\frac{H}{B_e}\right)^{3/2}$$

Comparison between the two theories

ΔA =	difference in the fluke area calculated by C&V (1977) and by Ovesen (1981)	0.40%
ΔB =	difference in the fluke diameter calculated by C&V (1977) and by Ovesen (1981)	0.20%

What would be the anchor static capacity calculated through C&V's (1977) theory with the anchor dimensions obatained from the application of Ovesen's (1981) theory?

Clemence S.P. & Veesaert C.J. (1977)

Anchor Properties

A =	fluke projected area for pullout = A (as calculated by Ovesen (1981))	4.505 m2	48.49 ft2
B =	fluke diameter = $\sqrt{(4A/\pi)}$	2.39 m	7.86 ft
R =	fluke radius = B/2	1.20 m	3.93 ft
H/B =	relative depth = (input)	3.0	
H =	embedment depth at the fluke = H/B*B	7.18 m	23.57 ft

Anchor static capacity

D_m =	diameter of the major base of the truncated cone = B+2H*tan(ϕ/2)	7.48 m	24.55 ft
R_m =	radius of the major base of the truncated cone = D_m/2	3.74 m	12.28 ft
V_s =	volume of sand in truncated cone = $(\pi*H/3)*(R^2+R_m^2+R*R_m)$	149.83 m3	5291.35 ft3
Q'_s =	ultimate anchor static capacity by C&V (1977) with A predicted by Ovesen (1981)	5114.4 kN	521.5 t
ΔQ_s =	difference between C&V's (1977) and Ovesen's (1981) theories abou the prediction of the ancohr static capacity	0.59%	

➔ Ovesen's (1981) results are accepted as somewhat more reliable and more conservative

ANCHOR DYNAMIC CAPACITY

Based on this difference between the two approaches, one can predict the dynamic holding capacity of the circular anchors. Even though, C&V (1977) are the only ones who suggested a formula to evaluate this resistance, the comparison with Ovesen's (1981) theory allows one to make a rough estimate of the dynamic capacity from a centrifugal model test perspective. Indeed, knowing the final anchor dimensions and the 0.59% difference for the static holding capacity, one can calculate the dynamic uplift resistance through the following C&V's (1977) equation and, then, correct it by the same percentage.

Clemence S.P. & Veesaert C.J. (1977)

Anchor dynamic capacity

D_f =	dynamic strain rate factor	1.15	
a =	accelaration of anchor in unit of g	0.36	
Q_d =	ultimate anchor dynamic capacity = (see formula below)	5377.8 kN	548.4 t

$$Q_d = \gamma_t V_s + \gamma K_0 \tan(\phi)\cos^2\left(\frac{\phi}{2}\right)\pi\left[\frac{BH^2}{H} + \frac{H^3\tan(\phi/2)}{3}\right]D_f + V_s\gamma_t a$$

Projection: Anchor dynamic capacity

Q_d =	ultimate anchor dynamic capacity according to C&V's (1977) theory with a correction of 0.59% = Q_d-(Q_d*0.59%), and verify that this $Q_d \geq Q_{rd}$	5345.8 kN	545.1 t

Thickness, Volume, and Weight of Final Anchor

According to the anchor dimensions determind through Ovesen's (1981) theory, thickness, volume, and weight of the anchor can be obtained as follows:

γ_t =	steel unit weight	77.0 kN/m3	490.1 pcf
t =	anchor thickness = estimated as 3% of B	0.07 m	0.24 ft
V =	anchor volume = A*t	0.32 m3	11.43 ft3
W =	anchor weight = V*γ_{steel}	24.92 kN	2.80 T

Legend

data to input

cell box to change during "goal seek" operation

cell box to "goal seek" for

PRELIMINARY PROTOTYPE ANCHOR DESIGN in DRY SOIL - Front Platform

Q =	required anchor total dynamic capacity =	1191.8 t	11687.5 kN
Q' =	required anchor static capacity = 90%*Q	1072.6 t	10518.7 kN
FS_s =	factor of safety recommended by API RP2SK for quasi-static load =	1.8	
Q_{rs} =	required ultimate anchor static capacity = Q'*FS_s	1930.6 t	18933.7 kN
FS_d =	factor of safety recommended by API RP2SKfor total dynamic load =	1.5	
Q_{rd} =	required ultimate anchor static capacity = Q*FS_d	1787.6 t	17531.2 kN

➔ repeat the same procedure as shown for the Back Platform.

PROTOTYPE ANCHOR DESIGN in SATURATED SOIL - Back Platform

Q =	required anchor total dynamic capacity =	320.0 t	3138.2 kN
Q' =	required anchor static capacity = 90%*Q	288.0 t	2824.4 kN
FS_s =	factor of safety recommended by API RP2SK for quasi-static load =	1.8	
Q_{rs} =	required ultimate anchor static capacity = Q'*FS_s	518.4 t	5083.9 kN
FS_d =	factor of safety recommended by API RP2SKfor total dynamic load =	1.5	
Q_{rd} =	required ultimate anchor static capacity = Q*FS_d	480.0 t	4707.4 kN

➔ replace the soil total unit weight with the soil buoyant unit weight γ'=12.9 kN/m^3

➔ repeat the same procedure

PROTOTYPE ANCHOR DESIGN in SATURATED SOIL - Front Platform

Q =	required anchor total dynamic capacity =	1191.8 t	11687.5 kN
Q' =	required anchor static capacity = 90%*Q	1072.6 t	10518.7 kN
FS_s =	factor of safety recommended by API RP2SK for quasi-static load =	1.8	
Q_{rs} =	required ultimate anchor static capacity = Q'*FS_s	1930.6 t	18933.7 kN
FS_d =	factor of safety recommended by API RP2SKfor total dynamic load =	1.5	
Q_{rd} =	required ultimate anchor static capacity = Q*FS_d	1787.6 t	17531.2 kN

➔ replace the soil total unit weight with the soil buoyant unit weight γ'=12.9 kN/m^3

➔ repeat the same procedure